Stochastic beach width prediction

At a recently nourished beach

M.O. Enschedé

Technische Universiteit Delft

Cover photo: The Hondsbossche Dunes after the nourishment in 2015 (www.hoogwaterbeschermingsprogramma.nl).

Stochastic beach width prediction

At a recently nourished beach

by

M.O. Enschedé

in partial fulfillment of the requirements for the degree of

Master of Science

in Civil Engineering

at the Delft University of Technology,

to be defended publicly on Tuesday Oktober 1, 2019 at 10:00 AM.

Student number: 4253817

Supervisor:	Ir. J. (Anna) Kroon,	TU Delft
Thesis committee:	Prof. dr. ir S.G.J. (Stefan) Aarninkhof	TU Delft
	Dr. ir. M.A. (Matthieu) De Schipper,	TU Delft
	Dr. ir. O. (Oswaldo) Moralis Napolis	TU Delft
	Dr. ir. W.S. (Wiebke) Jäger	Boskalis

TU Delft Delft University of Technology

Abstract

The insight in the behaviour of beach profiles is important for three main functions of a beach: limiting flood risk, ecological values and recreational values. A sufficient beach width contributes to these functions. Therefore, maintaining a minimal beach width can be relevant. This relevance of a sufficient beach width is for instance reflected in the requirement of maintaining a minimal beach width of 50 meters in the Design, Build & Maintenance contract for the 'Hondsbossche Dunes' nourishment project. The Hondsbossche Dunes are an artificial beach dune area with a length of 6 km at the Dutch coast. To ensure a certain minimal beach width, beach development predictions can be made to know when nourishments have to take place. These beach development predictions can be made using the numerical morphodynamic model XBeach. Morphodynamic developments are however hard to predict due to the many uncertainties. These uncertainties are in deterministic state of the art morphodynamic modelling not quantified. This study examines a method for stochastic beach width predictions with a process-based morphodynamic model. The uncertainties that are addressed in this stochastic assessment, are the hydrodynamic forcing conditions in a morphodynamic forecast.

The method to carry out a stochastic beach width model forecast is developed and described using a case study. In this case study, the beach profile development right after a beach nourishment is examined. The beach nourishment took place at the artificial beach of the Hondsbossche Dunes.

The first step is to analyse the beach profile development after a nourishment. This analysis is done by beach profile surveys with a GPS mounted on a walking wheel during the first four months after the nourishment. Initially, the nourishment creates a seaward perturbation in the shoreline. In the period after the nourishment the size of this perturbation decreases over time due to erosion. The shape of the nourishment disperses in longshore direction. The erosion is most severe at the largest cross-shore extent of the nourishment. At this location, the beach width decrease was 52 m over the first four months. At the north side there only was a decrease of 19 m, and at the south side, the beach width even increased with 1 m after four months. The location with the largest beach width decrease is used for the morphodynamic model. With satellite imagery the planform of the nourishment is analysed until one year after the nourishment took place. After one year, the shoreline perturbation disappeared and a smooth coastline remains.

The morphodynamic model used for the stochastic beach width prediction is XBeach. An XBeach model is calibrated based on observed hydrodynamic conditions and observed beach profiles. In the calibration process, the XBeach model settings are adjusted so that the model result matches with the values observed. Especially the parameter for the longshore transport gradient had to be set to -0.003 to achieve the correct amount of net sediment loss. The XBeach model settings are optimised to limit the computation time while maintaining sufficient accuracy. This was achieved by maximising the morphological acceleration factor and the grid size while preserving sufficient accuracy. Limiting the computation time is necessary because a stochastic forecast with a process-based model is relatively computationally intensive.

To make stochastic XBeach predictions, a range of possible hydrodynamic forcing conditions are required. For this, stochastic wave data are generated which consist of time series containing a full range of possible wave conditions. To generate these synthetic time series, historical offshore wave data are analysed. The offshore wave data is collected at three wave rider stations: IJmuiden Munitiestortplaats, Europlatform, and Eierlandsegat. First, the waves at IJmuiden Munitiestortplaats are simulated, as this location is the closest to the study location. The historical wave data at IJmuiden Munitiestortplaats are decoupled in a stationary and a non-stationary component. The non-stationary component is simulated by Fourier series and for the stationary component, an Autoregressive-Moving Average (ARMA)

model is developed. Combining these components leads to a synthetic wave time series at IJmuiden Munitiestortplaats. For the simulation of the wave data at Europlatform and Eierlandsegat, an ARMA model is estimated based on the differences between the waves at these two stations and the waves at IJmuiden Munitiestortplaats. These three wave time series are combined and transformed to the near-shore location of the Hondsbossche Dunes and can be used as input for XBeach. The resulting time series of the hydrodynamic forcing conditions consist of realistic time series containing natural variations such as seasonal differences, storm conditions, and calm conditions. However, seasonal differences are underestimated in the generated forcing conditions.

A total of 5000 stochastic wave time series are created for the offshore wave rider stations to describe a large range of possible wave conditions. It is computationally infeasible to process all these wave time series through XBeach, therefore Latin Hypercube sampling is applied. Latin Hypercube sampling is an efficient sampling method for selecting stratified samples. Twenty wave time series are selected which contain a well-spread coverage of the total wave energy in longshore and cross-shore direction.

These 20 wave time series of one year are used as input for the XBeach model. This results in 20 possible beach development profiles. With this stochastic forecast, the possible beach width development and the probability of occurrence is indicated. The results show that after one year, the beach width change is between -18 m and -98 m with an 80% probability. There is a 10% chance that the beach width decrease is larger than 98 m after one year.

With this method uncertainty ranges are taken into account when doing beach profile development forecasts. This gives a more realistic idea of the possible beach width development. One of the questions which can be answered by applying this method is the probability that nourishments will have to take place within a certain period. In beach nourishment contracts where maintenance is included, such as at the Hondsbossche Dunes, this insight can contribute to better budgeting decisions and optimisation of beach nourishment volumes.

Preface

Before you lies the master's thesis "Stochastic Beach Width Prediction at a Recently Nourished Beach". With this thesis, I conclude my study of Civil Engineering in Delft.

For me, the process of writing this thesis contained several distinct components to mention. It started with practical fieldwork experience, I enjoyed going out to the beach for the surveys. I learned how to analyse this data, and to calibrate an XBeach model with this data. Then I delved into the theory behind generating stochastic hydrodynamic conditions with great enthusiasm. But this thesis also contained parts I didn't particularly enjoy, mainly writing my findings down. Of course, writing *is* an essential part of a thesis, this caused it took longer than conventional to finish. But with this finished work in hand, I can proudly look back at what I have accomplished.

I want to thank all members of my thesis committee. Thank you, Anna Kroon, for being a great help in guiding the thesis process from start to end. In our numerous meetings, you provided me with thoughtful feedback which always resulted in new ideas and improvements for this thesis. You also arranged that I could use the computational Power at Svašek Hydraulics for my stochastic XBeach simulations which were key in my process. Thank you, Matthieu de Schipper, for your enthusiastic supervision, always with sharp remarks and constructive advice. Wiebke Jäger, thank you for sharing your expertise on the complex matter of generating time series of hydrodynamic conditions. Thank you Stefan Aarninkhof and Oswaldo Morales Nápoles for contributing in my committee.

Besides the professional help, I want to thank my friends for their support. The countless coffee breaks with Tom made the process of writing a thesis much more fun. The roommates from the Koornmarkt, and later from the Prinsegracht, were always there to for debating issues and to keep me motivated. My parents deserve a particular note of thanks: Their endless support and wise counsel have been of great help.

I hope you enjoy reading.

MEnschede

M.O. Enschedé
Den Haag, September 2019

Contents

List of Tables

List of Figures

1

Introduction

1.1. Background

Functions of sandy shorelines can be categorised into three groups: limiting flood risk, socio-economic functions, and ecological functions. Beach widths can contribute to all of these three functions. The water safety part mainly concerns the volume of the foreshore, beach, and dunes. For the water safety function, a larger beach width results in a larger foreshore volume. This affects the impact of storm activity due to an increased dissipation of wave energy. The beach also contributes to the aeolian sediment transport towards the dune area, which results in a larger dune volume (Ruessink & Jeuken, 2002). The socio-economic factor of coastal areas mainly concerns recreation. Coastal tourism is one of the fastest-growing areas in tourism (Hall, 2001). A sufficient beach width is a prerequisite for coastal tourism. The ecological functions of the beach vary per local climate of the beach. In general, beach areas are of great ecological importance and larger beach widths contribute to this. A sufficient beach width contributes to all three of these beach functions, beach widths can, therefore, be an important maintenance requirement. To fulfil beach width requirements, it is of importance to model the development of the beach behaviour over time. This need to maintain a sufficient beach width is also reflected in recent tenders using a Design, Build & Maintenance contract. In beach nourishment contracts where maintenance is included, such as at the Hondsbossche Dunes, a minimum beach width of 50 meter is required to be maintained. For a contractor, it is crucial to make a risk assessment, with the probability of the beach width falling below this minimum. Generally, current advance beach width prediction models result in an expected beach width development without showing the probability range. With beach width predictions within a stochastic framework examined in this study, the probability range is shown. This gives a better insight into the possible future development of the width of the beach concerned.

Beach width assessment models

For beach width predictions, morphological models can be used. Beach widths can be determined from cross-shore profiles, so cross-shore profile models are suitable for this analysis. Several models can be used to simulate cross-shore profile changes. Beach profile models can be categorised in behaviour models, process-based models, and hybrid models. Behaviour models are equilibrium forced and use empirical relationships to model the behaviour of a coastal profile over time. Behaviour models are typically applied with long time scales (multiple years). Process-based models describe the elementary processes of flows and the sediment response. Process-based models are typically used for medium-term time scales (multiple seasons) although covered time scales become longer. Hybrid models are a combination of behaviour models and process-based models. As this research is aimed at a medium-term time scale and not at an equilibrium profile only process-based models will be taken into consideration. Nowadays XBeach is the most widely used model to simulate hydrodynamic and morphodynamic processes both in the sub-aqueous as in the sub-aerial beach parts. XBeach is an open-source numerical model which is originally developed to simulate hydrodynamic and morphodynamic processes and impacts on sandy coasts (Roelvink et al., 2015).

1.2. Problem description

So XBeach is potentially a good model to forecast beach widths. However, the model output of an XBeach model is deterministic whereby no uncertainty in the climatic forcing is involved in the results. As a deterministic model gives no insight into the uncertainties and the probabilities of the outcome, a stochastic model could be more meaningful. With a deterministic model, uncertainties can be assessed by a scenario-based approach. In this approach, experts define a limited amount of critical scenarios which result in a range of model outcomes whereby the uncertainties can be assessed. However, the uncertainties cannot be quantified by this method as the likelihood of the scenarios is not taken into account (Scheel, de Boer, Brinkman, Luijendijk, & Ranasinghe, 2014). To ideally assess the uncertainties a full probabilistic approach, like a Monte Carlo simulation, would be applied on XBeach models. In a Monte Carlo simulation, a random combination of a range of possible input values are repetitively processed. The large number of results, each based on random input values, are used to describe the uncertainties of certain values in the model. However, an XBeach model requires significant computing power so the number of simulations required for a Monte Carlo approach is not feasible. In between, on the one hand, a scenario-based model and on the other hand the full probabilistic approach, are a wide range of probabilistic methods (Scheel et al., 2014). Within this range of options, a method has to be selected which gives sufficient uncertainty quantification and has efficient computational properties so that it can be used with XBeach. Calculating probability range for future beach width calculations improves the insight for the possible future development of the beach.

1.3. Research Objective

In this research, a method is examined to forecast the beach width under future forcing in a probabilistic manner in which the uncertainties of future hydrodynamic forcing conditions can be quantified. The research objective can be summarised as the following:

> ”Examine an uncertainty assessment method for beach width predictions by carrying out a beach width prediction within a stochastic framework at a recently nourished beach”

This research objective consists of two main parts, the beach width prediction part, and the stochastic framework part. The combination of these two parts has not been researched until now. When this research objective is met, the knowledge gap of understanding the effect of applying a stochastic synthetic time series to a beach width prediction model is filled. The approach of this research is to develop the stochastic beach width forecasting method by applying this to a case study. The case study based on which this method is developed is at a recent nourishment beach at the Hondsbossche Dunes, the Netherlands. To successfully carry out this research objective, it is split into four sub-questions:

- What is the morphological development of a recently nourished beach?
- What are appropriate XBeach model settings to model the development of a recently nourished beach?
- How can stochastic forcing conditions be generated for a near-shore location?
- What are the probability ranges of the expected beach width development for the study location?

Scope

This objective of this study is to examine a method for stochastic beach width forecasting. This includes a case study for the locating of the Hondsbossche Dunes, at the region where a nourishment took place in March 2018. A fieldwork analysis for the beach profiles focuses on the development of the shape of the nourishment in the four months after the construction.

To model the impact of the morphodynamic and hydrodynamic processes on the coast, an 1D cross-shore XBeach model is used. For XBeach, the surfbeat mode is used, which resolves short waves on the wave group scale, and the long waves associated with them.

In the field of uncertainty analysis, a distinction can be made between the sources of the uncertainties. In this study, only intrinsic uncertainties, related to the uncertainty in future forcing conditions, are taken into account.

For the method of creating synthetic stochastic hydrodynamic forcing conditions, an exploration is made for the use of Autoregressive-Moving Average (ARMA) models. For this, the focus lies more on the development of an engineering model, and the methodology used than on the quality of the results. The synthetic forcing conditions consist of significant wave heights, peak wave periods, mean wave directions, and water levels.

The stochastic XBeach forecast has a time scale of one year. With the results of this forecast, the focus lies on the development of the beach width and its statistical spreading.

1.4. Outline

This thesis contains eight chapters, the outline of these chapters is as follows. Chapter 2 contains the theoretical framework, where the background of the theory used in this study is given. In chapter 3 the methodology is explained. The data used for this study, and the collection method, are described in chapter four. In chapter 5 the XBeach model settings are calibrated. In chapter 6 the generation of synthetic wave time series are described. These synthetic wave time series are thereafter the input for XBeach for the stochastic forecast in chapter 7. Chapter 8 contains the discussion and in chapter 9 the conclusions of this study are given.

2

Theoretical Framework

This chapter provides background information for the theories, concepts, and models used in this study. The current state of knowledge of the relevant topics is reviewed from the literature. The beach is defined in section 2.1. Methods for beach width development modelling are discussed in section 2.2, containing a general introduction to XBeach. In section 2.3 the uncertainties associated with beach width modelling are explained.

2.1. Beach width definition

In this research, the most important parameter is the width of the allocated beach. But how is the beach width defined? After all, with a varying water level as a result of the tide, the beach width also varies constantly. In general, the beach width is defined as distance between the dune-foot X_{DF} and the shoreline X_{SL}. (Keijsers, Poortinga, Riksen, & Maroulis, 2014). Both the dune-foot X_{DF} and the shoreline X_{SL} are however dynamic locations.

The dune-foot X_{DF} is the most seaward position of the dune, which is dynamic due to hydraulic and aeolian processes. The definition of the dune-foot is arbitrary. The dune-foot can be defined by the position of the maximal storm surge level (Guillén, Stive, & Capobianco, 1999). In the situation at the Hondsbossche Dunes, this is not a useful definition as the beach and the dunes are artificial, so the location of the dune-foot might not be fully adjusted to the maximal storm surge level. A more useful definition of the position of the dune-foot at the Hondsbossche Dunes is the location where there is a change in slope of the cross-shore profile, from the gentle slope of the beach face to the steep dune face. In this research the dune-foot is defined as a fixed point, so the dune-foot variation is neglected. In the case study of this thesis, the beach widths are calibrated and validated for a summer period during which it is not expected that the dune-foot will erode due to the milder conditions during summer. Accretion due to aeolian processes could be expected at the dune-foot, however, this is expected to be of such minor quantities in the period of this project and will hence be neglected.

For the position of the shoreline, there are several possible definitions. According to (Verhagen, 1989) the shoreline location X_{SL} can be obtained by a volume integration of the profile between mean high water (MHW) and mean low water (MLW) (figure 2.1). For the location of the Hondsbossche Dunes, the levels of MHW and MLW are 0.84 m and -0.76 m respectively (Dillingh, 2013).

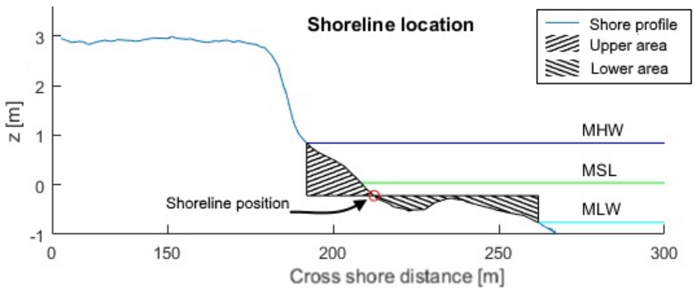

Figure 2.1: Determination of the shoreline position in the beach profile. The upper area between mean high water and the shoreline position is equal to the area between the shoreline position and mean low water.

2.2. Beach width modelling

To model beach widths several modelling approaches are possible. The available modelling methods are discussed in section 2.2.1. The morphodynamic model used in this study is XBeach, which is introduced in section 2.2.2.

2.2.1. Modelling methods

Beach profile models can be categorised in data-driven models, process-based models, and hybrid models. Data-driven models are models based solely on the analysis of measurements, whereby no knowledge of the physical process is used. Data-driven models use measurements of past conditions to identify patterns of behaviour. An example of data-driven modelling is the convolution method for time-dependent beach profile response by Kriebel and Dean (1993) which is a simple beach erosion and accretion model. Callaghan, Nielsen, Short, and Ranasinghe (2008) applied this data-driven method within a stochastic framework to analyse extreme beach erosion on Narrabeen Beach, Sidney. Data-driven models have a relatively low computation demand. Therefore these are suitable for long term and large scale forecasting. Process-based models are based on physical processes and include the interactions between hydrodynamic forcing and the morphodynamic response, resulting in a bed-updating module. Originally, this approach is developed for short-term forecasting, such as single or multiple storm events. However, due to the development of the understanding of hydrodynamic and sediment transport processes, and the growing availability of computational power, the use of process-based models grows (Davidson, Turner, Splinter, & Harley, 2017). Examples of process-based models are XBeach, UNIBEST TC, and Delft3D. In hybrid models, elements of the two model types are combined to reduce the complexity of the model. SBEACH is an example of a hybrid model.

2.2.2. XBeach

XBeach is a model that can be used to calculate sediment transport and morphological changes to determine beach width evolution. XBeach is a process-based model which is used to compute sediment transport and dune erosion. In the model, both short and long waves are transformed towards the shore and their interactions are taken into account. XBeach was developed to simulate hydrodynamic and morphodynamic processes and impacts on sandy coasts. XBeach has a 1D mode, where long-shore gradients are ignored, and a 2DH mode where detailed analysis of long-shore processes on erosion are possible. Large 2DH simulations are significantly more computationally intensive than the 1D simulations. For a complete description of XBeach, see Roelvink et al. (2015).

Longshore Transport Gradient

As explained in section 1.3 this study focuses on a prediction of beach width reduction after the implementation of a nourishment. When after a nourishment, the shoreline has a seaward perturbation, a long-shore transport gradient is expected, as the shape of the nourishment diffuses along the shoreline. Cross-shore profile models are not able to calculate longshore transport gradients. However, a recent implementation for longshore transport gradients in XBeach made it possible to implement a longshore transport gradient for 1D models. A recent implementation for longshore transport gradients in XBeach can be manually implemented with the factor f_{lsgrad}. The factor f_{lsgrad} is implemented in the volume balance equation for bed level updating (see equation 2.1).

$$\frac{\partial z_b}{\partial t} + \frac{MorFac}{(1-\rho)}\left(\frac{\partial q_x}{\partial x} + \frac{\partial q_y}{\partial y} f_{lsgrad}\right) = 0 \tag{2.1}$$

In this volume balance equation z_b is the bed level, ρ is the porosity, $MorFac$ is the morphological acceleration factor, and q_x and q_y represent the sediment transport rates in x- and y-direction. The change is sediment transport rate in y-direction is multiplied by the factor f_{lsgrad}. In cross-shore profile XBeach models there is no grid size in y-direction, therefore $\partial y = 1$.

In XBeach, the longshore transport gradient factor is a fixed factor, it can not be changed over time. When the shape of the coastline changes, the longshore transport properties change. This effect is not included in cross-shore profile models for XBeach. For long term simulations, containing multiple seasons, this can be a limiting property.

2.3. Uncertainties

Box (1979) mentioned that "All models are wrong, but some are useful" (p. 202). This aphorism is often referred to, underlying that a model is a simplification of reality, and hence always contains deficiencies. Uncertainties are inherently associated with morphodynamic models. The uncertainties present in morphodynamic models can be distinguished between epistemic and intrinsic uncertainties (Van Gelder, 2000). Intrinsic uncertainties result from the random behaviour of natural systems in time and space. Stochastic processes such as wave heights, water levels, or number of storms are examples of intrinsic uncertainties. These intrinsic uncertainties can be addressed, but not reduced. Epistemic uncertainties are related to the misfit between the model and the real phenomenon and can be reduced by acquiring further knowledge or additional data. Kroon, de Schipper, van Gelder, and Aarninkhof (2019) provided a scheme with the different uncertainty sources for morphological modelling 2.2. The intrinsic uncertainty, for example, the uncertainty in future wave heights, can be divided in an intrinsic uncertainty in time and space. The epistemic uncertainty is divided in a model uncertainty and an observation uncertainty. The model uncertainty refers to the model inadequacy, numerical uncertainty, and the parameter uncertainty. The observation uncertainty is the difference between the measured values and the true values, resulting from inaccuracies in survey instruments and data processing. In Kroon et al. (2019) the relative importance of the model uncertainty versus the effect of wave climate variability in a probabilistic assessment of a large scale nourishment is examined. For a 2.5 year simulation period the model uncertainty was found to be in the same order of magnitude as the wave climate variability. These uncertainties are related to the fundamental properties of predictive process-based morphodynamic modelling. Therefore it is not possible to fully remove or overcome these uncertainty sources. A way to cope with these uncertainties is to quantify them. Ignoring these uncertainties leads to incomplete model outcomes.

Previous research

The interest in predictions of the beach and dune profile development within a probabilistic framework is increasing among coastal zone managers (Scheel et al., 2014). A single deterministic outcome

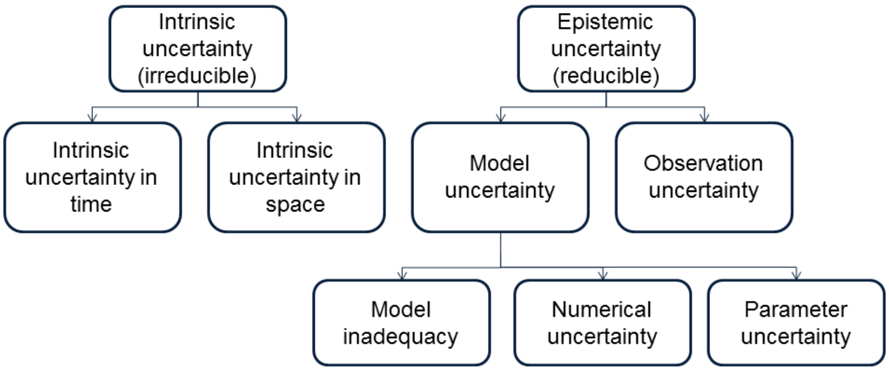

Figure 2.2: Types of uncertainties for morphological modelling (Kroon et al., 2019).

of a coastal change prediction is less meaningful than coastal predictions in a probabilistic manner since forcing conditions which govern future coastal change can be predicted in a statistical sense only (Ruggiero, List, Hanes, & Eshleman, 2007). In Jäger (2018) a method to create synthetic wave time series based on auto-regressive moving average (ARMA) models is described. A knowledge gap lies in the combination of an extensive stochastic wave forecasting method combined with a process-based sediment transport model for morphological changes in the nearshore area. Filling this knowledge gap contributes to the understanding of the uncertainty range of a beach width forecast.

2.4. Stochastic forecasting of hydrodynamic forcing conditions

Stochastic modelling can be used to incorporate the above-mentioned uncertainties in beach profile forecasting. With stochastic modelling, the outcome is not deterministic anymore but has a certain probability of occurrence. For the example of a beach width model, a deterministic model results in one beach width after the modelling period, and a stochastic model results in a range of possible beach width, with their probability of occurrence.

Examples for stochastic modelling for beach profiles are:

In den Bieman et al. (2014) a probabilistic approach, namely Adaptive Directional Importance Sampling, is applied to a 1D XBeach model for flood risk. Flood risk is assessed by a Limit State Function and the sample size is decreased by Adaptive Directional Importance Sampling. In this study, a probabilistic approach is used in combination with XBeach. However, the focus in den Bieman et al. (2014) lies on the probability of failure, using the limit state function, while in this thesis the whole probability distribution is assessed to examine the uncertainties of the beach width development.

In Ruggiero et al. (2007) a method is developed in which a deterministic shoreline change model is applied in a probabilistic manner. A one-line model (UNIBEST-TC) in which the wave height, wave period and wave direction are varied with different sediment budget scenarios. The resemblance with this study is that it also uses a deterministic coastal model in a probabilistic manner. However, the modelling is scenario-based, focusing on the effect of changing the sediment budget, rather than a complete probability range.

In (Davidson et al., 2017) a shoreline displacement model is developed for annual time scales by a probabilistic approach. A Generalised Extreme Value (GEV) analysis is applied to extrapolate the probability of occurrence for the shoreline response within a return period of one year. The correspondence with this study is that also beach width development is modelled. This study uses an equilibrium based model 'ShoreFor', and a simplified method for creating stochastic wave time series by random monthly selection.

So several previous studies contained stochastic modelling for beach profiles. However, the method whereby the hydrodynamic conditions are generated varies per study, as well as the morphological models applied. A method with advanced process-based modelling, in combination with long term (one year) stochastic hydrodynamic forcing conditions, has not been examined yet.

2.4.1. Generating synthetic time series

For building a stochastic XBeach model for beach width predictions, an essential uncertainty comes from the wave input. So a fundamental part of this study is generating a time series of wave heights, wave periods, wave directions and water levels.

When the time series of the wave heights are generated by random sampling from its distribution, a signal as given in figure 2.3 is the result. Although the magnitudes and the bivariate correlation between the wave heights and the wave periods are realistic, their arrangement is not. This signal contains no seasonality nor natural swell or storm behaviour.

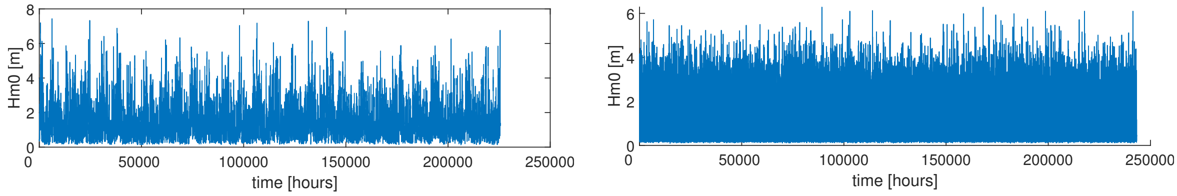

(a) (b)

Figure 2.3: Time series of the (a) observed significant wave heights and (b) random generated significant wave heights. The duration is 28 years and the data points are one hour apart.

When this random time series is used as input for XBeach, the sediment transport is underestimated. This underestimation is because in random wave time series intense conditions generally last only one time-step, to be followed by average conditions. While natural a storm lasts a few hours so stirred-up sediments stay longer in suspension and therefore more sediment is transported.

Therefore a more natural behaviour must be incorporated in the synthetic time series. In literature more applications demand the generation of time series of hydro-meteorological conditions, e.g. (Jäger, 2018) and (Davidson et al., 2017). Methods to generate synthetic time series with natural hydro-meteorological behaviour are random monthly sampling, Vine-Copula modelling, and Auto Regressive-Moving Average (ARMA) processes. These methods are explained below. In a study by Jäger (2018) time series of significant wave heights and mean zero-crossing periods are generated both using Vine-Copulas and ARMA processes.

Random Monthly Sampling

A way to generate synthetic time series is by selecting random month-long segments from a randomised pool of data containing only data from an equivalent month (Davidson et al., 2017). So when generating one year of synthetic data, first one random month of the past observed data from January is selected. Then a randomly selected February month is added, etc. This method preserves seasonality, storm behaviour, and joint probabilities of parameters. This is convenient for simulating data in XBeach the wave heights, wave periods, wave directions, and water level surge are correlated. This method of random monthly sampling requires a large set of years of observed data. Davidson et al. (2017) used two sets of data, one with 63 years and one with 36 years. A disadvantage of this method is that random sampling has no physical origin. It is possible that in one year of generated data, only extreme months are sampled, while this might be physically impossible. Furthermore, only the extremes which are included in the observed data can reoccur in the generated data. The spreading of the total wave energy per year is therefore expected to be larger than in reality. Moreover, with random sampling as simulation method, inter-annual seasonal variability is not taken into account.

Vine-Copula modelling

Vine-copulas are used to simulate time-series in the financial field, for energy research, and in the social science. Jäger (2018) used vine-copulas to simulate time series of significant wave heights and mean zero-crossing periods with an hourly resolution. With this method, stormy behaviour and daily wave conditions are successfully described. However, this method is highly sensitive to the selected vine structure, the chosen copula families, and the parameter estimates. Furthermore, the model is complex and requires long simulation times.

Auto Regressive-Moving Average (ARMA) processes

Besides a method for vine copulas, Jäger (2018) also explored a less complex time series approach based on ARMA models.

An ARMA model describes a weakly stationary stochastic process in terms of two polynomials, one for the auto-regression (AR) and the second for the moving average (MA). An ARMA process is described by equation 2.2 (Box, Jenkins, Reinsel, & Ljung, 2015).

$$X_t = c + \sum_{j=1}^{p} \phi_j X_{t-j} + \epsilon_t + \sum_{j=1}^{q} \theta_j \epsilon_{t-j} \tag{2.2}$$

An ARMA(p,q) model is an ARIMA(p,d,q) with $d = 0$. The d term gives the degree of difference. With stationary models, the degree of difference is 0. In this study, the seasonality of the time series where the ARMA model is applied is modelled separately. Therefore this study refers to ARMA models instead of ARIMA models. The notation ARMA(p,q) refers to the model with p auto-regressive terms and q moving average terms. In this model, the current value of the AR(p) part is expressed as a regression of its previous values and a random shock ϵ_t (or residual). The MA(q) part involves modelling the random shock as a linear combination of a finite number q of previous random shock terms ϵ_t (Box et al., 2015). Including both auto-regressive and moving average terms in the model leads to the mixed auto-regressive-moving average (ARMA) model.

An indication of suitable values of the orders p and q in the ARMA(p,q) model can be found by inspecting the auto-correlation function (ACF) and the partial autocorrelation function (PACF) (Brockwell, Davis, & Calder, 2002). For an AR(p) process, the ACF decays slowly, and the PACF has a cut off at lag p, while for an MA(q) process, the ACF has a cut off at lag q and the PACF decays slowly (Box et al., 2015). When the orders of p and q are determined, their coefficients are by found maximum likelihood estimation. Determining the coefficients p and q is a built-in function in MATLAB.

2.5. Sampling

The computation time of an XBeach model with a simulated period of one year is minimised to approximately 7 hours. With a computation time of 7 hours, it is unfeasible to run a large amount (1000) of XBeach calculations. An optimum has to be found with the minimal number of XBeach calculations, which gives a good representation of the characteristics of the whole population. To find this optimum, different sampling methods are examined.

2.5.1. Sampling methods

To select a subset which represents the characteristics of the whole population, different sampling techniques are available. A usual way to choose a subset of individuals chosen from a larger set is by simple random sampling. With simple random sampling, every individual has an equal chance of being selected in the population sample (Acharya, Prakash, Saxena, & Nigam, 2013). An advantage of this method is that limited knowledge is required about the characteristics of the data. However, a limitation is the sample size, which has to be larger compared to stratified sampling to reach the same precision. With stratified sampling, the population is partitioned in various sub-groups (strata). From each sub-group, a random sample is drawn by simple random sampling. A multidimensional version of stratified sampling is Latin Hypercube sampling (Pebesma & Heuvelink, 1999). With Latin Hypercube sampling a sample size is drawn from multiple variables in such a way that for each variable the sample is fully stratified (McKay, Beckman, & Conover, 1979). Due to this stratification of various variables Latin Hypercube sampling is an efficient and widely used technique to limit computation time while preserving the characteristics of the data e.g. (Dagalaki, 2018), (Pebesma & Heuvelink, 1999), (Ţene, Stuparu, Kurowicka, & El Serafy, 2018). Besides simple random sampling and stratified sampling, other sampling techniques are available, such as Importance Sampling, Directional Sampling, etc. Dagalaki (2018) compared these different statistical methods for the applicability on process-based model. According to Dagalaki (2018) for process-based models with a large computational demand, Latin Hypercube sampling should be preferred.

2.5.2. Latin Hypercube sampling

Latin Hypercube sampling is often used to save computation time when running Monte-Carlo simulations with a high computational demand. Latin Hypercube sampling aims to select evenly distributed samples from a large data set. Near-random samples are generated based on multiple parameters. This process is summarised as follows: For selecting n samples, the range of each variable is divided into n equal probable intervals. In each interval one value is selected, so that the Latin Hypercube requirements are satisfied; with only one sample at each axis-aligned hyperplane (figure 2.4). For the example in figure 2.4 with two parameters, one value in the axis-aligned hyperplane means that there is one sample in each row and each column.

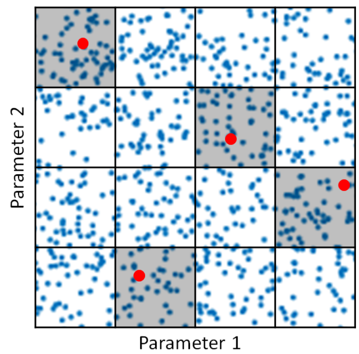

Figure 2.4: Illustration of the Latin Hypercube method for two parameters. For each parameter the range is divided into four equal probable intervals. From each interval one sample is selected, so that each hyperplane contains one sample only.

Correlation

When the parameters used for Latin Hypercube sampling are correlated, the selected samples will not copy the correlation with the simple Latin Hypercube procedure, resulting in an unevenly distributed sample. Iman and Conover (1982) proposed a method to induce correlation in Latin Hypercube sampling.

With this method, the selected squares in the hyperplane (the grey squares in figure 2.4) have the same correlation coefficient as the total set of original samples (blue points in figure 2.4). The procedure to induce correlation in Latin Hypercube sampling is part of MATLAB function 'lhsgeneral'.

Sample size

A drawback of Latin Hypercube sampling is that the sample size cannot simply be increased by adding new sample elements, as the stratification will not be maintained if the sample size is simply increased. In Sallaberry, Helton, and Hora (2008) a method for extension of Latin Hypercube samples is proposed in combination with correlated variables. This method starts with a Latin Hypercube sample of size m, and an associated rank correlation matrix **C**. A new Latin Hypercube sample is created with the size $2m$ and a rank correlation close to the original rank correlation **C**. This procedure is as follows:

- Generate a Latin Hypercube sample with size m. (see figure 2.4)
- Select a second set of Latin squares (see figure 2.5).
- Divide all squares in four sub-squares.
- Each previous selected square, contains a sub-square with no sample in its row and column. From each of these sub squares, one sample is selected. (see figure 2.5)

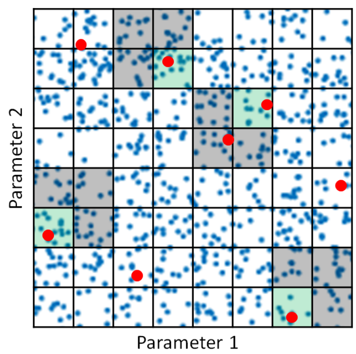

Figure 2.5: Extension of the Latin Hypercube sample size. The Latin Hypercube sample given in figure 2.4 of size 4, is doubled to a sample size of 8, while maintaining the Latin Hypercube properties.

This results in a Latin Hypercube sample of the size $2m$. This process can be repeated until the desired sample size is reached.

2.6. Model performance evaluation

In the calibration and validation of the XBeach model, the generated output is compared to an observed profile to determine the performance of the model. This performance is analysed both visually and quantitatively. To quantitatively determine the performance of the morphodynamic predictions two single-number metrics are used.

Following Bosboom, Reniers, and Luijendijk (2014) the method used to quantify the performance of the morphodynamic simulation is by obtaining both the accuracy and the skill of the data. The accuracy of the data is given by the root-mean-square error (RMSE), defined in equation 2.3:

$$RMSE = \sqrt{\sum (z_p - z_m)^2} \tag{2.3}$$

where z_p is the predicted profile, and z_m is the measured profile. A common method to quantify the skill, or relative accuracy, of morphodynamic simulations, is the means-square error skill score (MSESS) (also known as Brier skill score or BSS). The relative accuracy of a morphological prediction is compared to a baseline prediction using the mean square error (MSE) (Bosboom et al., 2014). This MSE based skill score is expressed by equation 2.4 (Murphy, 1988):

$$MSESS = 1 - \frac{MSE(p,m)}{MSE(i,m)} = 1 - \frac{\sum(|z_p - z_m|)^2}{\sum(|z_i - z_m|)^2} \tag{2.4}$$

where z_i is the initial profile. The MSESS is a value between 0 and 1, where a value of 1 represents a perfect agreement of the model prediction with observed data. Table 2.1 shows the classification of MSESS values proposed by (Van Rijn et al., 2003). The accuracy and skill values are calculated using

Table 2.1: Classification of Mean Square Error Skill Score (MSESS) values (Van Rijn et al., 2003).

Qualification	Score
Bad	< 0
Poor	$0 - 0.3$
Reasonable/fair	$0.3 - 0.6$
Good	$0.6 - 0.8$
Excellent	$0.8 - 1.0$

only the data between MLW and the dune foot of the initial beach profile. This reflects the focus of this study on the beach width, as the beach width is by definition between MLW and the dune foot (see section 2.1).

3

Research Methodology

The research objective of this study, as stated in section 1.3, is ”to develop an uncertainty assessment tool for beach width predictions by carrying out a beach width prediction within a stochastic framework at a recently nourished beach”. The method whereby this research objective is fulfilled is described in this chapter.

To successfully carry out this research objective, a case study is made where a stochastic beach width prediction is made for the location of the Hondsbossche Dunes. At the Hondsbossche Dunes, an artificial dune area in North Holland, an additional nourishment took place in March 2018. A brief introduction to this case study location is given in section 3.1. The process of carrying out a stochastic

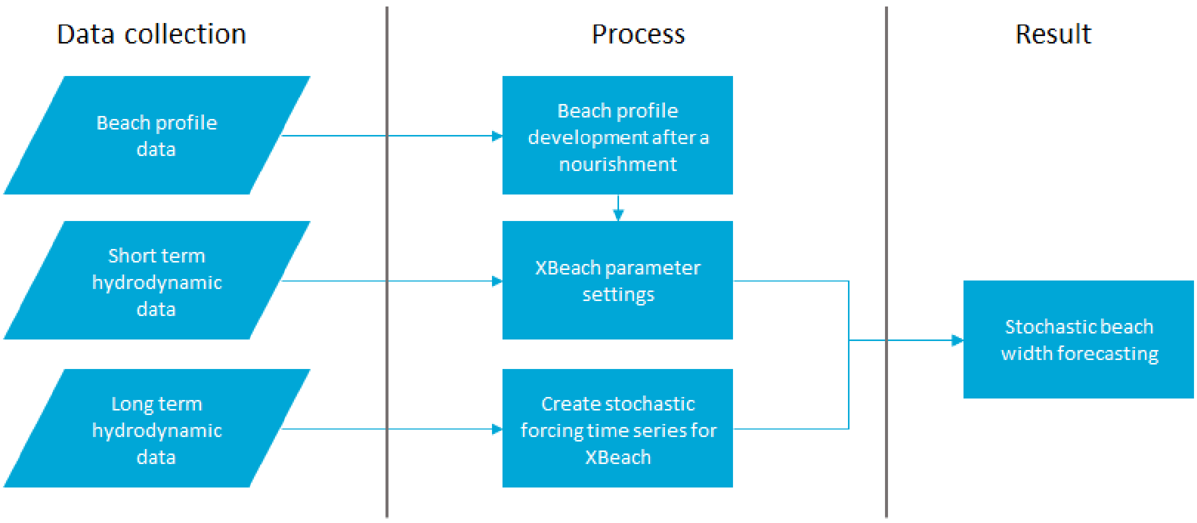

Figure 3.1: Flow chart of the research methodology. The flow chart shows the steps in the process for a stochastic beach width forecast with XBeach.

XBeach forecast for the Hondsbossche Dunes is divided into several steps (figure 3.1). First, the required data are gathered. These data consist of periodic beach profile data, short therm hydrodynamic data, and long term hydrodynamic data. The method whereby these data are collected is described in section 3.2. The beach profile data are analysed to answer the first sub-question: ”What is the development of beach profiles at a recently nourished beach?”. Insight in the development of a beach profile after a nourishment is required to set up the parameters for an XBeach model. The method of this analysis is given in section 3.2.1. The next step is to determine XBeach parameter settings to answer the sub-question: ”What are appropriate XBeach model settings to model the development of a recently nourished beach?". The method whereby the XBeach model settings are determined is given in section 3.3. The next step is to create stochastic forcing time series for XBeach. The method for the creation of stochastic forcing time series is given in section 3.4. With this the sub-question "How are stochastic forcing conditions generated for the study location?" is answered. The final sub-question to be answered is: "What are the probability ranges of the expected beach width development for the study location?". This question is answered by applying the stochastic forcing conditions to the calibrated XBeach model. The method for this is described in section 3.4.6.

3.1. Case study

The location used for the case study is the Hondsbossche Dunes, an artificial dune area at the Dutch coast. To give context to the project location, the area of interest where the addition nourishment took place in March 2018 is described in this section.

3.1.1. History Hondsbossche Dunes

In the middle ages the coastline of North-Holland consisted of a beach-dune area. The coastal area nearby Petten, where nowadays the Hondsbossche Dunes are, was located in this beach-dune region. In this part of the coast, structural erosion made the coastline shift landwards. This erosion was mainly caused by the sediment-import capacity of the neighbouring tidal inlet of the Wadden Sea. To counteract the retreat of the coastline groynes and seawalls were constructed. This resulted in the Hondsbossche and Pettemer Sea defence (figure 3.2a). During the reassessment of the safety of the Dutch coast in 2003, some parts of the Dutch coast, which did not comply with the safety standards were appointed "weak links". The Hondsbossche and Pettemer sea defence was one of these weak links, hence had to be reinforced. The design of the improvement of the Hondsbossche en Pettemer sea defence had the two main requirements: 1) Improve coastal safety to be able to withstand the revised 1/10 000 hydraulic boundary condition for the next 50 years, and 2) maintain, and where possible, improve environmental quality. This resulted in a multi-functional beach-dune area in front of the old seawall providing safety against flooding, room for nature development, and providing recreational areas. These became the Hondsbossche Dunes (figure 3.2b).

(a)

(b)

Figure 3.2: Situation before and after nourishment in 2015. In (**??**) the Hondsbossche en Pettemer Zeewering is shown before the nourishment and in figure (b) the Hondsbossche dunes are shown after the nourishment.

3.1.2. Hondsbossche Dunes

The construction of the Hondsbossche Dunes started in 2014 and was completed in March 2015. The new dune-beach area is constructed with a total volume of 35.6 million m^3 sediment. The nourishment is divided in three zones: Recreation zone North, Nature zone, and Recreation zone South (figure 3.3). The construction of the Hondsbossche Dunes tender contract also included a maintenance obligation of 20 years. Among the maintenance obligations, maintaining a sufficient beach width and a sufficient beach volume, are the most relevant for this study. The beach width and volume are maintained by sand nourishments. The expected nourishments are: (1) for the nature zone 1.5 million m^3 in 2026 and (2) for the recreation zones 1.6 million m^3 and 1.1 million m^3 in 2023 and 2030 respectively (de Jongh, 2017). However, if the beach width, or the beach volume, decreases faster than expected, additional nourishments have to be applied to guaranty the minimum required beach width.

Figure 3.3: Area of interest, adapted from The Netherlands Space Office Satellietdataportaal (2018)

At the recreational zone South, a beach width of minimally 50 meter has to be maintained according to the maintenance contract. The location where the minimal beach width of 50 meter is mainly an issue, is at the location of beach pavilion "Luctor et Emergo" (figure 3.4). When the beach width decreases further than 50 meters at that location the stability and accessibility of the beach pavilion are at stake. As the beach width is the main issue here, this research is focused on this region.

3.1.3. Additional nourishment in 2018

In March 2018 an extra nourishment had to be applied to ensure the minimal beach width of 50 meters. This additional nourishment was required earlier than expected. The additional nourishment is applied on the coastal region near "Camperduin" with a length of $1.400m$. At the location of beach pavilion "Luctor et Emergo" the beach width before the additional nourishment was approximately $100m$, after the nourishment this beach width was increased to $230m$. The additional nourishment contained 0.85 million m^3 of nourished sediment. With satellite images, the differences between the situation before, and after the nourishment can be observed (figure 3.4a, and figure 3.4b). Recent nourishments tend to be highly dynamic in the months after completion, as the coastal profile is out of equilibrium. This is convenient for this research, as within a relatively small period large differences can be expected in the coastal profile.

3.2. Methods for data collection

For this study, three main data sets are used, beach profile data, long term hydrodynamic data, and short term hydrodynamic data.

(a)

(b)

Figure 3.4: Situation before and after the additional nourishment of April 2018 (The Netherlands Space Office Satellietdataportaal, 2018). In (a) the satellite image of the study location from $06-07-2017$, before the additional nourishment. In (b) the satellite image of the same location at $07-04-2018$, after the additional nourishment.

The beach profile data are used to determine the behaviour of the beach profile after the additional nourishment. This information is used to compare the behaviour of the XBeach model with the local conditions at the Hondsbossche Dunes. Beach profile data are collected during the first four months after the nourishment in March 2018. The method whereby the beach profile data are collected is described in section 3.2.1.

For generating stochastic wave time series, long term hydrodynamic data are used. The period of these long term hydrodynamic data is from 1990 to 2017. The method to collect these data is given in section 3.2.2.

For the calibration of the XBeach model, local hydrodynamic forcing conditions are used. These local hydrodynamic forcing conditions are from the same four months as those of the beach profile survey data. These data are therefore considered as short term data. The short term hydrodynamic data collection is described in section 3.2.3.

3.2.1. Beach profile survey

To analyse the beach profile development after nourishment, a beach profile survey is performed. With the beach profile survey, the morphological development of the beach after the nourishment is analysed. With this survey, an answer can be given to the first research question: "What is the dynamic development of a recently nourished beach?".

Field measurements are executed periodically by walking with an RTK GPS mounted on a walking wheel (figure 3.5). In these measurements, the position of the GPS antenna is measured on centimetre-level accuracy. This accuracy is sufficient for beach profile measurements. With the fieldwork, the total project area is mapped in sections from the dune foot to the shoreline. At the focus area close to beach pavilion "Luctor et Emergo" every 50 meters a profile is measured. To the north and the south of this area of interest, the sections lie 100 meters apart. An example of a field measurement is shown in figure 3.6 where all data points are indicated by the red dots. The beach profile survey is always carried out around the time where the tide reaches low water, as then the largest part of the beach can be measured with a walking wheel. During the summer period, eight beach profile surveys were conducted (figure 3.10). The collected data consist of x, y, and z coordinates. These coordinates

Figure 3.5: Fieldwork in progress

are transformed into a grid by linear interpolation. This results in an elevation map for each survey (appendix B.1). Erosion and accretion is analysed by subtracting the elevation map of the first survey from the successive surveys (appendix B.2).

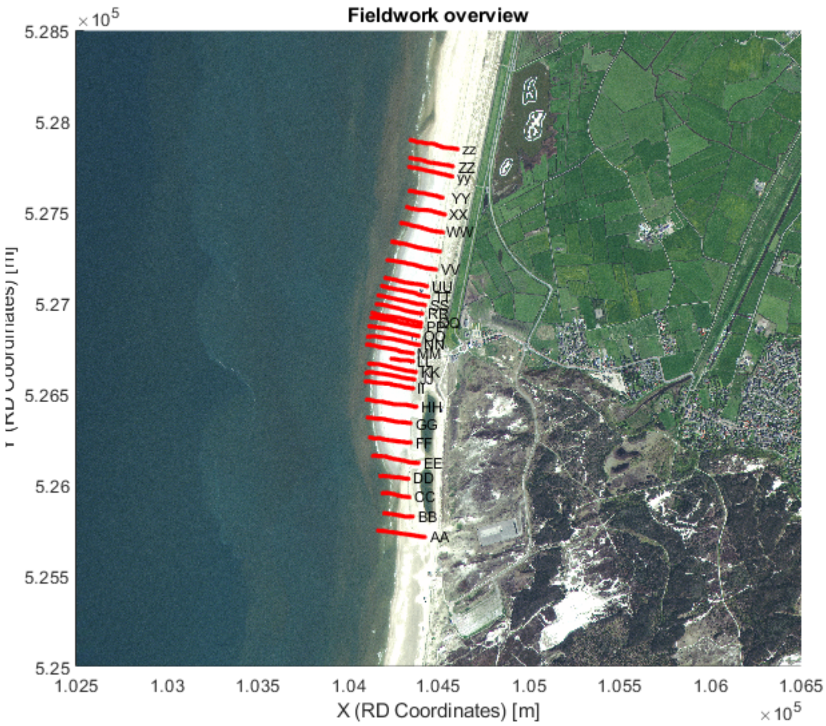

Figure 3.6: Fieldwork overview with each individual data point indicated by a red dot.

Besides field measurements, optical satellite imagery is used to analyse the development of the shape of the coastline. These satellite images are retrieved from The Netherlands Space Office Satellietdataportaal (2018) and analysed with ArcGIS. Satellite images from the before the additional nourishment (June 2017) until one year after the additional nourishment (April 2019).

Both local beach profile survey and the optical satellite imagery are used to analyse the development of the nourishment at the Hondsbossche Dunes in chapter 4.

3.2.2. Long term hydrodynamic data

To generate synthetic time series the local wave data have to be characterised based on wave time series of a sufficiently long period (e.g. 10 to 30 years). Such a data set is not available for the location of the Hondsbossche Dunes. As a sufficiently long time series of wave data is available for offshore locations, common practice is to transform the hind-cast data to the near-shore data using spectral wave models such as SWAN. To minimise calculation time, the wave look-up table developed by (Fockert & Luijendijk, 2010) is used to obtain local wave conditions.

Wave look-up table

The purpose of the wave look-up table is to transform wave time series of three offshore wave rider stations to an arbitrary location near-shore. The wave rider stations this wave lookup table is based on are: IJmuiden Munitiestortplaats (YM6), Eierlandsegat (ELD) and Europlatform (EUR) (figure 3.7. Fockert

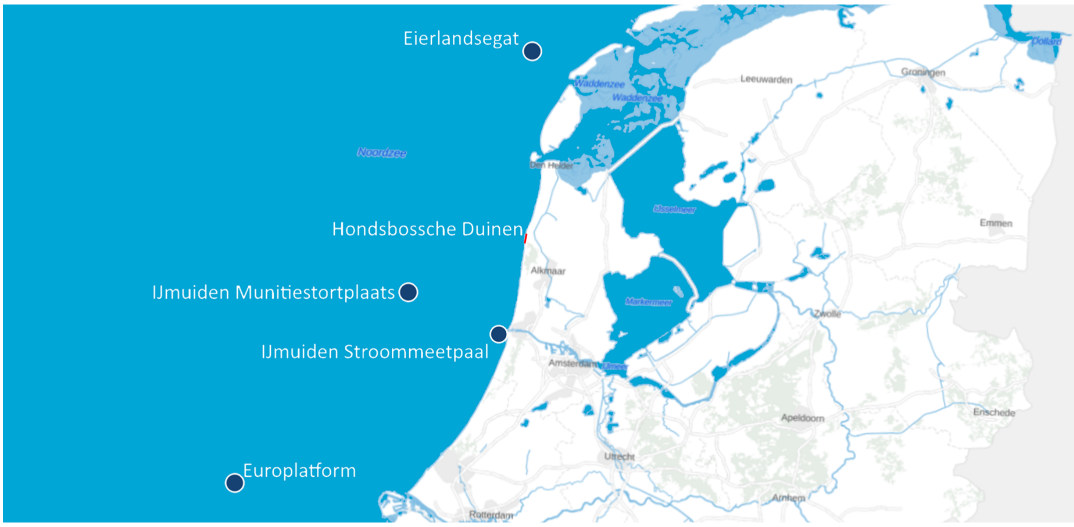

Figure 3.7: Overview of the measurement locations. The offshore wave stations at Europlatform, IJmuiden Munitiestortplaats, and Eierlandsegat are depicted in blue. The wave level data are gathered at IJmuiden Stroommeetpaal, and the study location is at the Hondsbossche Dunes, indicated in red.

and Luijendijk (2010) developed a wave transformation matrix by a set of 269 stationary SWAN calculations whereby the relationship between offshore and nearshore wave parameters are specified. The parameters used from these wave ride stations are the significant wave height (H_{m0}), the mean zero-crossing period (T_{m02}), and the main wave direction (Th0). In the transformed nearshore wave time series the mean zero-crossing period is translated to the peak period (T_p). So the resulting nearshore time series contain the parameters H_{m0}, T_p, and T_{h0}.

Water level

Local water level data can not be transformed with the use of the transformation table, but are important input parameters for XBeach. The water level consists of an astronomical tidal term and a surge term. Local astronomical tidal data are available at the study location of the Hondsbossche Duinen. However, this does not take surge into account. The nearest station where both the astronomical and the surge component of the water level are available is at IJmuiden Stroommeetpaal (SPY). This is approximately 30 kilometres away from the project area. The position of the coast of IJmuiden is similar to the position of the Hondsbossche Duinen. Therefore the surge is comparable for both locations. The astronomical tide differs approximately 30 minutes between these two locations. The time step of the water level observations is 60 minutes, so the 30-minute difference considered to be minor.

Data coverage

The hydrodynamic data are derived from DONAR data (`http://waterinfo.rws.nl`). This data set contains some data gaps, which is undesirable for the generation of synthetic wave time series. Therefore periods with stable data coverage are selected from these data sets. The data at YM6, ELD, and EUR have a relatively stable coverage with hourly data from 1990. Therefore the parameters H_{m0}, T_{m02}, and T_{h0} are used from 1990. The DONAR data end in November 2017. For the implementation of seasonal differences, years with large amounts of missing data are removed, so the used wave data are from January 1990 to January 2017. The data from SPY start in January 2012 and end in 2017. A total overview of all available hydrodynamic data is given in figure 3.8. The hours where data is available are indicated in blue, and the missing data are indicated in orange. The period of the data used is given by the black dashed line. A summary of the data coverage is given in table 3.1.

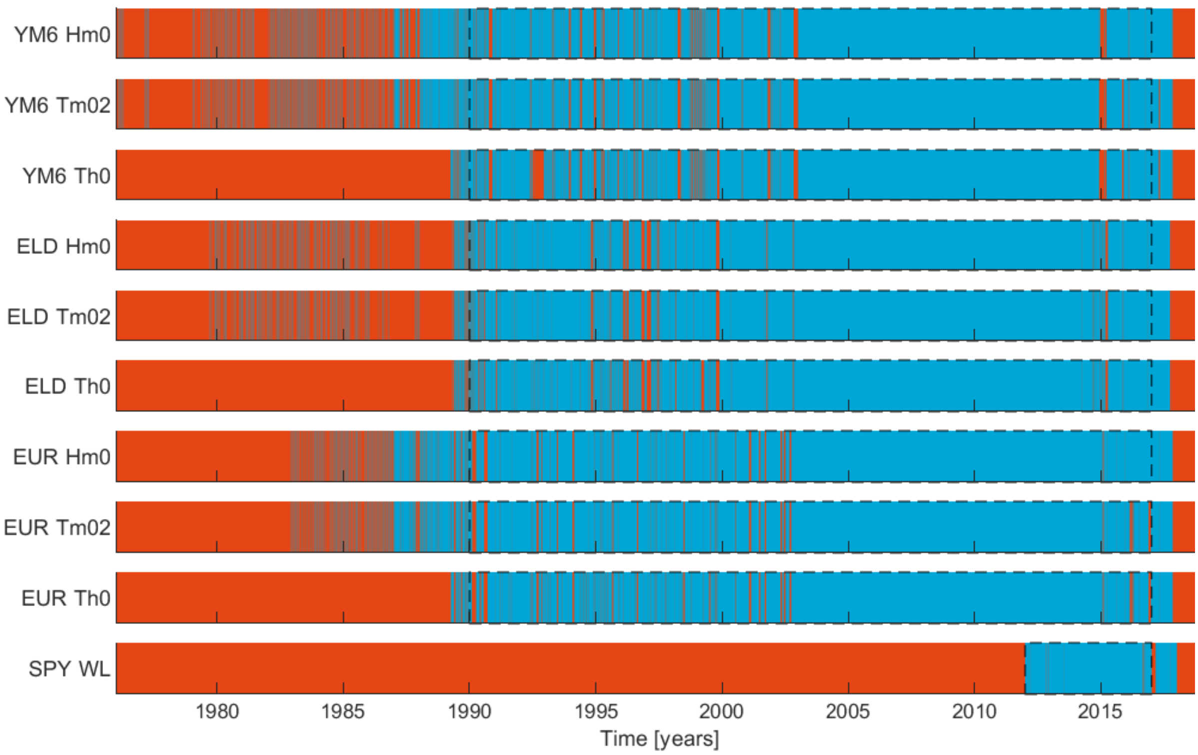

Figure 3.8: Timeline of the available data of long term hydrodynamic conditions. The blue areas indicates that data are available and missing data are given with orange areas. The dashed line surrounds the data period that is used in this study.

3.2.3. Short term hydrodynamic data

Besides the beach profile data after the nourishment, hydrodynamic forcing conditions are also required for the calibration and the validation of the XBeach model. For calibrating the XBeach parameter settings, the results of the XBeach model are compared to local beach measurements. Essential in this calibration is that the used hydrodynamic conditions are accurate and available for the whole calibration period. Local hydrodynamic conditions can be provided by a wave buoy, placed approximately 800 meters offshore to the project area, or by transformation of offshore wave data to the nearshore data, similar to the long term wave data (section 3.2.2). The data coverage is examined for both the transformed wave data from the transformation matrix and the local wave buoy (figure 3.10). From both these methods hourly observations of the wave heights, wave periods, and wave directions are obtained. The transformed time series show many short periods with missing values. These missing

Table 3.1: Available long term hydrodynamic data with the data coverage.

Location	x, y coordinates [m; RD]	Parameter	Used data	Missing values	Data coverage
YM6	64779, 507673	Hm0	01/01/1990 - 01/01/2017	18332	92%
YM6	64779, 507673	Tm02	01/01/1990 - 01/01/2017	19299	92%
YM6	64779, 507673	Th0	01/01/1990 - 01/01/2017	25315	89%
ELD	106514, 587985	Hm0	01/01/1990 - 01/01/2017	12914	95%
ELD	106514, 587985	Tm02	01/01/1990 - 01/01/2017	12915	95%
ELD	106514, 587985	Th0	01/01/1990 - 01/01/2017	16037	93%
EUR	10056, 447687	Hm0	01/01/1990 - 01/01/2017	11651	95%
EUR	10056, 447687	Tm02	01/01/1990 - 01/01/2017	13612	94%
EUR	10056, 447687	Th0	01/01/1990 - 01/01/2017	17777	92%
SPY	95902, 497709	WL	01/01/2012 - 01/01/2017	625	99%

values occur when the wave direction is offshore, i.e. between $30°$ and $200°$. For offshore directed wave conditions the waves from the offshore wave stations can not be transformed to the nearshore. During offshore directed wave conditions the nearshore waves are low and have little influence on the beach profile. For this reason, the missing values are neglected as they do not influence the measurement data in this study.

The time series collected by the local wave buoy shows a more continuous signal with some large data gaps. The wave buoy was placed on June 7, 2018. Between June 15, 2018, and June 25, 2018, as well as between July 17, 2018, and July 27, 2018, the buoy was caught in a fishing net. Due to the large areas with missing values in the buoy measurements, for this study, it is more convenient to use the transformed data as input. The accuracy of the wave data at the offshore boundary generated by the transformation table is reviewed by analysing the differences between data from the local wave buoy and the data from the transformation table in appendix A. When comparing the time series of the significant wave heights, the transformed data appear to match the buoy data reasonably well, with $R^2 = 0.85$ (figure A.1. The differences between the wave buoy data and the transformed data are occasionally larger than 1 m. The standard deviation of the differences is 0.23 m.

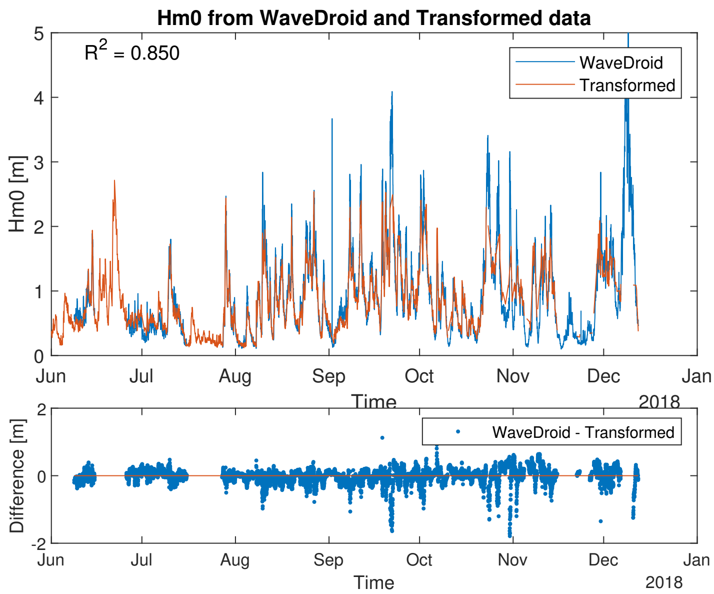

Figure 3.9: On the top the comparison between the significant wave height of the wave buoy and wave transformation table. In blue the wave buoy data and in red the transformed data. Below the differences between the wave buoy data and the transformed data.

With a density scatter plot the correlation between the transformed significant wave height and the significant wave height of the wave buoy is derived, resulting in a correlation factor of 0.922 (see Appendix A, figure A.2). Note that the R^2 in figure A.1 corresponds to the squared correlation factor in figure A.2. For the peak period, the correlation factor is only 0.54 (see Appendix A, figure A.3). The wave direction gives a correlation factor of 0.74 (see Appendix A, figure A.4).

For the significant wave height and the wave direction, the similarity between the transformed waves and the waves measured by the wave buoy is high. The correlation factor for the wave peak period performs not as good. A possible reason for the differences between the transformed wave peak periods and the wave peak periods from the wave buoy is that the wave buoy was situated relatively close to the shore, at a distance of approximately 700 m from the shoreline. At this location the tidal streaming is relatively strong, causing disturbances in the data, especially in the peak parameters. To minimise this effect, the buoy data are filtered. Despite the filtering, the difference in peak periods between the transformed data and the buoy data remains relatively large. Another explanation can be that the performance of the transformation table for wave periods is relatively poor. The performance of the SWAN model is often worse for the wave period than for the wave height. In Fockert and Luijendijk (2010) the transformation table is also validated against local measurements near Petten. This validation showed for the significant wave height and wave direction correlation factors above 0.92. For the wave peak period, a correlation factor of less than 0.60 is found (Fockert & Luijendijk, 2010). This also shows a poor performance of the wave periods in the SWAN model compared to the wave heights.

The performance of the transformed data for the significant wave height and wave direction is approved. For the peak wave period, the difference between the transformed data and the wave buoy data is significant. Despite the difference in the peak wave period, the transformed data are used for the calibration of XBeach. The buoy data are not used as short term hydrodynamic data because of the large data gaps in the buoy data (figure 3.10). The possibly inaccurate wave period for the transformed data has to be kept in mind.

Water level data

For the observed hydrodynamic conditions, the wave level data are derived from IJmuiden Stroommeetpaal (SPY) similar to the long the hydrodynamic data (section 3.2.2).

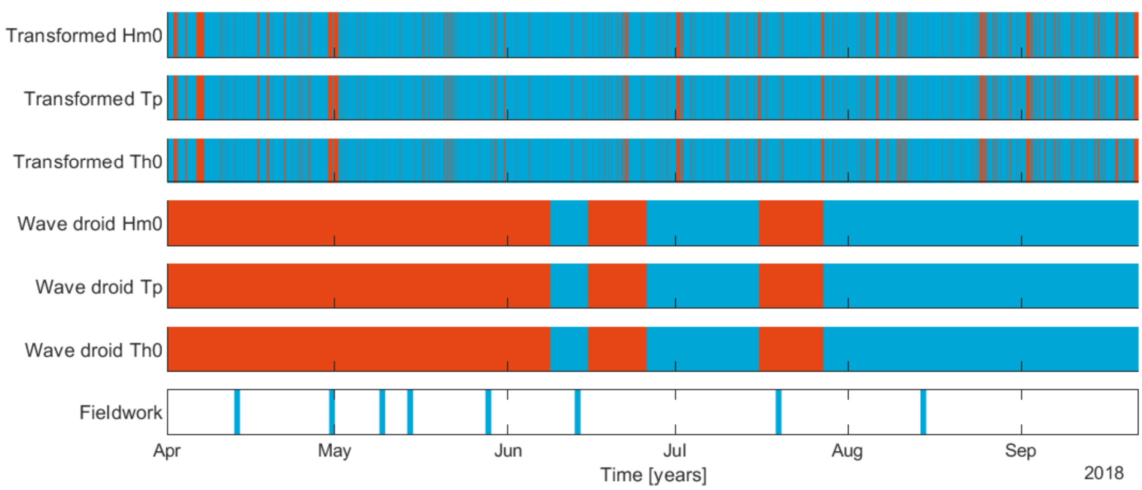

Figure 3.10: Timeline of the short term hydrodynamic data from April 2018 to September 2018. The blue area indicates collected nearshore data, orange areas indicate missing data. For the transformed data, the missing values indicate offshore directed wave conditions with small significant wave heights. For the wave buoy data, the missing values are due to the displacement of the buoy.

3.3. XBeach modelling

Before the stochastic data are used as input for XBeach, first the model settings are determined. The model settings are calibrated based on observed beach profile measurements. This is done with the short term observed hydrodynamic data as input for XBeach. The resulting beach profile from XBeach is compared to the observed beach profiles from the survey in the calibration period (figure 3.11). After the XBeach model is calibrated, the performance is checked by validating the XBeach model with the data from the validation period (figure 3.11).

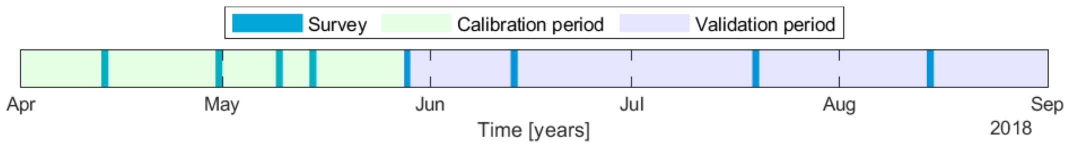

Figure 3.11: Timeline of the beach surveys. The calibration period is shaded in green and the validation period is given by a blue shade.

3.3.1. Model Settings

To successfully carry out an XBeach forecast, the XBeach model settings have to be set. The settings in the XBeach model have to meet two requirements. On the one hand, the model is aimed to accurately replicate the reality, and on the other hand, the model has to be efficient with a limited computation time. The computation time is limited by optimising the following parameters.

- MorFac: Morphological acceleration factor
- Wave Threshold: Neglect waves below a certain threshold
- Grid size: Increasing the grid size decreases the number of grid cells, decreases the number of calculations in XBeach.

In section 5.1 this is explained in detail and the results are presented. Calibrating the model performance based on accuracy is done by calibrating the following parameters:

- Facua: Calibration factor for wave asymmetry and wave skewness
- LsGrad: Longshore transport gradient

The performance of the model settings is quantified by the determination of the root-mean-square error and the mean-square error skill score. When optimising the model settings for a limited computation time, the performance of the model settings is compared to a base case where the computation time is not limited. For the model settings where the accuracy is optimised, the model settings performance is compared to the observed beach profile from the survey data.

After optimising these model settings, the XBeach model is considered fast and accurate enough. There are more important calibration settings that can be optimised, but for these parameters, the default settings suffice.

3.3.2. Validation

The XBeach model settings are validated using the data of the validation period. For this validation, the XBeach model for the calibration period is extended to the validation period. The resulting beach widths from the XBeach model are compared to the observed beach widths in the validation period.

3.4. Simulate stochastic forcing conditions

To obtain a stochastic result from the XBeach model, stochastic forcing conditions are generated. These stochastic forcing conditions consist of a range of wave time series, based on the long term hydrodynamic conditions of the three offshore wave platforms at IJmuiden Munitiestortplaats, Europlatform, and Eierlandsegat. Creating these stochastic wave time series requires several modelling steps (figure 3.12).

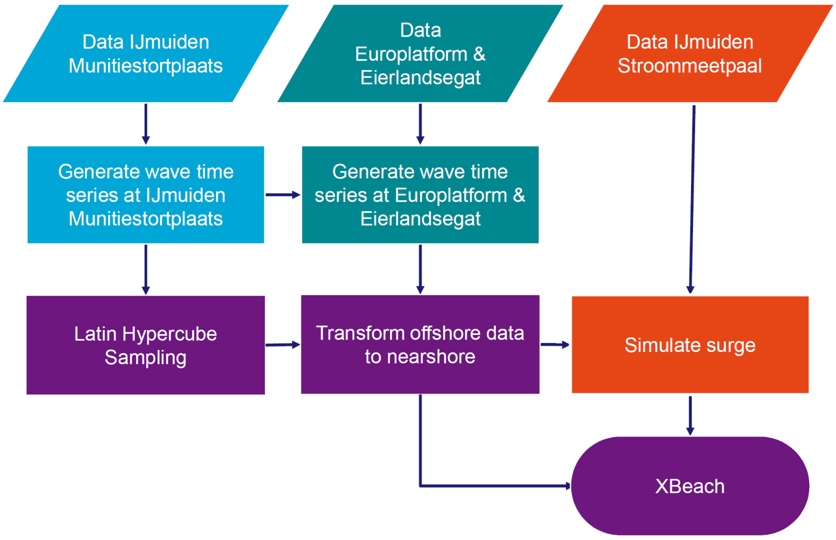

Figure 3.12: Flow chart containing the modelling steps for generating the stochastic forcing conditions.

First, a wave time series for the location of IJmuiden Munitiestortplaats is created based on the long term wave data of this location. A set of 5000 wave time series of one year is generated. Then wave time series at Europlatform and Eierlandsegat are generated based on the differences between the waves at these two stations and the waves at IJmuiden Munitiestortplaats.

To limit the computation time, the sample size is decreased from 5000 to 40. Latin Hypercube sampling is used as sampling method to maintain a good representation of the variability. These samples are selected based on the total wave energy in long- and cross-shore direction at IJmuiden Munitiestortplaats.

The sampled wave time series of all three stations are transformed from offshore time series to the nearshore location of the Hondsbossche Dunes. Synthetic water level data is added by a model for the surge at IJmuiden Stroommeetpaal. Note that this model for the surge is based on the nearshore wave data at the Hondsbossche Dunes, and the nearshore water level data at IJmuiden Stroommeetpaal. Combining the data results in stochastic time series for the hydrodynamic forcing conditions for XBeach. In this section, the method for each modelling step is explained. In chapter 6 generating the time series is described in more detail together with the results.

Considering the structure of the modelling steps, it seems to be more efficient to first transfer the observed data from offshore to the nearshore, and to use this transformed time series as the basis for the synthetic wave time series. This reversed modelling structure was used in earlier stages of this study. However, this resulted in a persistent underestimation of the total wave energy. A likely reason for this inaccuracy is that in the process of transforming the offshore data to nearshore, offshore directed wave heights are assumed to be zero and treated as data gaps. The transformed wave time series contain considerable more missing data than the original offshore data. Therefore a choice was made to turn around the modelling process, and first create synthetic data based on the offshore time series, and thereafter transform the offshore data to the nearshore. The drawback of this method is that this requires stochastic wave time series of all three wave stations.

3.4.1. Simulate time series for IJmuiden Munitiestortplaats

Simulation of the time series at IJmuiden Munitiestortplaats is done using an autoregressive-moving-average (ARMA) model. Following the method used by Jäger (2018), additional transformations are applied besides the ARMA model to account for complex dependencies.

For simulating time series of the significant wave height, the mean zero-crossing period, and the wave direction for IJmuiden Munitiestorplaats, the observed wave time series are first analysed and decoupled with the following steps:

1. *Limiting wave steepness condition:* The first step is to set a wave steepness limit condition. The steepness limit is introduced to account for the dependency between the wave steepness and the wave height. A deterministic part of the relationship between the mean zero-crossing period and the significant wave height is separated from the stochastic part. At the end of the wave modelling steps, the deterministic part of the wave steepness is combined with the generated stochastic part. If this step is ignored, the dependency between the significant wave height and the mean zero-crossing period is not simulated correctly and too steep waves can occur in the synthetic data.
2. *Normalisation:* The time series of the significant wave height and the stochastic part of the wave period are normalised, which means that they are transformed to time series with a mean of zero and a standard deviation of one. This modelling step is convenient because it removes the wave skewness and strictly positive behaviour of the time series. Furthermore, an ARMA process, used in a later modelling step, can only be applied to data with a zero mean and constant standard deviation.
3. *Reduction to directional regime time series:* Significant wave heights and mean zero-crossing periods are related to the wave direction. To include the dependency of the wave height and the mean zero-crossing period of the wave direction, the wave directions are simplified to two directional regimes. The observed wave directions mainly originate from either northwest (NW) or southwest (SW) direction. The duration of the observed directional regimes are analysed per season.
4. *Seasonal model for regime switches:* To model the directional regimes, the duration of the observed directions is modelled as an altering binary renewal process. This model is based on the duration of the directional regimes. A distinct model is made for every astronomical season.
5. *Select wave direction per switch:* For each simulated directional regime switch, a direction angle is sampled randomly to create a directional time series with all possible directions. During a directional regime, the sampled wave direction is constant.
6. *Decomposition into stationary and non-stationary components:* Time series of the significant wave height and the mean zero crossing-period contain seasonal behaviour, which are also transformed to the normalised processes Y^{Hm0} and Y^{Tm02}. To incorporate this behaviour in the synthetic data, the data are de-seasonalised and the seasonal components and stationary components are modelled separately. The same approach as (Jäger, 2018) is used to depersonalise the data whereby the non-stationary components are extracted using a sliding window kernel.
7. *Model for stationary components:* The high-frequency stationary component is described by an autoregressive moving-average (ARMA) process. First adequate orders of p and q are estimated for northwestern and southwestern waves. Their orders of p and q are used to model the stationary components of the time series.
8. *Model for non-stationary components:* The non-stationary components of the time series are modelled using Fourier series. For each observed year, a Fourier series is fitted to the non-stationary component. For the synthetic data, terms for Fourier series are generated based on the distributions and correlations of the observed Fourier terms. This results in realistic synthetic time series for the non-stationary components.

9. *Simulate wave time series at IJmuiden Munitiestortplaats:* The last step in creating synthetic time series for the significant wave height and the mean zero-crossing period is to combine the previous steps to create wave data. 5000 wave time series of one year are created for the stationary and non-stationary components of the significant wave height and the mean zero-crossing period based on the models estimated in step 4 and 5. Combining these time series results in synthetic normalised time series of the significant wave height and the mean zero-crossing period. This normalisation is reversed and the deterministic part of the mean zero-crossing period is added to the time series to create synthetic wave time series of the significant wave height and the zero-crossing period.

3.4.2. Simulate time series Eierlandsegat and Europlatform

After creating synthetic wave time series at IJmuiden Munitiestortplaats (IJM), the wave time series are extended to the locations of Europlatform (EUR) and Eierlandsegat (EIE). The time series of EIE and EUR are created by modelling the differences between these stations and the time series at IJM. This method is relatively simple as the wave time series of EIE and EUR are not examined in detail. By modelling the differences between the stations, correlations between these stations are taken into account. Potential inaccuracies due to this simplification are small because in the process of the wave transformation to the nearshore, the data from IJM is dominant and the data from EIE and EUR only have little influence due to their distance and the angle to the coastline of the Hondsbossche Dunes (Fockert & Luijendijk, 2010). The modelling step taken to create synthetic time series for EIE and EUR are the following:

1. *Limited steepness condition:* For the data at EIE and EUR, the same steepness condition is taken into account as at IJM. This is to prevent the simulation of too steep waves. At EIE and EUR, the same steepness limit as for IJM is used.

2. *Normalisation:* Similar to the data at IJM, the Hm0 and Tm02 are normalised. This is to reduce the skewness and to remove the property that the data are strictly positive. When this step would be ignored, the resulting data contain negative values and the skewness is not modelled properly.

3. *Model for differences:* The differences between the stations are modelled by analysing the differences between the wave directions, the normalised wave heights and the normalised wave periods between the data from IJM and EUR and IJM and EIE. Synthetic time series of these differences are created by estimating an ARMA model for each of these time series.

4. *Simulate time series EIE & EIM:* With the synthetic time series of Hm0, Tm02, and Th0 in IJM, together with the model for the differences of these parameters with the parameters in EIE and EUR, the synthetic time series for EIE and EUR are created.

3.4.3. Simulate surge

Besides time series of the local wave data, time series of the local water levels are also required as input for XBeach. Water level consists of two parts namely an astronomical component and a hydrodynamic component. Accurate predictions are available for the astronomical tide. When subtracting the astronomical tide from the water level, the tidal residual or surge remains (Sterl, Brink, Vries, Haarsma, & Meijgaard, 2009). An attempt was made to only use the astronomical component of the water level, but the influence of the surge appears to be significant. The surge is mainly dependent on the wind speed and wind direction. An extensive analysis of the behaviour of the surge and a detailed model similar to the model of the waves would be optimal. However, as this is not feasible within the period of this study. A model is created to obtain a time series for the surge, based on the correlation between the surge and the wave height. Modelling the surge contains the following steps:

1. *Average surge per wave height:* The correlation between the observed surge and observed wave height is subtracted from the surge. A function of this relationship is determined by a linear regression. The remaining signal can be simulated without considering the correlation between the surge and the wave heights because this relation is added again after the simulation.

2. *Model for surge:* After removing the linear regression between the surge and the wave height, a hydro-meteorological time series remains, which is suited to be simulated by an autoregressive–moving-average (ARMA) model. The orders and terms of a suitable ARMA model are estimated for the remaining surge time series.

3. *Simulate surge:* With the ARMA model, synthetic data is created for the surge. The average surge per wave height is added to this time series using the previously generated synthetic time series of the significant wave heights. For the input of XBeach, the surge is added to the astronomical component. The astronomical tidal data for the year 2019 is derived from waterinfo.rws.nl (Rijkswaterstaat, n.d.).

3.4.4. Latin Hypercube sampling

The simulated data consist of 5000 time series of one year with hourly values of the significant wave heights, mean zero-crossing periods, and main wave directions. The number of 5000 time series is considered large enough to take into account the occurrence of forcing conditions which result in extreme large, or small beach width differences. Simulating all these time series with XBeach is unfeasible, so Latin Hypercube sampling is used to save computation time. Furthermore, the transformation 5000 wave time series of one year from offshore to the nearshore would, even with a wave transformation matrix, take a significant amount of time. Therefore Latin Hypercube sampling takes place before the transformation to the near-shore and is based on the synthetic time series at IJmuiden Munitiestortplaats.

The sampling is used to select a small amount of time series which show a similar results as all 5000 time series. The change in coastal profile is strongly dependent on the wave energy reaching the coast. Therefore, the wave time series are sampled with the total cross- and longshore wave energy for one year as variables. This assumes that there exists a strong correlation between the total wave energy in cross- and longshore direction and the beach width development. So two wave times series with a similar total wave energy in cross- and longshore direction, result in approximately the same coastal profile change. This assumption is checked in section 8.2.

As explained in section 2.5 a drawback of Latin Hypercube sampling is that when increasing the sample size, the former samples have to be taken into account. In this study, the correct sample size is determined by starting with a sample size of 5, then doubling this sample size to 10. When the distribution of the resulting beach widths from the XBeach model does not significantly differ for a sample size of 5 or 10, the number of samples is considered sufficient. When the distribution of the beach width does differ, the sample size is increased to 20. This process is repeated until the sample size is large enough.

3.4.5. Transform offshore data to nearshore

The same wave lookup table developed by Deltares as was used for the short term hydrodynamic data is used to transform the synthetic data to the nearshore (Fockert & Luijendijk, 2010). The generated wave time series of IJM, EIE, and EUR are transformed to the nearshore location at the Hondsbossche Duinen. This results in one wave time series containing the significant wave height, the peak wave period (Tp) and the wave direction. When the waves are directed offshore (between 30° and 200°) no transformation to the nearshore takes place. This leaves gaps in the data. With offshore directed waves at the offshore stations, the waves at the nearshore are assumed to be low and of little influence on the beach profile. Therefore these gaps in the data are skipped in the model, and the beach profile is considered to be constant during offshore wave directions.

3.4.6. XBeach model with synthetic data

After the XBeach model is calibrated, the stochastic forecast can be made by using the sampled time series as input. This results in a range of possible beach profile developments of time. From these beach profiles, the evolution of the beach width is calculated. This range of possible beach widths can be summarised in a fan chart. From this fan chart, the probability of occurrence of a certain beach width decrease can be determined. These probability ranges of the possible beach width development are the main result of the case study.

Validation of stochastic prediction

The resulting beach widths are validated using the observations in the validation period. For this validation, the beach width difference per day of the synthetic results are analysed with the beach width difference per day of the survey data.

4

Beach profile development after a Nourishment

To successfully carry out a stochastic beach width forecast at a recently nourished beach, the first step is to analyse the actual development of a recently nourished beach. This section answers the sub-question ”What is the development of beach profiles at a recently nourished beach?”.

The 0.85 million m^3 of additional nourished sediments creates a seaward perturbation in the coastline (figure 4.1a). Irregularities in an otherwise straight sandy shoreline, are usually smoothed by along-shore sediment transport (Ashton & Murray, 2006). Nourishments tend to diffuse over time following a flattening bell-shaped curve (Dean, 2003).

At a location further south on the Dutch coast, the Sand Engine is constructed in 2011. This is a mega-nourishment, which also creates a seaward perturbation in the shoreline. The Sand Engine shows a decrease in cross-shore extent and a large longshore increase in lateral dispersion to both sides (de Schipper et al., 2016). Albeit on a smaller scale, a similar response was expected at the nourishment at the Hondsbossche Dunes, with a decrease in cross-shore extent and a longshore increase.

The development of the beach after the nourishment is analysed by field measurements (section 3.2.1). With these measurements the elevation of the beach and shoreline is mapped (figure 4.1b). The erosion and accretion patterns are analysed by the differences between the elevation maps of two surveys. Four months after the first survey, the erosion and accretion pattern shows that the erosion is the most sever at the coastline where the nourishment has the largest cross-shore extend (figure 4.1c). Furthermore, accretion takes place to the North and South of the Nourishment (figure 4.1c). This is in line with expectations. The erosion and accretion patterns of the intermediate surveys show a similar, although less severe, pattern (Appendix B.2).

4.1. Beach width development

To analyse the beach width development after the nourishment, some profiles are selected from the survey data. The selected profiles are: BB, GG, KK, OO, VV, and YY (figure 4.2c). The profiles at the largest cross-shore extent (i.e. profile GG, KK, and OO) show the larges beach width decline (figure 4.2a). In the four months after the nourishment, the beach width at the profiles GG and KK decreases by 52 m from 260 m to 208 m from the dune foot. The beach profiles during every survey at section KK are given in appendix B.3 with the locations of the shoreline. At the northern and southern bounds of the nourishment, where profiles BB and YY are selected, the beach width initially decreases after the

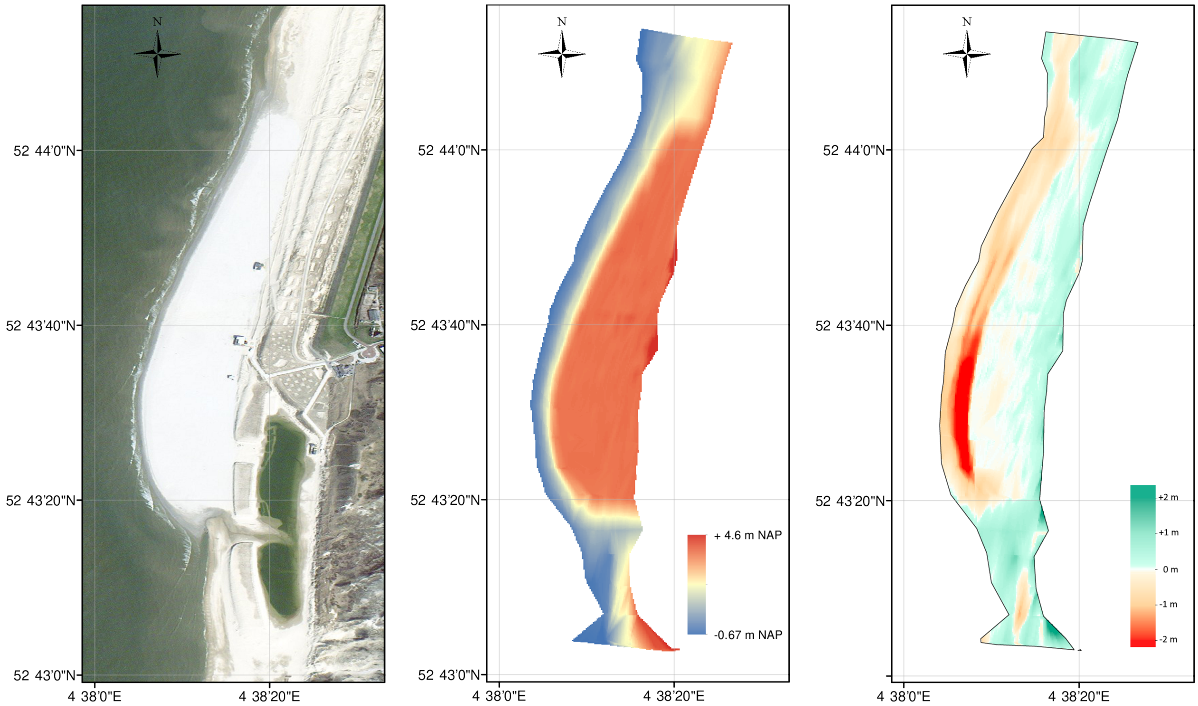

(a) (b) (c)

Figure 4.1: Overview of the Hondsbossche Dunes, with in (a) the satellite image of April 7, 2018, after the nourishment (The Netherlands Space Office Satellietdataportaal, 2018). (b) shows the elevation map of the survey data obtained at April 13, 2018 with a GPS wheel. The high beach and dunes (red colours) and low shoreline (Blue colours) can be distinguished. The erosion and accretion pattern of the study site is given in (c) where the bed level differences between the survey at August 14, 2018 and April 7, 2018 are given. Accretion is given by the green colours and erosion in red.

nourishment. However, approximately two months after the nourishment, from halfway June, the beach width at BB and YY starts to increase again. The rapid decrease of the beach width at sections GG, and KK, and the eventually increasing beach width at BB and YY, indicate alongshore diffusion of the nourished sediment. At profile OO, where the cross-shore extent of the nourishment is similar to KK, the total decrease in beach width over four months after the nourishment is 29 m. This is substantially less than the 52 m beach width difference at GG and KK. The net sediment transport at the dutch coast is directed northward. So section OO is at the leeward side of the planform nourishment.

The morphological response of the nourishment is expected to be the strongest in the first months after the nourishment, thereafter the change is expected to be less pronounced. This effect was seen at the initial development of the Sand Engine (de Schipper et al., 2016). At the Hondsbossche Dunes, the measurements appear to show a non-linear behaviour, with a strong morphological response at the first measurements, and slowing down morphological response at later surveys. However, the survey period is too short to confirm this.

During the survey period, a scarp has formed in the region with the largest cross-shore extent of the nourishment. This scarp developed during the survey period to a height in the order of 1 m. The survey period spans the summer period where the conditions are mild. At the Sand Engine, a similar scarp formation is observed during the summer months (de Schipper, Darnall, de Vries, & Reniers, 2017).

4.2. 1st year development

The survey with the walking wheel spans approximately four months after the nourishment. For the long term development, satellite images are reviewed. Periodic satellite images until one year after the additional nourishment are available (appendix B.4). A clear flattening pattern of the initial planform

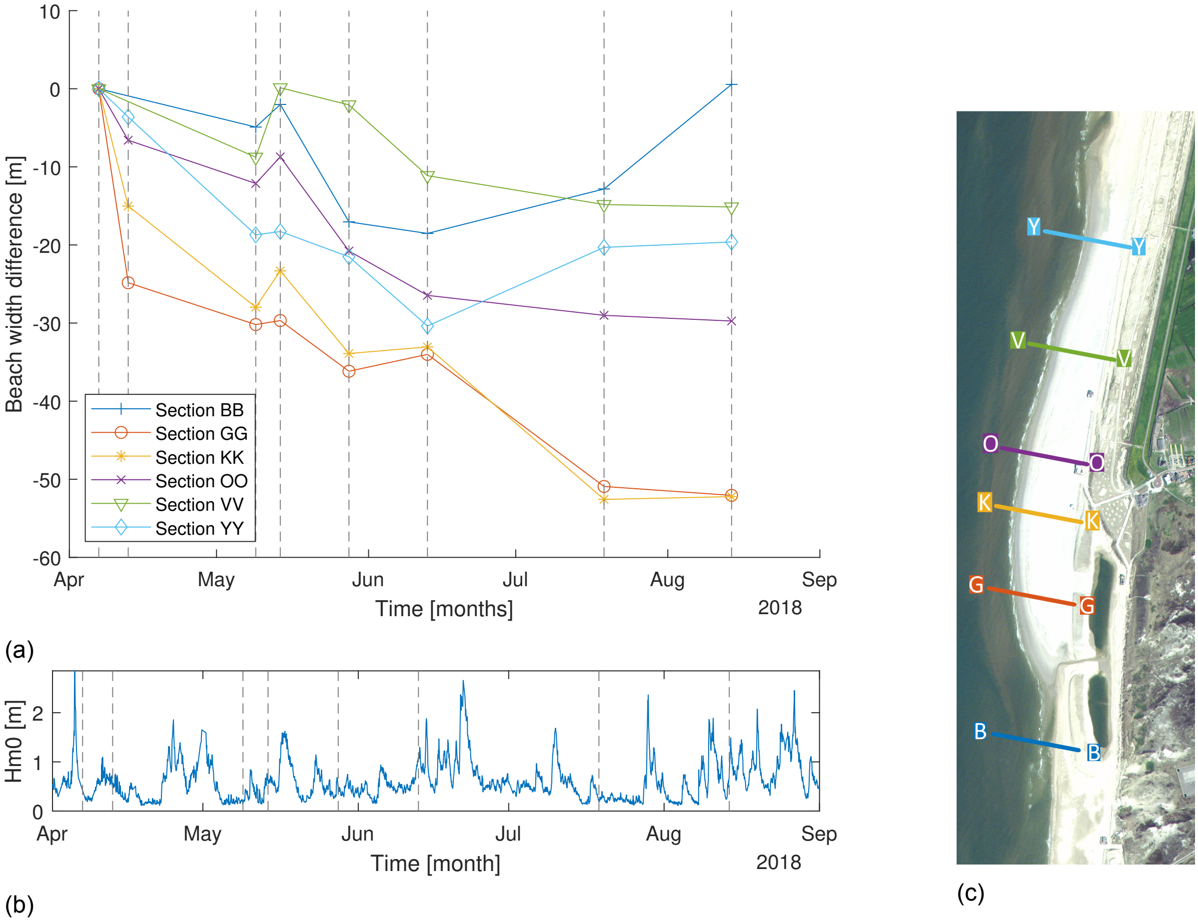

Figure 4.2: Beach width development after the additional nourishment in figure (a). The beach width difference is given with respect to the beach width from the first survey. For eight surveys, each observed beach width is indicated by a marker. Six beach profiles are selected, each denoted by a different colour. The locations of the beach profiles are given in figure (c). The significant wave heights during the survey period are given in figure (b).

can be observed. After one year, the convex-seaward perturbation has entirely disappeared. Although the shape of the coastline is smoothed, the shape of the coastline remains a bit convex-seawards.

4.3. Conclusion

The development of the beach profiles at a recently nourished beach are analysed for the nourishment at the Hondsbossche Dunes in March 2018. The most severe erosion takes place at the largest cross-shore extent of the additional nourishment. At both ends of the nourishment, accretion takes place eventually, after an initial beach width decrease. This indicates that the nourishment diffuses in long-shore direction over the coastline. The longshore diffusion appears to be gradual, with a decreasing erosion intensity over time. However, the survey period is too short to confirm this. The total beach width decrease in the first four months after the nourishment is 52 meter at profile KK. On the long term, the shape of the additional nourishment keeps flattening. After one year the perturbation disappeared and a smooth coastline remains.

5

XBeach model settings

The beach width predictions in this study are carried out using an XBeach model. In this chapter, the XBeach model settings are presented. The model settings are first calibrated and thereafter validated.

In this study, the XBeach model settings have to meet two requirements. On the one hand, the settings have to be accurate for the case study location, and on the other hand, the model must be fast enough to run time series which contain a year of wave data in a reasonable time. Sometimes these two requirements contradict, then concessions have to be made.

For efficiency, the model settings are first adjusted to limit the computation time by maintaining accuracy, and then the model is calibrated to represent the local conditions. However, this is an iterative process, so the profiles in section 5.1 and 5.2 are not all with the same 'base settings'. So apart from the varying parameter, the other model settings can also differ per calibration step. Therefore these settings are given in with each XBeach figure.

In the process of optimising the model settings, the model performance is quantified using the root mean square error (RMSE) and mean square error skill score (MSESS). A description of quantification of the model performance with the definitions of the RMSE and MSESS is given in section 2.6. For the model settings where the computation time is limited, the RMSE and MSESS are with respect to a base case scenario where the computation time is not decreased. While during the calibration of the shape of the profile, the RMSE and MSESS are with respect to the observed profile.

For the parameters that are not calibrated the default settings are used. The default settings in XBeach are configured for normal conditions on the Dutch coast and applicable to this study (Roelvink et al., 2015). The input file containing the model settings of the final XBeach model is given in appendix C.

5.1. Limit computation time

Without limiting the XBeach computation time, a stochastic approach for long-term XBeach modelling is unfeasible. A reference model without an optimised computation time took 36 hours to model the coastal development of the coastal profile for one month with hourly wave data. The final stochastic model contains 20 runs of one year, which would take approximately one year of computation time. Fortunately, there are several ways to limit the computation time in XBeach. In the final stochastic forecasting model, the computation time for 20 runs is decreased to approximately 5 days. Decreasing the computation time can lead to a decrease in accuracy, the challenge is to find an optimum between an acceptable accuracy and a feasible computation time.

MorFac

A typical way to decrease the computation time in XBeach is by increasing the morphological acceleration factor $MorFac$. In every morphological time step the bed level change is multiplied by the $MorFac$, this results in much faster computations (Ranasinghe et al., 2011). The speed of the changes in morphology can be scaled up to a rate where it does not yet have a significant impact on the hydrodynamic flows (Li, 2010). To optimise the computation time, different values of $MorFac$ are tested with the calibration model. The calibration model is based on data from April 7, 2018, to May 28, 2018, so it spans 52 days. An increase in $MorFac$ leads to an increase in erosion, especially at the higher part of the beach profile (figure 5.1). With a $MorFac$ above 10, the increase in erosion becomes significant while the difference between a $MorFac$ of 1 or 10 gives only a minor change. The duration of the model with a $MorFac$ of 1 is 36 hours on the computer used for the computation. With a $MorFac$ of 10 the computation time is a factor 10 faster so takes about 3:30 hours.
For a quantified comparison, the root mean square error (RMSE) and mean square error skill score (MSESS) are determined for every profile (table 5.1). The values of RMSE and MSESS indicate the performance with different $MorFac$ settings compared to the case where $MorFac = 1$. An MSESS of 0.79 for a $MorFac$ of 10 indicates that the model is classified as good according to Van Rijn et al. (2003). Therefore in further simulations for this study, the $MorFac$ is set on 10.

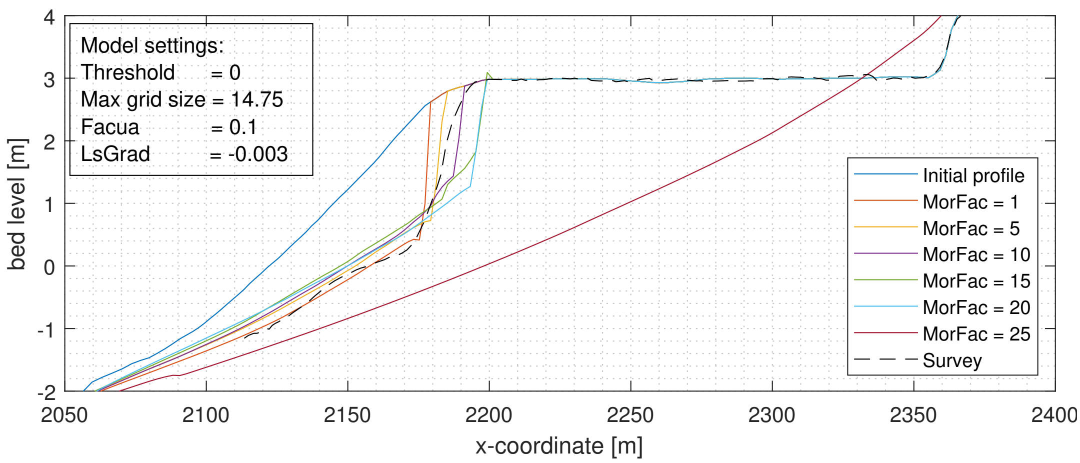

Figure 5.1: Comparison of the beach profiles resulting from the XBeach model with varying values of $MorFac$. The simulation time is 52 days.

Table 5.1: Root mean square errors (RMSE) and mean square error skill scores (MSESS) for calibrating MorFac

	MorFac 1	MorFac 5	MorFac 10	MorFac 15	MorFac 20	MorFac 25
RMSE	0.0000	0.2315	0.3338	0.4275	0.4764	1.6410
MSESS	1.0000	0.8971	0.7862	0.6494	0.5646	-4.1658

Wave Threshold

In Bart (2017) a method to reduce computation time is examined which is a data input reduction method. In this method wave conditions with a significant wave height below a certain threshold are removed. Wave spectra with low wave conditions have a limited influence on the behaviour of the beach profile and wave spectra with high wave conditions are often significant. Removing wave conditions below a certain threshold can decrease the computation time substantially, depending on the threshold level. In figure 5.2 results of the calibration model are given with different threshold levels. The reference model is with a wave threshold of zero, no waves are removed. These results are compared to models with a wave threshold of 0.5, 1, and 1.5. These wave thresholds result in a significant different beach profile, with more erosion especially at the higher part of the beach (Figure 5.2). In table 5.2 the root mean square error and the mean square error skill score are given. The model with a wave threshold of one gives a reasonable result with a mean square error skill score of 0.7 which is classified as ”good” according to Van Rijn et al. (2003). Also, a root mean square error of 0.24 is reasonable. However, when comparing the models to the observed profile data, indicated by the black dashed line in figure 5.2 the wave threshold affects the shape of the beach profile significantly. Above $2mNAP$ all models with a wave threshold show a considerable increase in erosion. Therefore a wave threshold is not used in this study to decrease the computation time.

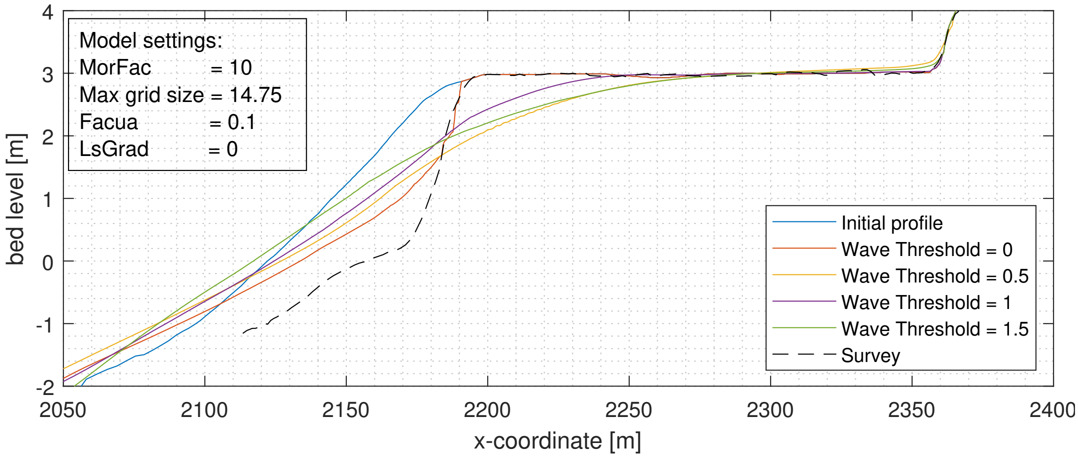

Figure 5.2: Comparison of the beach profiles resulting from the XBeach model when varying the $WaveThreshold$.

Table 5.2: Root mean square errors (RMSE) and mean square error skill scores (MSESS) for calibrating the wave Threshold

	Wave Threshold = 0	Wave Threshold = 0.5	Wave Threshold = 1	Wave Threshold = 1.5
RMSE	0.0000	0.3274	0.2408	0.3864
MSESS	1.0000	0.4690	0.7128	0.2602

Grid size

In XBeach the minimum grid size influences the computation time. In every cell centre the depths, water levels, wave action, and sediment concentrations are calculated for each time step. Increasing the minimum grid size reduces the number of cells so the computation time decreases. However, this can be at the cost of accuracy.

The computational grid is generated by the use of the OpenEarthTools Matlab Toolbox. The minimum grid spacing is based on the incident minimum short wave period. For the calibration data the minimum wave period is $min(Tm) \approx 1.67s$ and for the final data the minimum wave period is $min(Tm) = 1.22s$. To examine the influence of changing the grid size, different minimal wave period inputs are used for the calibration data. For wave periods of 1, 2, 3, and 6 seconds, the maximum grid sizes are $2.1m$, $8.0m$, $14.8m$, and $33.1m$ respectively. The minimum grid size is $2m$ for all models. The resulting profiles for each grid size are relatively close to each other (figure 5.3). In table 5.3 the performance of the different models quantified. The different models are compared to the model with the highest number of grid points with $min(Tm02) = 1$. Both the root mean square error and the mean square error skill score indicate that no matter the grid size, the model performs very well. Also, the computation time decreases significantly. However, shorter wave periods appear in the synthetic data than in the observed waves during the calibration period. A total number of 520 grid points with a maximum grid size of $14.75m$ is considered to a safe choice with a sufficiently fast model.

Summary accelerated settings

With optimised values of the Morfac, the wave threshold, and the grid size, the computation time of the XBeach model is considered to be low enough. The finally determined settings for these parameters are Morfac = 10, wave threshold = 0, and the number of grid points = 520. This decreases the computation time for the calibration period of two months from several days to approximately one hour.

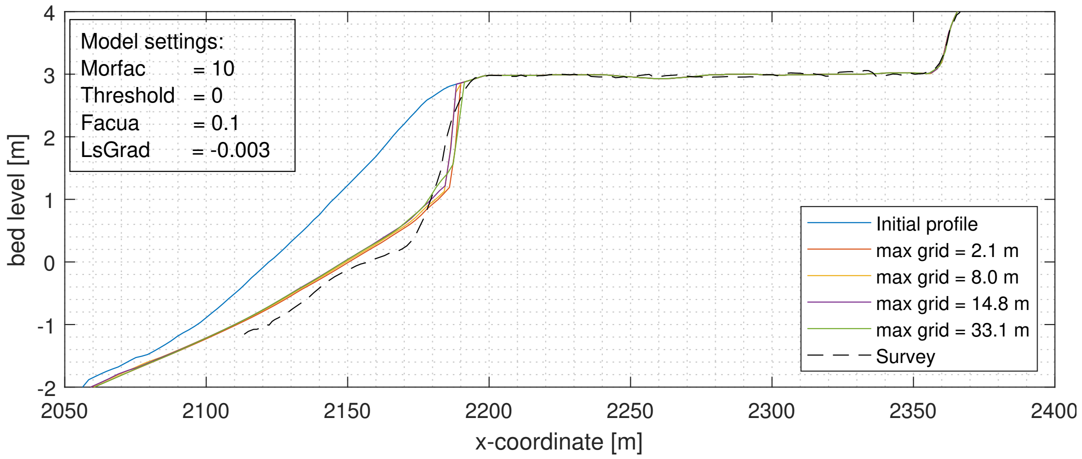

Figure 5.3: Comparison of the beach profiles resulting from the XBeach model when varying the Grid size

Table 5.3: Root mean square errors (RMSE) and mean square error skill scores (MSESS) for calibrating the grid spacing

Max grid size	2.08 m	8.00 m	14.75 m	33.11 m
Min wave period	1	2	3	6
Calculation time [HH:MM]	09:23	01:11	00:43	00:37
Number of grid points [-]	1619	570	520	497
RMSE [-]	0	0.07	0.08	0.05
MSESS [-]	1	0.99	0.99	0.99

5.2. Calibration

For the calibration based on accuracy, the main calibration factors are changed until the model performance is sufficient. First, the wave asymmetry and skewness is calibrated, then the longshore transport gradient is calibrated. Especially this longshore transport gradient gives a great improvement to the model. After the calibration of these two factors, the model accuracy is adequate.

Wave asymmetry and skewness

The effect of the wave shape on sediment transport is determined by the factors $facAS$ and $facSK$, which are the calibration factor for time-averaged flow due to wave asymmetry and wave skewness respectively. The $facua$ parameter is a parameter whereby both the $facAS$ and the $facSK$ can be varied at once. This makes the $facua$ an adequate and common calibration tool. In figure 5.4 results with different values of $facua$ are given. To quantify which setting performs best, the models with different $facua$ settings are compared to the observed profile. The root mean square errors and the mean square error skill scores are given in table 5.4. The default value of 0.1 seems to fit best with a root mean square error of 0.09 and a mean square error skill score of 0.96.

Table 5.4: Root mean square errors (RMSE) and mean square error skill scores (MSESS) for calibrating the $facua$

	Facua = 0.05	Facua = 0.1	Facua = 0.2
RMSE [-]	0.16	0.09	0.18
MSESS [-]	0.87	0.96	0.84

Longshore transport gradient

A major disadvantage of a 1D model is that long-shore transport gradients are zero as the total volume of the profile is preserved in this model. The case study location is at a convex-seaward crest of a

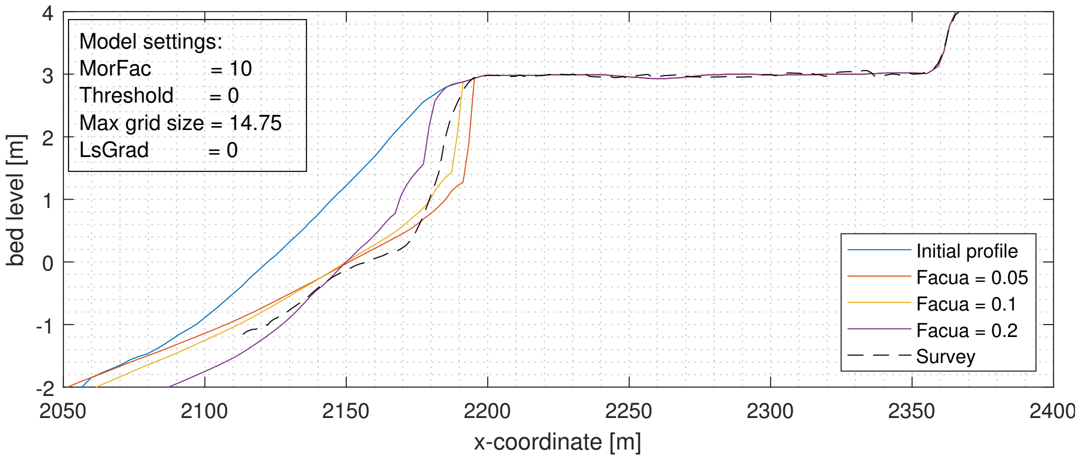

Figure 5.4: Comparison of the beach profiles resulting from the XBeach model with varying values of $Facua$.

perturbation due to the recent nourishment. This perturbation causes a longshore transport gradient. For 1D calculations XBeach assumes a constant volume balance. This assumption does not hold in case of a longshore transport gradient.

A recent implementation of the f_{lsgrad} factor in XBeach makes it is possible to include a longshore transport gradient in 1D XBeach applications. The factor f_{lsgrad} is implemented in the volume balance equation for bed updating (see equation 2.1 in section 2.2.2).

This longshore transport gradient has a significant influence on the calibration of the model. Without this factor, attempts to calibrate the beach profile model failed, especially in the lower region of the profile around MLW at -0.76 m NAP. In figure 5.5 the long-shore gradient is varied. For calibration of the f_{lsgrad} the model performance is compared to the observed profile from the survey. In figure 5.5 can be seen that a positive value of f_{lsgrad} leads to net sediment input and a negative value of f_{lsgrad} leads to a sediment loss. In table 5.5 the root mean square error and mean square error skill score show that a value of $f_{lsgrad} = -0.003$ performs best for the calibration data. With the default value of $f_{lsgrad} = 0$ the mean square error skill score is 0.79. With $f_{lsgrad} = -0.003$ the mean square error skill score is 0.93 which is a significant improvement.

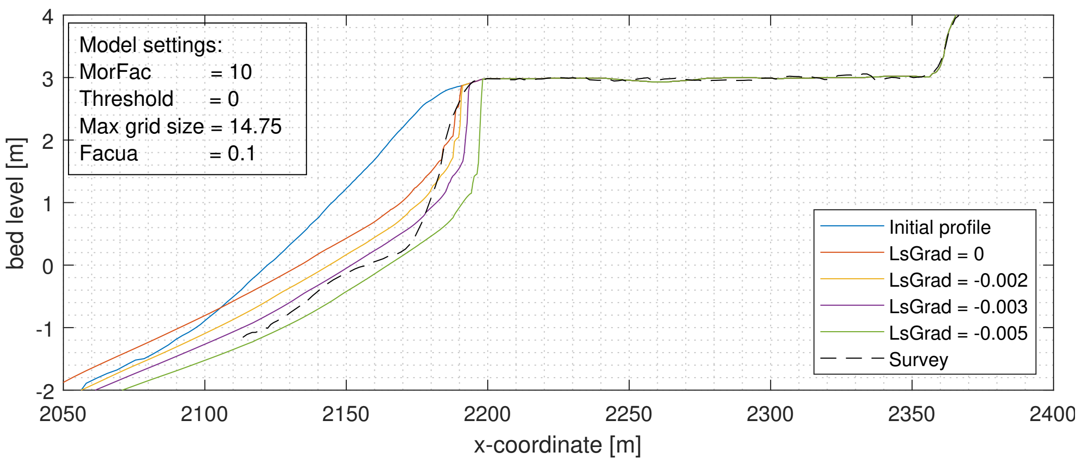

Figure 5.5: Comparison of the beach profiles resulting from the XBeach model with varying values of $LsGrad$.

Table 5.5: Root mean square errors (RMSE) and mean square error skill scores (MSESS) for calibrating the wave Longshore transport Gradient

	LsGrad = 0.05	LsGrad = 0	LsGrad = -0.002	LsGrad = -0.003	LsGrad = -0.005
RMSE	0.70	0.35	0.22	0.20	0.40
MSESS	0.17	0.79	0.91	0.93	0.73

Beach width difference

In previous calibration results, the beach profile of the model is compared to the observed beach profile after the calibration period of two months. The intermediate observations which are available are not tested in this calibration process. To test these intermediate observation profiles on the calibration model, the beach widths of the model data are compared to the beach widths of the calibration data for the whole calibration period. This results in the observed and modelled beach widths given in figure 5.6. The beach widths measured in the survey are given with the red line, and the beach width differences obtained with XBeach are given in blue. The observed beach width from the survey on April 30 is missing because the mean low water level was not reached and therefore the beach width can not be obtained. At the end of the calibration period, the beach widths of the observed profile and the XBeach profile are close to each other. In the intermediate period, the XBeach beach widths are less accurate, with the largest difference between the model and the observations at May 9th, where the difference between both beach widths values is $14.2m$.

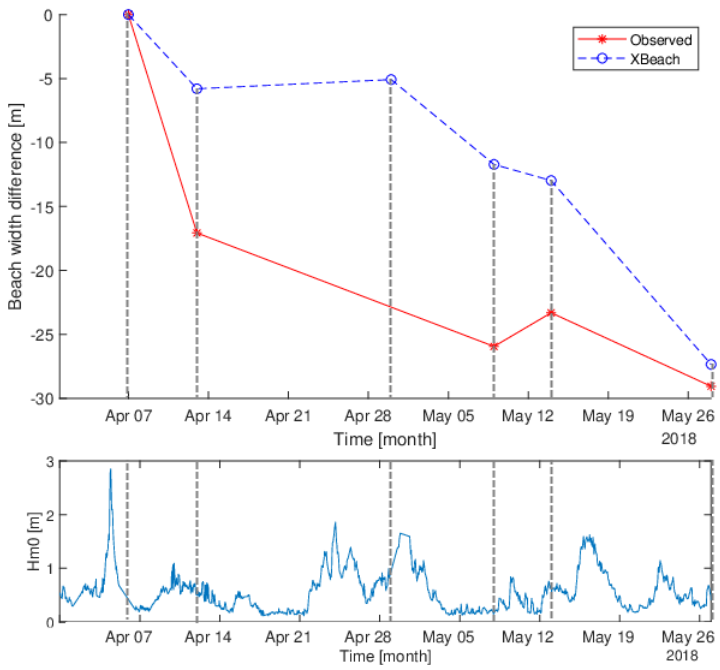

Figure 5.6: On top a comparison of the beach width difference of the observed profile and the XBeach model profile with respect to their initial beach width. Below the significant wave heights for this same period.

By visual interpretation on the beach widths during the calibration period, the difference between the model and the observations appear to be rather large. However, when not only the beach width but the whole profile of these intermediate observations is analysed, the model appears to be quite accurate. The root mean square error and the mean square error skill score between the observed profiles and the XBeach profiles are given in table 5.6. The profiles where these values are based on, are given in appendix D. The mean square error skill scores for the performance of the calibrated XBeach model on the intermediate dates are relatively high, indicating a good performance of the calibrated model. Especially at the last three measurement dates, the model performs excellently. The first two observation dates perform less good, as here both the observed profile and the XBeach profile are close to the initial profile, so relatively small differences between the XBeach profile and the observed profile are larger with respect to the initial profile. Therefore, the calibration data are considered to be sufficiently accurate.

Table 5.6: Root mean square errors (RMSE) and mean square error skill scores (MSESS) of the XBeach profiles compared to the observed profiles for each measurement date.

	07-Apr-2018	13-Apr-2018	30-Apr-2018	09-May-2018	14-May-2018	28-May-2018
RMSE	0.00	0.71	0.60	1.02	0.96	0.22
MSESS	1.00	0.59	0.63	0.91	0.92	0.95

5.3. Validation

To review the performance of the calibrated XBeach model, the data from the validation period are used. In the validation period three surveys were carried out on June 13, July 19, and August 14, 2018. For this period, the XBeach model is used with the final settings of the calibration (table 5.7). To start the validation period with the measured beach profile at the end of the calibration period, the whole time series including both the calibration and the validation period are computed at once.

Table 5.7: Calibrated parameters for XBeach

XBeach parameter	Value
Morfac	10
Threshold	0
Max grid size	14.75
Facua	0.1
LsGrad	-0.003

During the validation period, the beach width resulting from the XBeach model is very similar to the observed beach width (figure 5.7). This indicates that the XBeach model settings perform good for modelling the beach width. When looking at the root mean square error (RMSE), and then mean square error skill score (MSESS), the error increases for the last two profiles (table 5.8). Contrary to the calibration period, when analysing the individual profiles for the validation, the erosion on the higher part of the beach is significantly larger in the XBeach model than in the observed beach profiles (Appendix D).

Table 5.8: Root mean square errors (RMSE) and mean square error skill scores (MSESS) of the XBeach profiles compared to the observed profiles for each measurement date.

	13-Jun-2018	19-Jul-2018	14-Aug-2018
RMSE	0.0100	1.8700	2.2100
MSESS	0.8800	0.7600	0.7500

5.4. Conclusion

In this chapter appropriate settings for the XBeach model are found. First, the settings are adjusted to limit the computation time. This is done by adjusting the morphological acceleration factor, and the minimum grid size. Also, the possibility to introduce a minimum wave threshold is tested, but this decreased the accuracy of the XBeach considerably and is therefore not used. The total computation time for the calibration period of two months is decreased from several days to approximately one hour without a substantial loss of accuracy. After limiting the computation time, the XBeach model is calibrated based on accuracy. The effect of the wave asymmetry and wave skewness on sediment transport is adjusted by varying the $facua$. At the study location of the Hondsbossche Dunes, a longshore transport gradient is present. A longshore transport gradient factor is implemented in the XBeach model with f_{lsgrad}. This greatly improves the accuracy of the model. With these calibrated parameters, the XBeach model is considered to be accurate enough (table 5.7. For all other parameters that are not

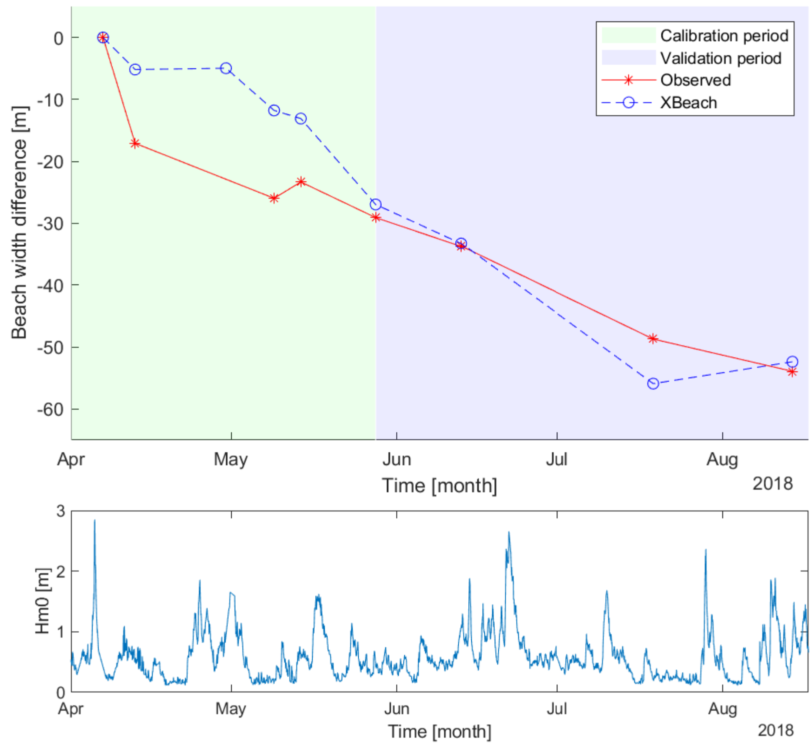

Figure 5.7: Beach width difference for the calibration period (green) and the validation period (purple). The observed beach width is given in red and the beach width derived from XBeach is given in blue. Below the significant wave heights are given for the same period.

calibrated the default value is used. After the calibration, the model is validated with the data from the validation period. Based on the beach width the model performs well for the validation period. At the higher part of the beach, however, the XBeach model profile deviates from the observed profile.

6

Generating stochastic forcing time series for XBeach predictions

In this section, the synthetic time-series for the wave heights, wave periods, wave directions, and water levels are generated. The flow chart in figure 6.1 gives an overview of the steps taken to generate the synthetic time series. The modelling steps used to create the synthetic time series are mostly based on the approach of Jäger (2018). In Jäger (2018) a method is developed for generating synthetic time series of the significant wave height, and the mean zero-crossing period for the offshore location Europlatform.

In this chapter the modelling steps are treated in detail and applied in the case study. Also, the intermediate outcomes are discussed. Simulation of synthetic data for IJmuiden Munitiestortplaats is described in section 6.1. The simulation of wave time series for Eierlandsegat and Europlatform is described in section 6.2. In section 6.3 generating the water level time series with the surge is described. Significant wave time series are selected by Latin Hypercube sampling in section 6.4 and in section 6.5 the offshore wave data is transformed to nearshore data.

6.1. Simulate time series for IJmuiden Munitiestortplaats

In this section, the simulation of a synthetic wave time series for IJmuiden Munitiestortplaats is explained. The observed historic data, where the simulated synthetic wave time series are based on, are the significant wave height H_{m0} (figure 6.2a), mean zero-crossing period T_{m02} (figure 6.2b), and the main wave direction T_{h0} (figure 6.3). The collected data are described in section 3.2.2.

Limit steepness condition

The wave steepness is the relation between the wave height and the wavelength. The ratio between H_{m0} and T_{m02} is for the most part stochastic. However, wave heights become too large compared to the wavelength white-capping occurs and waves breaks. This lower limit of the wave steepness can be seen as the deterministic part of the relation. To assure the generated wave periods do not result in values below this limit, this deterministic part is first removed from the wave period, and at the end of the simulation, this deterministic part is added to the wave periods again.

$$\widetilde{T}_{m02} = T_{m02} - T_{m02_{min}},$$

Holthuijsen (2010) states that the wave steepness is physically limited to $Steepness < 1:15$. In figure 6.4 this wave steepness boundary is shown, applied to the observed data in IJmuiden Munitiestort-

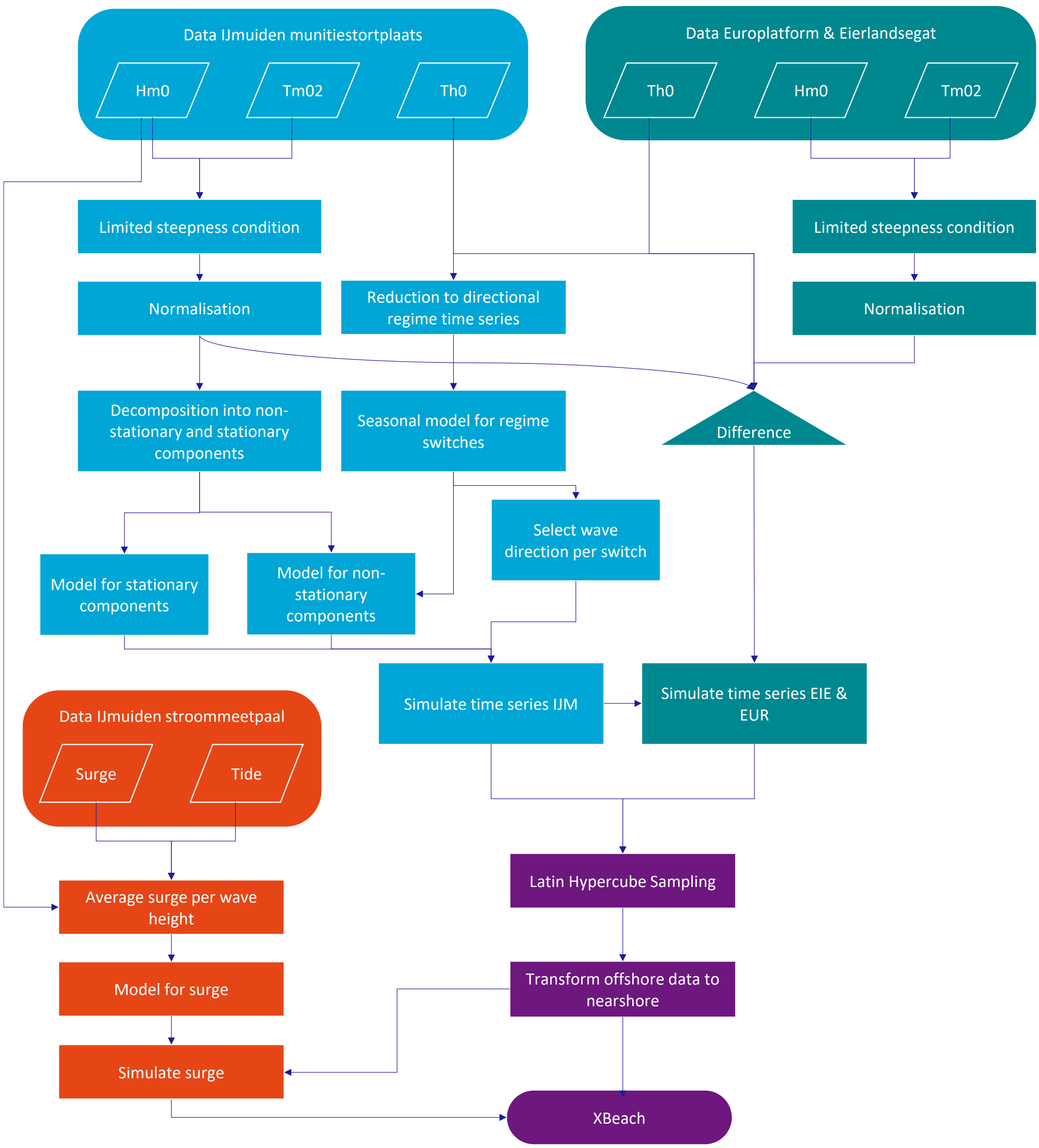

Figure 6.1: Flow chart for generating stochastic forcing conditions. In the blue part, the steps to create synthetic data at IJmuiden Munitiestortplaats are given. The green part contains the steps to extend the offshore wave data at IJmuden Munitiestortplaats to the wave rider locations of Europlatform and Eierlandsegat. The orange boxes describe the process of adding water level data. In the purple part the time series are sampled, transformed to nearshore data, and combined to prepare the XBeach data.

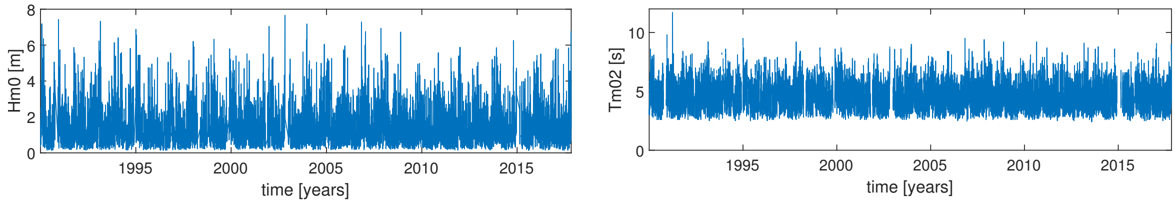

(a) (b)

Figure 6.2: Time series of the observed ((a)) significant wave heights and ((b)) the mean zero-crossing periods at IJmuiden munitiestortplaats for the period from January 1990 to September 2017.

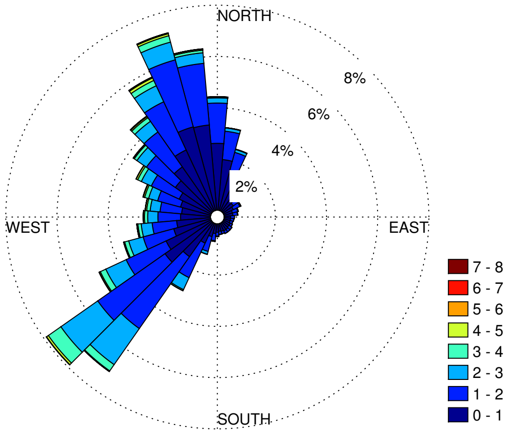

Figure 6.3: Circular histogram of observed wave directions at IJmuiden Munitiestortplaats.

plaats. In figure 6.4 the red + signs fall outside the steepness limit and are therefore ignored. 1223 values are hereby removed and treated as missing values. The data coverage of the data at IJmuiden Munitiestortplaat is now 91.9 % and 91.4 % for H_{m02} and $\widetilde{T}_{m02}$ respectively.

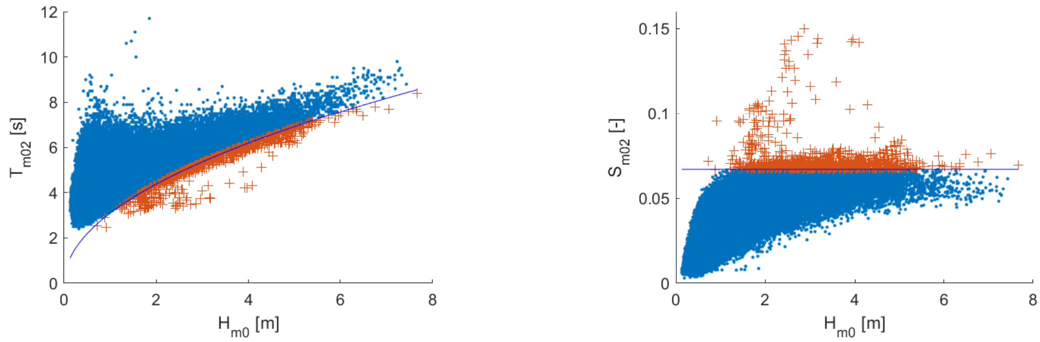

(a) (b)

Figure 6.4: In ((a)) the relation between the mean zero-crossing period T_{m02} and the significant wave height H_{m0}, and in ((b)) the relation between the wave steepness S_{m02} and the significant wave height H_{m0}. In both figures she blue line gives the wave steepness limit of $steepness < 1:15$. The blue dots indicate values that fall in the wave steepness limit, and the values that fall outside the wave steepness limit are indicated by a red +.

Transformation to standard normal distribution

The processes H_{m0} and $\widetilde{T}_{m02}$ are both skewed processes with only positive values. To remove this skewness the data are transformed to standard normal processes i.e. with a mean of $\mu = 0$ and standard deviation of $\sigma = 1$. When H_{m0} and $\widetilde{T}_{m02}$ are modelled without reducing the time series to standard normal, the resulting synthetic time series contains negative values, which is not possible for H_{m0} and T_{m02}. The data are transformed to standard normal by using the empirical distribution function (6.1) in the probability integral transform (6.2).

$$F_n(x) = \frac{\text{number of } x_i =< x}{n+1}. \tag{6.1}$$

where $F_n(x)$ is the empirical distribution function estimated for data $x_1, ..., x_n$ and n is the number of data points.

$$f(x) = \Phi^{-1}(F_n(x)), \tag{6.2}$$

where Φ^{-1} is the inverse of the standard normal cumulative distribution function. The transformation to standard normal results in data series given in figure 6.5.

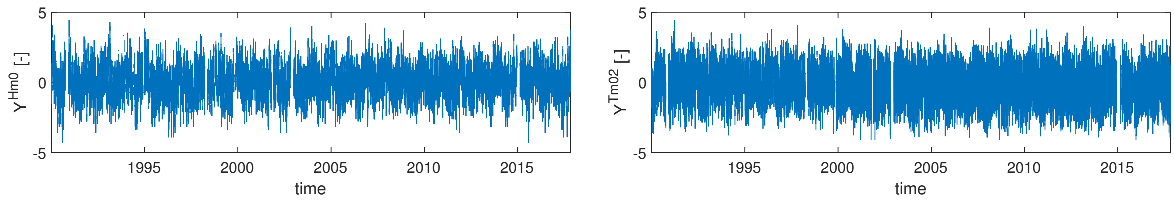

(a) (b)

Figure 6.5: Time series of the normalised observed (a) significant wave heights and (b) mean zero-crossing period.

When at the end of this section, the synthetic time series for Y^{Hm0} is created, the data have to be transformed back to a non-normalised X^{Hm0} time series. Since the empirical distribution function is a step function it does not have a unique inverse. Therefore the relation between the regular observed data and the normalised observed data are analysed (figure 6.6). The original data are denoted on the x-axis by X^{Hm0} and X^{Tm02} and the standard normal data are given on the y-axis denoted by Y^{Hm0} and Y^{Tm02}. The transformation from synthetic normalised data to synthetic regular data is by linear interpolation between the observed data points. At the tails of the observed data, the points are linearly extrapolated to be transformed back (figure 6.6). The data of the normalised wave height shows a logarithmic increase until the highest several data points (figure 6.6a). At high values of X^{Hm0} and Y^{Hm0} the curve tails to a 1:1 ratio. Neglecting this tail results in extreme high values of generated wave heights. To take this tail into account, linear interpolation and extrapolation is used rather than fitting a curve through the data points. For the mean zero-crossing period, this tail is also present, although less pronounced.

Decomposition into stationary and non-stationary components

The signals Y^{Hm0} and Y^{Tm02} are split in a stationary and a non-stationary component. This is done by describing the data as in function 6.3 where the mean μ_t and the standard deviation σ_t are slowly varying non-stationary components and z_t is a high-frequency stationary component.

$$y_t = \mu_t + \sigma_t z_t, \quad t = 1, ..., T \tag{6.3}$$

The slowly varying mean μ and standard deviation σ are extracted from this signal using a moving window with an Epanechnikov kernel as weighting function. This is illustrated in figure 6.7. A window

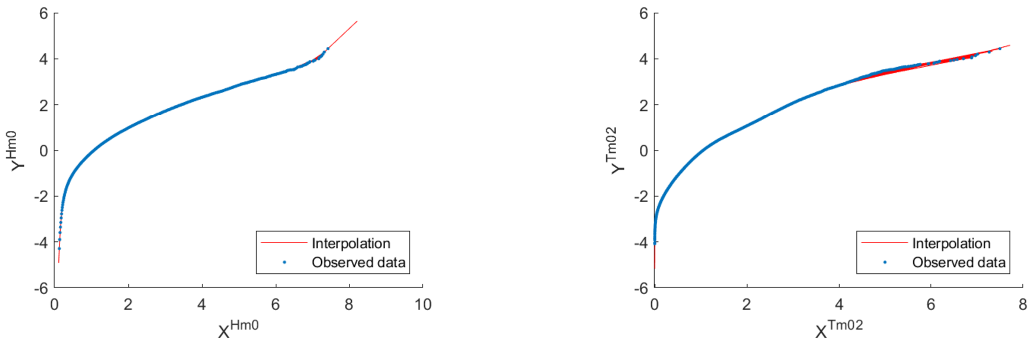

(a) (b)

Figure 6.6: Relations between original and normalised values of (a) the significant wave height and of (b) the mean zero-crossing periods.

is slid through the time series. For every time step, the mean and the standard deviation of the window is calculated. The weighting function of the sliding window is described by an Epanechnikov kernel, meaning that the values in the centre of the window weight more than the values at the edges of the window. The function of the Epanechnikov kernel K is given in equation 6.6. The functions describing

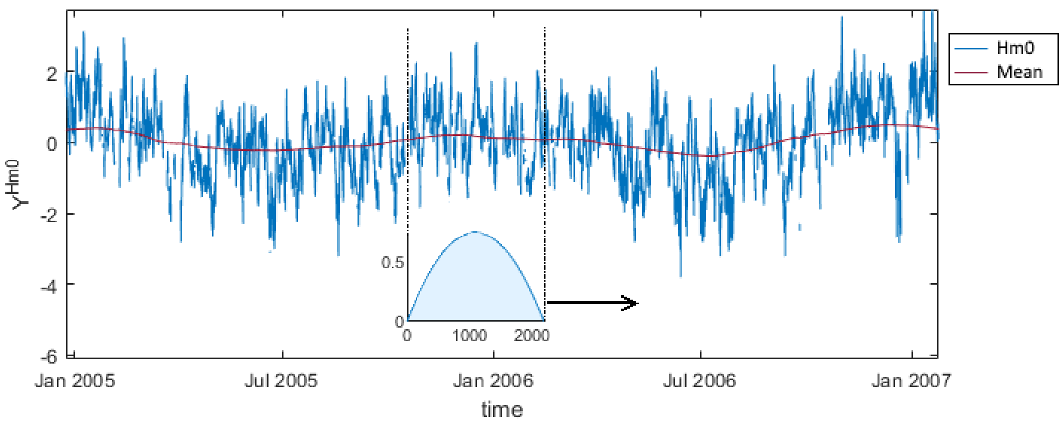

Figure 6.7: Illustration of alternating binary renewal process with the normalised wave time series of January 2005

the moving mean and moving standard deviation are given in equation 6.4 and 6.5 respectively.

$$\mu_t = \frac{1}{2t'} \sum_{k=t-t'}^{t+t'} K_{2t'}(x_t - x_k) \tag{6.4}$$

$$\sigma_t = \sqrt{\frac{1}{2t'} \sum_{k=t-t'}^{t+t'} K_{2t'}(x_t - \mu_t)^2 - (x_k - \mu_k)^2} \tag{6.5}$$

where

$$K(u) = \frac{3}{4}(1 - u^2) \tag{6.6}$$

A window size of $t = 2191$ is chosen, which corresponds to three months. This window size is optimised to a value where the slowly-varying mean and standard deviation are well described by a five-term Fourier curve, used for modelling these components.

With the decoupling process, the seasonality of the first two moments, i.e. the mean and the variance, are removed from the time series. Higher moments, like the skewness and the kurtosis, may contain seasonal behaviour as well. As these higher moments are not removed from the time series, the stationary time series may still contain some seasonality. This decomposition into stationary and non-stationary components is applied on both Y^{Hm0} and Y^{Tm02}. This results in slowly varying means μ_t^{Hm0}, and μ_t^{Tm02}, and slowly varying standard deviations σ_t^{Hm0}, and σ_t^{Tm02}, and fast varying stationary components z^{Hm0} and z^{Tm02}.

Model for non-stationary components

The time series is now decoupled in a stationary and a non-stationary component. The slowly varying non-stationary components can be described by Fourier series. To do this, the data are separated in yearly segments. For each year a Fourier series with two terms is estimated. The two-term Fourier series for μ and σ are given in equation 6.7 and 6.8.

$$f^{(\mu_k^{(i)})}(\tau) = a_0^{(\mu_k^{(i)})} + a_1^{(\mu_k^{(i)})} cos\left(\frac{2\pi\tau}{T}\right) + b_1^{(\mu_k^{(i)})} sin\left(\frac{2\pi\tau}{T}\right) + a_2^{(\mu_k^{(i)})} cos\left(\frac{4\pi\tau}{T}\right) + b_2^{(\mu_k^{(i)})} sin\left(\frac{4\pi\tau}{T}\right) \tag{6.7}$$

and

$$f^{(\sigma_k^{(i)})}(\tau) = a_0^{(\sigma_k^{(i)})} + a_1^{(\sigma_k^{(i)})} cos\left(\frac{2\pi\tau}{T}\right) + b_1^{(\sigma_k^{(i)})} sin\left(\frac{2\pi\tau}{T}\right) + a_2^{(\sigma_k^{(i)})} cos\left(\frac{4\pi\tau}{T}\right) + b_2^{(\sigma_k^{(i)})} sin\left(\frac{4\pi\tau}{T}\right) \tag{6.8}$$

Where $T = 8765$ is the number of hours per year and $i = \{H_{m0}, \widetilde{T}_{m02}\}$. At the transitions from one year to the other discontinuities are present. To smooth these discontinuities smoothing spline is fitted to the time series. This eliminates the discontinuities but does not affect the shape of the Fourier curve. The time series of the observed moving average and moving standard deviations are given in figure 6.8 together with the fitted Fourier curves for every year. From visual diagnostics can be assets that the Fourier curve corresponds to the data sufficiently. The coefficients of determination (R^2) are all above 0.89, this confirms the visual assessment of well corresponding data 6.1.

Table 6.1: Coefficients of determination R^2 for the fitted seasonal mean and seasonal standard deviation

	μ_t^{Hm0}	μ_t^{Tm02}	σ_t^{Hm0}	σ_t^{Tm02}
R^2	0.95	0.89	0.95	0.90

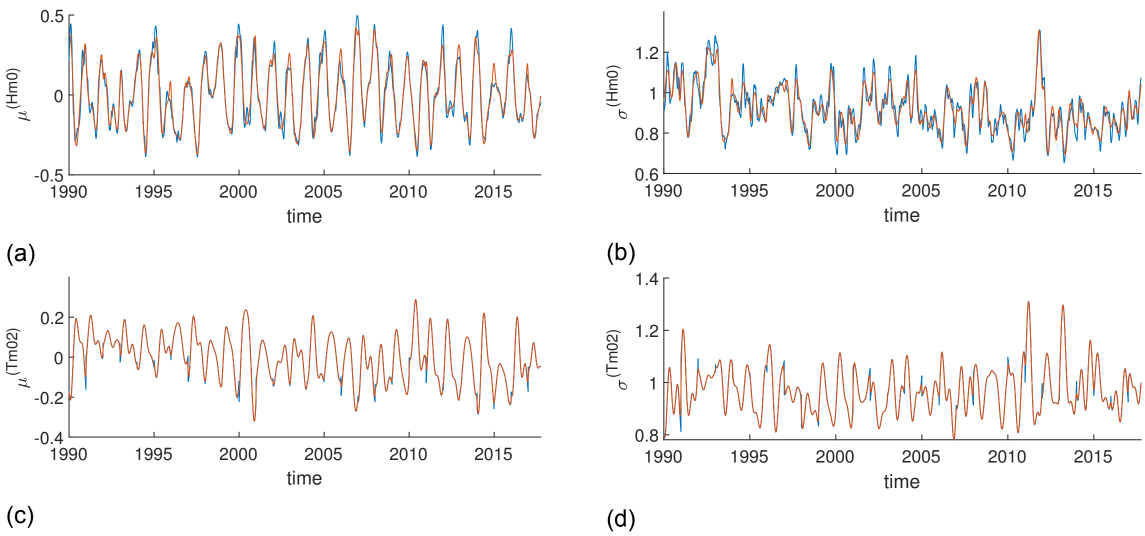

Figure 6.8: Observed non-stationary components in red and the fitted and smooth Fourier series in blue

Table 6.2: Mean and standard deviations of the observed Fourier coefficients. Noted as (mean, standard deviation).

	a0	a1	b1	a2	b2
$\mu^{H_{m0}}$	(0.01, 0.05)	(0.21, 0.05)	(-0.05, 0.06)	(0.01, 0.05)	(-0.01, 0.06)
$\mu^{T_{m02}}$	(0.00, 0.05)	(-0.15, 0.05)	(0.08, 0.06)	(-0.02, 0.03)	(0.00, 0.05)
$\sigma^{H_{m0}}$	(0.92, 0.06)	(0.01, 0.06)	(-0.02, 0.07)	(-0.02, 0.03)	(0.01, 0.05)
$\sigma^{T_{m02}}$	(0.95, 0.04)	(0.05, 0.05)	(0.04, 0.04)	(-0.03, 0.03)	(0.00, 0.04)

For each year the Fourier variables are now known. To be able to generate Fourier variables for the simulation, the distributions and their correlations of the observed Fourier variables are analysed. Each fitted Fourier series with its variables represents one year. Since the sample size is small (N = 28) it is unfeasible to analyse the distributions. Therefore, they are assumed to be multivariate Gaussian. The significant correlations found between the Fourier variables are:

$$
\begin{aligned}
\rho\left(a_0^{(\mu^{(Hm0)})}\ ,\ a_0^{(\mu^{(Tm02)})}\right) &= -0.57,\\
\rho\left(a_1^{(\mu^{(Hm0)})}\ ,\ a_1^{(\mu^{(Tm02)})}\right) &= -0.78,\\
\rho\left(b_1^{(\mu^{(Hm0)})}\ ,\ b_1^{(\mu^{(Tm02)})}\right) &= -0.73,\\
\rho\left(a_2^{(\mu^{(Hm0)})}\ ,\ a_2^{(\mu^{(Tm02)})}\right) &= -0.84,\\
\rho\left(b_2^{(\mu^{(Hm0)})}\ ,\ b_2^{(\mu^{(Tm02)})}\right) &= -0.78.
\end{aligned}
$$

The correlations are considered statistical significant when the p-value is below 0.05. Significant correlations are only found between the terms $a_n^{\mu^{Hm0}}$ and $a_n^{\mu^{Tm02}}$, and between $b_n^{\mu^{Hm0}}$ and $b_n^{\mu^{Tm02}}$ for different values of n. This physically represents the correlation between the seasonal variability of the mean of the significant wave height and the mean of the mean zero-crossing period. For the standard deviation no significant correlations are present. When simulating the non-stationary components, the Fourier coefficients are generated randomly with the same mean, standard deviation, and correlation as the observed Fourier coefficients. The means and standard deviations of the observed coefficients are given in table 6.2.

Model for stationary components

The stationary component $z_t^{(i)}$ of the wave time series is extracted by removing the non-stationary components according to equation 6.9.

$$z_t^{(i)} = \frac{y_t^{(i)} - \mu_t^{(i)}}{\sigma_t^{(i)}} \tag{6.9}$$

The observed stationary components z^{Hm0} and z^{Tm02} are given in figure 6.9. These stationary pro-

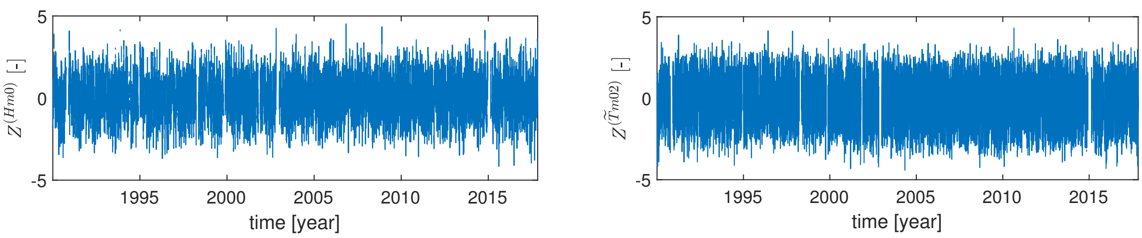

(a) (b)

Figure 6.9: Observed stationary components of wave time series with in (a) the stationary part of H_{m0} and in (b) the stationary part of T_{m02}.

cesses are simulated as Autoregressive-Moving Average (ARMA) processes. A brief introduction into

ARMA processes is described in section 2.4. The function of the ARMA process is given in equation 6.10. The orders of q and p in ARMA(p,q) are estimated by analysing the auto correlation function (ACF) and the partial auto correlation function (PACF), both shown in figure 6.10. The ACF shows the correlation with a time series with a delayed copy of itself. The x-axis shows the number of lags the copy is delayed and the y-axis shows the correlation. A PACF gives the correlation of a time series with its own lagged values, removing the effect from all shorter lags.

The ACF of an AR process of order p tails off, whereas its PACF has a cutoff after lag p. In contrast to an MA process of the order q, which PACF tails off and ACF has a cutoff after lag q. When both the ACF and the PACF tail off, a mixed process is suggested (Box et al., 2015).

Besides the visual interpretation of the ACF and PACF, the orders of q and p are also determined by minimising Akaike's Information Criterion (AIC) (Jones, 1980). AIC estimates the relative amount of information lost by a given model. When AIC does not decrease significantly while increasing the orders of q and p, the performance does not increase. An optimum is found between the smallest AIC by trial on error (table 6.5).

$$X_t = c + \sum_{j=1}^{p} \phi_j X_{t-j} + \epsilon_t + \sum_{j=1}^{q} \theta_j \epsilon_{t-j} \tag{6.10}$$

In the ARMA model for the stationary components, a distinction is made between wave time series originating from northwestern directions and waves from southwestern directions. For both directional regimes, an ARMA model is estimated. For each wave directional regime switch, the ARMA model switches with the wave direction. The segments of the time series derived with the ARMA model are concatenated. While concatenating the segments, the ARMA properties of the correlation with its own delayed lagged values is lost at the model switches. With this model, the assumption is made that the stationary component of the wave heights, and the wave periods before a binary direction switch, are independent from the stationary component of the wave heights and wave periods after the directional switch. In practice, this can result in a sudden change in sea-state when the wave direction changes. The ACF and PACF for the wave origin from the northwest are given in figure 6.10. The ACF and PACF of the southwestern waves show a very similar pattern.

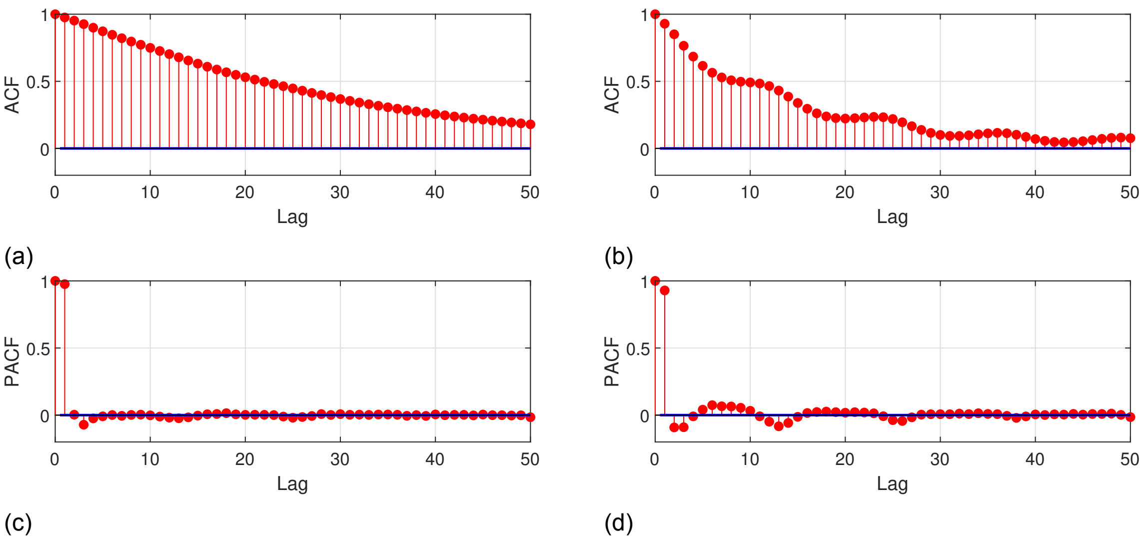

Figure 6.10: Auto correlation functions (ACF) and partial auto correlation functions (PACF) to find an appropriate choice for orders p and q in ARMA(p,q) of northwestern waves: (a) ACF of z^{Hm0}, (b) ACF of z^{Tm02}, (c) PACF of z^{Hm0}, (d) PACF of z^{Tm02}.

The ACF of z^{Hm0} in figure 6.10a shows a geometric decay (i.e. the autocorrelation decays exponentionally when increasing the number of lags), while the PACF in figure 6.10c has a cut off at lag one. This indicates that the ARMA process is of the order $(1,0)$.

With the ACF and the PACF of the residuals, it is verified that for z^{Hm0} an ARMA process of the order $(1,0)$ suffice. Also, AIC does not decrease significantly while increasing the orders of q and p. With this ARMA model, the residuals should behave like "white noise", i.e. show no autocorrelation. For z^{Hm0}, the lags of the ACF of the residuals show very little auto-correlation so the white noise behaviour is verified (figure 6.11a). For z^{Tm02} the ACF shows a decay but this decay is not geometric. The PACF is only significant in the first lag. The process which performs best for z^{Tm02} is an ARMA process of the order $(3,2)$. The ACF of the residuals verifies white noise behaviour (figure 6.11b). For both the stationary component of the significant wave height and the mean zero-crossing period, the residuals are best approximated by a Gaussian distribution.

The estimated ARMA coefficients are given in table 6.5.

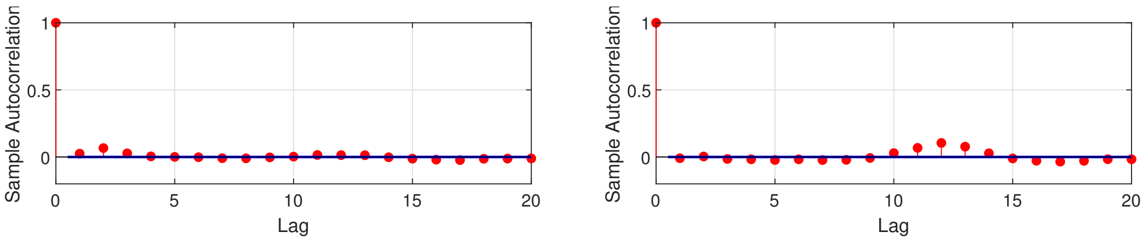

(a) (b)

Figure 6.11: Auto correlation functions (ACF) for the residuals of the (a) significant wave height (Hm0) and the (b) mean zero-crossing period (Tm02) for the north-western wave regime

Table 6.3: Estimated ARMA coefficients for the stationary components of the significant wave height and the mean zero-crossing period. The north-western and south-western component are distinguished. The standard errors are given in parentheses. The accompanying AIC values and the parameters for the residuals (ϵ) are also given. The residuals are approximated by a Gaussian family which can be parameterized by the mean (μ) and standard deviation (σ).

	AR(1)	AR(2)	AR(3)	MA(1)	MA(2)	AIC	ϵ (μ, σ)
$z^{(Hm0)}$ (NW)	0.98 (0.00)	-	-	-	-	-2.9e4	(0,0.22)
$z^{(Hm0)}$ (SW)	0.97 (0.00)	-	-	-	-	-2.6e-3	(0,0.24)
z^{Tm02} (NW)	2.00 (0.03)	-1.50 (0.05)	0.46 (0.02)	-0.97 (0.03)	0.48 (0.02)	8.9e4	(0.01,0.35)
z^{Tm02} (SW)	2.10 (0.01)	-1.70 (0.02)	0.50 (0.01)	-1.11 (0.01)	0.58 (0.01)	1.0e5	(-0.04,0.42)

Reduction to directional regime time series

The wave directions at the location of IJmuiden Munitiestortplaats in the North Sea are mainly from the north-north-western (NNW) and from south-western (SW) directions. For the model for stationary components a distinction is made between waves from these two directions. The waves form the NNW direction can contain swell, while the waves from the SW directions are mainly wind seas. This is because at the North sea the swell propagates mainly from the north and north western directions, i.e. from the Norwegian and Greenland Seas (Boukhanovsky, Lopatoukhin, & Soares, 2007). Therefore these wave directions are treated as binomial wave regimes. First the wave regimes Θ_t are simulated as an alternating binary renewal process (figure 6.12). The wave heights and periods of the two directional regimes are expected to behave differently, hence for each directional regime, H_{m0} and T_{m02} are simulated separately. The wave directional regimes are defined as follows:

$$\Theta_t = \begin{cases} 0, & \text{mean wave direction at time } t \in (275°, 90°), \\ 1, & \text{mean wave direction at time } t \in [90°, 275°]. \end{cases}$$

The north-western wave directions are indicated by zeros and the south-western wave directions are indicated by ones.

Seasonal model for regime switches

With an alternating binary renewal process, the duration of each regime is modelled. An example is given in figure 6.12, where the initial directional regime is 1 for time SW_1, then it switches to 0 for time NW_1, and so on.

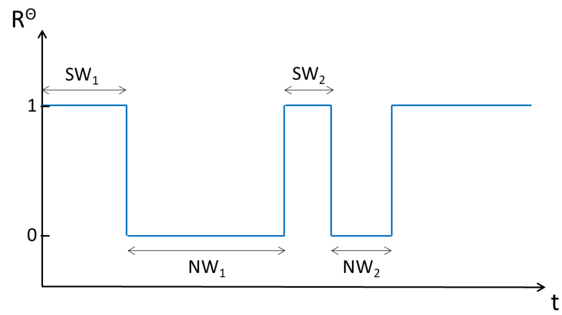

Figure 6.12: Illustration of alternating binary renewal process

Sequences SW and NW may be dependent on each other and the season. For each season bivariate copulas are constructed for the duration of each directional mode. To asses which copula families perform well in this simulation, the Multivariate Copula Analysis Toolbox (MvCAT) is used. With MvCAT the bivariate copula families are ranked based on three criteria of goodness of fit; likelihood, Akaike Information Criterion (AIC), and Bayesian Information Criterion (BIC) (Sadegh, Ragno, & AghaKouchak, 2017). Copula families which are tested are Gaussian, t, Clayton, Frank, and Gumbel. For all seasons a t copula appears to perform best on all three criteria based on the analysis with MvCAT. For the simulation of the binary directional regimes, values for the duration for each regime are randomly generated with the parameters of the estimated copulas (table 6.4).

Table 6.4: Estimated copula families and parameters of the directional fit for each season.

Season	Copula family	Parameters
Winter	t	$(\rho, \nu) = (0.32, 4.23)$
Spring	t	$(\rho, \nu) = (0.27, 5.83)$
Summer	t	$(\rho, \nu) = (0.29, 7.05)$
Autumn	t	$(\rho, \nu) = (0.25, 5.04)$

Select wave direction per switch

Besides binary directional regimes used for the stationary part of the models for wave heights and mean zero-crossing period, the exact wave direction is an important input value for XBeach. Furthermore, to transform the wave time series from offshore to nearshore, wave directions are also required. Although the waves have two main wave directions, the waves at IJmuiden Munitiestortplaats can originate from all directions. To modify the binary directional model to a more realistic wave directional model, for each regime switch, an exact wave direction is sampled randomly from the observed time series. The observed wave data show waves from all wave directions, therefore an extreme value analysis is not required and simple sampling suffices. The main difference with the sampled wave directions and the observed wave directions is that in the observed time series the wave direction can vary within a binary directional regime, while with the synthetic data only one wave direction per directional regime is applied. So small variations within a directional regime, which are present in reality, are neglected in this model. Furthermore, in this model, the exact wave direction is independent on the duration of the directional regime. So an uncommon wave direction, which in reality is likely to last shortly, can last unrealistically long with this model. These simplifications can be the reason for the differences between the observed wave directions (figure 6.13a) and the simulated wave directions (figure 6.13b).

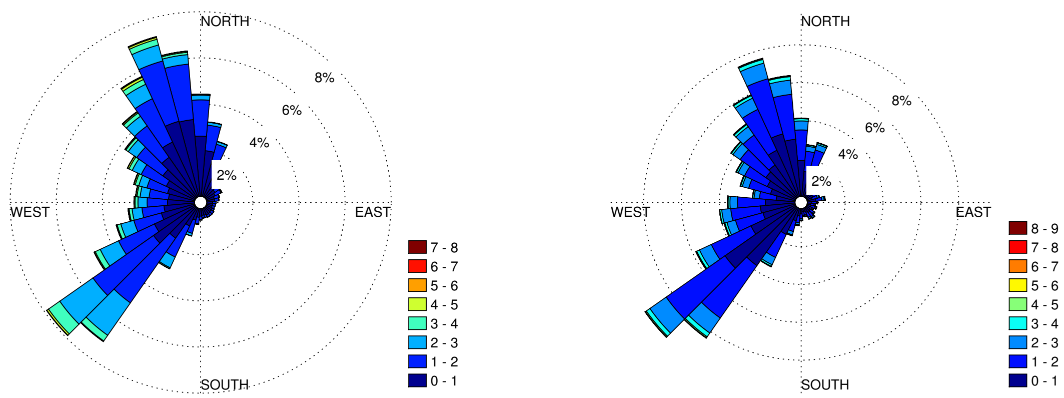

(a) (b)

Figure 6.13: Observed and synthetic wave directions for 28 years of wave data. In (a) the observed wave directions and in (b) the synthetic wave directions.

Simulate time series IJM

In previous subsections, models are estimated to simulate synthetic data parts of the wave time series in IJmuiden Munitiestortplaats. By combining these models, synthetic wave time series are generated. With this wave modelling method, any sample size of wave time series with any length can be generated. For this study, the duration of the simulated time series is set to one year. To include possible extreme values in the generated data, the simulation size is set to 5000. This results in a set of 5000 time series of one year with hourly intervals.

To generate the time series the following steps have to take place:

- Simulate binomial wave directions
- Generate Fourier series for the non-stationary components of the time series.
- Simulate stationary components with the estimated ARMA processes
- Combine the stationary and non-stationary components
- Transfer the standard normal time series back to all positive and skewed time series
- Add the deterministic part to the mean zero-crossing period
- Sample realistic wave directions for each binary wave direction.

The resulting set of 5000 time series of one year are analysed using fan charts (figure 6.14 and 6.15). In a fan chart, multiple line chart time series are combined, showing the ranges of possible values with the probability of occurrence. The fan charts of the observed significant wave height and observed mean zero-crossing period consist of the 28 years of observed data (figure 6.14a). To compare the observed data with the synthetic data, 20 of the 5000 synthetic wave time series are selected by Latin Hypercube sampling which is explained later in section 6.4 (figure 6.14b).

For the significant wave heights, the observed wave time series and the synthetic wave time series follow a similar behaviour (figure 6.14). The synthetic wave time series at IJmuiden Munitiestortplaats contains natural storm behaviour, as well as seasonal differences. Compared to the randomly generated waves without these effects, this is a large improvement (see figure 2.3). A noteworthy difference between the observed wave data and the synthetic wave data is, that the seasonal behaviour is more pronounced in the observed values than in the synthetic values. This difference will be further discussed in section 6.6. The mean of the significant wave heights for the simulated and the observed data are 1.25 m and 1.29 m respectively.

For the mean zero-crossing periods, the main difference between the observed and synthetic values

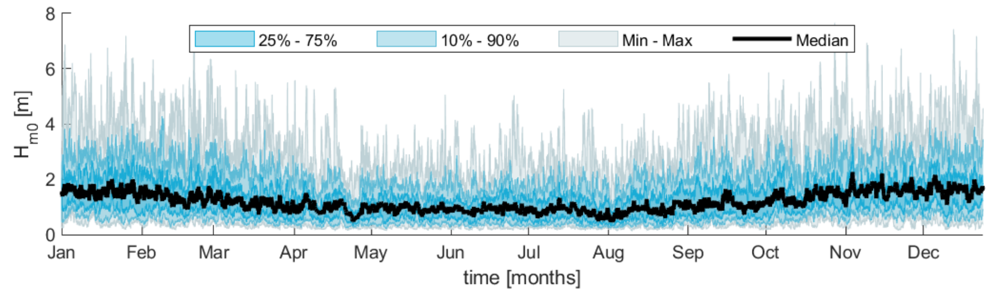

(a)

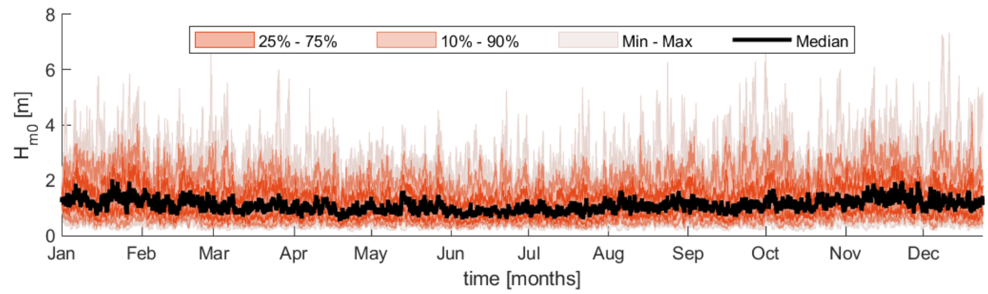

(b)

Figure 6.14: Fan chart time series of the significant wave heights at IJmuiden Munitiestortplaats. In (a) the observed wave time series and in (b) the synthetic time series.

is that the standard deviation in the synthetic values appears to be larger (figure 6.15). Furthermore, the synthetic data show more short term fluctuations than the observed data. The total means of the observed and the synthetic data are 4.52 s and 4.48 s respectively, so the wave periods of the synthetic data are slightly lower on average.

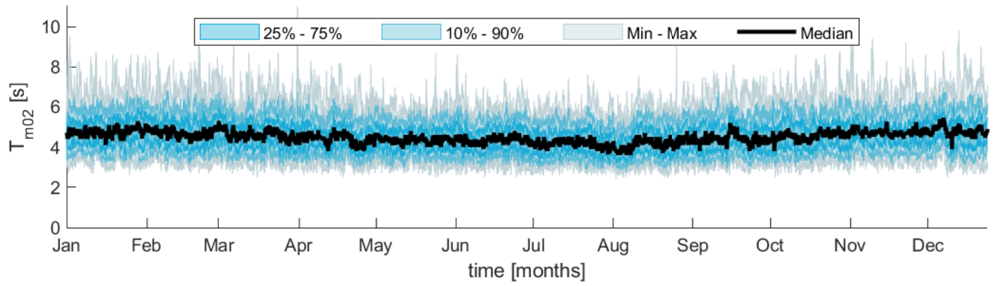

(a)

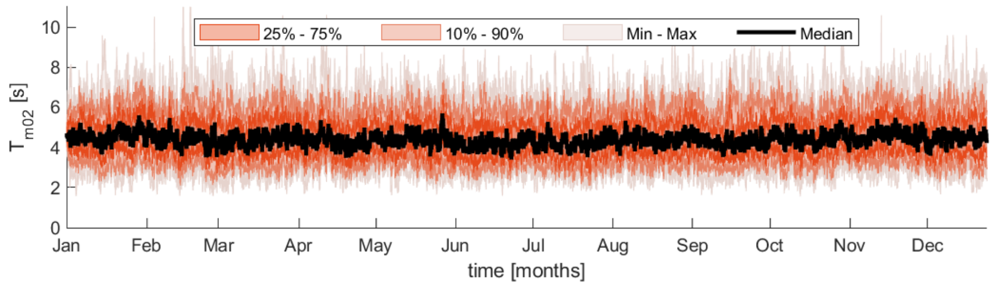

(b)

Figure 6.15: Fan chart time series of the mean zero-crossing period at IJmuiden Munitiestortplaats. Time series of the mean zero-crossing wave period for 28 years. In (a) the observed wave time series with the blue colours and in (b) the synthetic time series with the red colours.

6.2. Simulate time series for Eierlandsegat and Europlatform

For the wave transformation from offshore to nearshore, wave data from IJmuiden Munitiestortplaats (IJM), Europlatform (EUR), and Eierlandsegat (EIE) are required. Until now only the data at IJM are simulated. When the wave time series at EUR and EIE are simulated separately from the time series at IJM, unrealistic momentary differences between the time series will occur because the wave time series are correlated in time. Therefore, the time series in EUR and EIE are generated only by modelling the differences between IJM and EUR, and between IJM and EIE. The location of IJM is relatively nearby the Honsbossche Dunes compared to the locations of EIE and EUR. Therefore the time series at EIE and EUR are of minor influence to the waves at the Hondsbossche Dunes, given that they are in the same order of magnitude. As their influence is small, the models for EIE and EUR are highly simplified. Similar to the simulation of wave time series at IJM, for the waves at EIE and EUR the H_{m0} and T_{m02} are first transformed to standard normal and the deterministic part of the mean zero down-crossing period is removed. Instead of decoupling the data into a seasonal and a stationary component, an ARMA model is estimated for the differences between the normalised time series. With these ARMA models, the difference between the time series at IJM, and EUR and EIE can be simulated (figure 6.16). This method incorporates the behaviour of the synthetic wave time series at IJM in EUR and EIE.

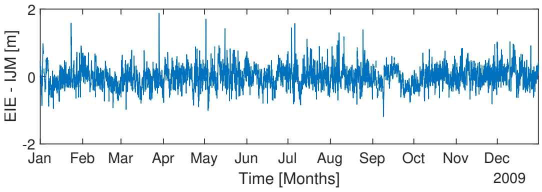

(a)

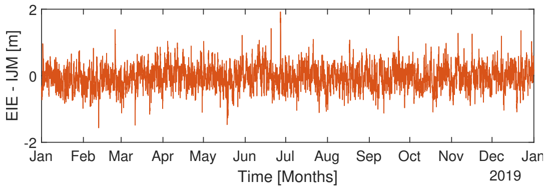

(b)

Figure 6.16: One year of the time series of the observed and simulated differences between the normalised significant wave height at Eierlandsegat and the normalised significant wave height at IJmuiden Munitiestortplaats. In (a) the observed differences in blue, and in (b) the synthetic time series in orange.

Table 6.5: Estimated ARMA coefficients for the differences between the stationary components of the data at IJmuiden Munitiestortplaats with the data at Europlatform and Eierlandsegat. For both the locations, ARMA models are estimated for the significant wave height (Hm0), the mean zero-crossing period (Tm02), and the wave direction (Hdir). Also, the parameters for the model for the surge are given. The accompanying AIC values and the parameters for the residuals (ϵ) are also given. The residuals are approximated by a Gaussian family which can be parameterized by the mean (μ) and standard deviation (σ).

	AR(1)	MA(1)	MA(2)	AIC	ϵ (μ, σ)
$[\text{IJM-EIE}]^{(\text{Hm0})}$	0.87	-0.12	0.03	-1.48e5	(0,0.18)
$[\text{IJM-EIE}]^{(\text{Tm02})}$	0.74	-0.03	-	1.68e5	(0,0.38)
$[\text{IJM-EUR}]^{(\text{Hdir})}$	0.84	-0.04	0.06	-1.31e5	(0,0.18)
$[\text{IJM-EUR}]^{(\text{Hm0})}$	0.69	0.12	-	2.2e5	(0,0.42)
$[\text{IJM-EUR}]^{(\text{Tm02})}$	0.90	0	-	1.59e6	(0.42,22.87)
$[\text{IJM-EIE}]^{(\text{Hdir})}$	0.89	-0.04	-	1.58e6	(0.31,22.32)
Surge	0.88	-	-	2.48e5	(0.02,0.09)

6.3. Simulate surge

Water levels are an important parameter for the XBeach model. As explained in section 3.2.2 the astronomical and water level data from IJmuiden Stroommeetpaal (SPY) are used. First, the surge data are derived by subtracting the astronomical tide from the water level. The surge is correlated with the significant wave heights (figure 6.17). Observed values of the significant wave height, which are transformed to the nearshore location of the Hondsbossche Dunes, are compared with surge levels at (SPY). A linear regression is fit through the relation between the surge and the significant wave height of the observed data. With the MATLAB curve fitting toolbox a relation in the form of $y = Surge - x * Hm0$ is determined. Whereby x is found to be 0.15 and y is the surge without correlation with the significant wave height (figure 6.17). For the remaining surge time series, an ARMA model is estimated. The model which describes the remaining surge time series best is an ARMA process of the order $(1, 0)$.

With this ARMA model surge levels are generated for every time step in the generated time series for IJM. The linear relation with the wave height is added to the surge after transforming the waves to nearshore. One year of astronomical tidal data is added to this surge time series to obtain water levels. For this, the astronomical tide at Petten is used from January 2019 until December 2019. This method is not very accurate as the relation between the surge and the significant wave height is not linear (figure 6.17). Furthermore, besides the relation of the mean of the surge, and the significant wave height, the variance of the surge is also influenced by the wave height. This is not taken into account in this model, hence the large differences between the observed and simulated data in figure 6.17. However, the larger part of the water level is the astronomical tide, therefore this simplified method to simulate the surge is considered to be accurate enough.

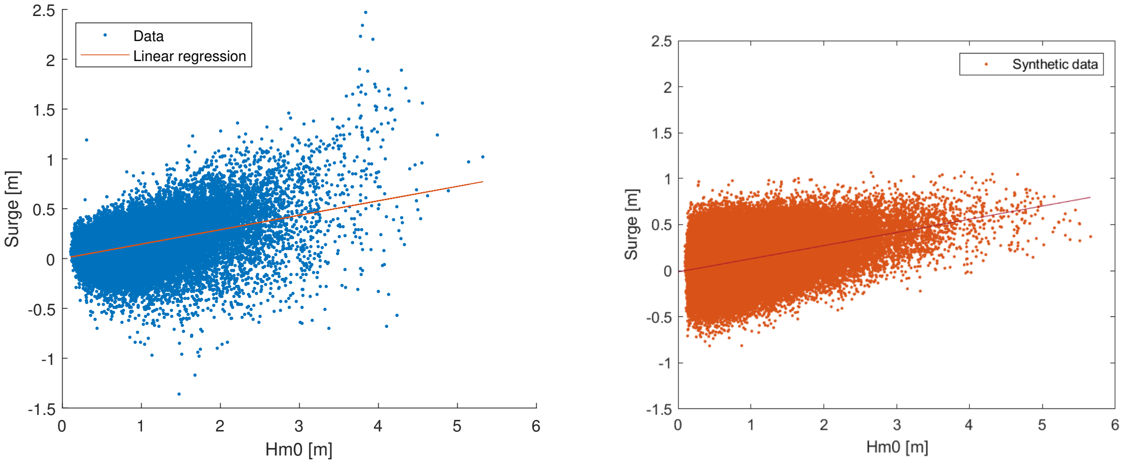

(a) (b)

Figure 6.17: Scatterplots with significant wave height transformed to the Hondsbossche Dunes on the x-axis, and surge levels at IJmuiden Stroommeetpaal on the y-axis. The red line indicates the linear regression. In (a) the observed data and in (b) the synthetic data

6.4. Latin Hypercube Sampling

As the simulation time in XBeach must be limited, Latin Hypercube sampling (LHS) is used to efficiently sample time series where the variability of all time series is represented by the least possible samples. In section 2.5 LHS is briefly explained. In section 3.4.4 the method whereby LHS is used in this study is explained. In this section, LHS is further elaborated and the results are presented. The first step is to determine the variables on which the sampling is based. Thereafter the sampling itself is explained together with its results.

Wave energy

An important parameter in the simulation is the average wave energy per simulated year. This parameter is important because the change in beach width is expected to be strongly related to the average wave energy. Therefore, the average wave energy per year is the parameter whereby the data series are sampled. As the direction of the wave energy is also expected to be important for the change in beach width, the average wave energy is split into average wave energy in x-direction representing the longshore direction, and average wave energy in y-direction, representing the cross-shore direction. It is evident that the distribution of the simulated average wave energy has to resemble the distribution of the observed average wave energy. In figure 6.18 the wave the observed wave energy is compared to the simulated wave energy. Each data point gives the average wave energy for one year in x- and y-direction. Next to the x- and y-axis the probability density plots for the average wave energy per year are given. It can be observed that there is some difference between the observed and the simulated average wave energy per year. The probability density of the simulated wave energy in x-direction is reasonably similar to observed wave energy in x-direction. In y-direction, the observed wave energy has a larger spreading than the wave energy of the synthetic data. Furthermore, the observed values have a stronger correlation between the wave energy in x- and y-direction.

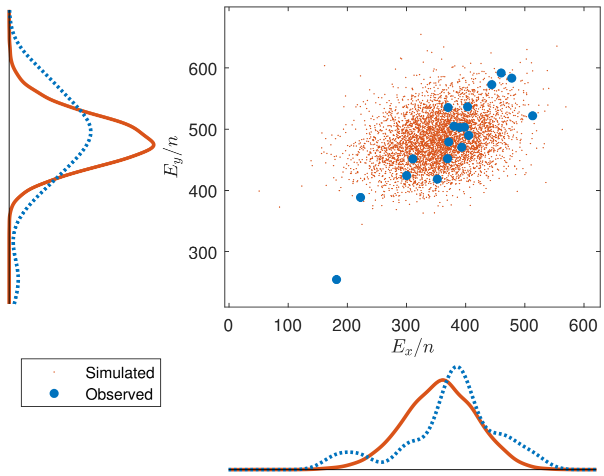

Figure 6.18: Scatter plot with the weighted wave energy in x and y directions on respectively the x and y axis.

Latin Hypercube sampling

The sampling of representative wave time series is described here step-by-step. In this study two variables are used for sampling, resulting in a 2-dimensional space which is convenient for visualising the sampling procedure.

For the generation of the first 5 samples, the first step is to rank the samples for both variables. This results in figure 6.19a, where the data has a uniform distribution in both the x- and y-direction. The next step is to divide each column and row in 5 equal density spaces. In Latin Hypercube sampling one square is randomly selected in every row and every column so that each row and column only contain one selected square. However, this does not consider correlated values. Since the wave energy in x- and y-direction are correlated, the selected squares must be correlated as well.

Iman and Conover (1982) described a method whereby Latin Hypercube sampling can be applied on correlated variables. A Cholesky decomposition is used to generate correlated random variables with a correlation similar to the correlation of the original data (Iman & Conover, 1982). This is an option in the MATLAB function *lhsgeneral* by which correlated Latin squares are selected. These selected Latin squares are given by the purple areas in figure 6.19b. In each of the squares, one random value is selected by simple random sampling, given by the red marks in figure 6.19b.

When increasing the sample size, the first samples have to be taken into account to maintain the Latin Hypercube properties (see section 3.4.4. To increase the sample size form 5 to 10 samples, 5 additional samples have to be selected taking the first 5 into account. The procedure, as described by Sallaberry et al. (2008) is as follows: Similar to the first 5 samples, 5 additional Latin squares are selected using the Cholesky matrix, regardless of the first 5 samples. These additional squares are given in light green in figure 6.20a. These squares are divided into four equal squares. Every larger light green square contains one smaller square which has no sample in its row or column. These are indicated by red squared lines in figure 6.20b. In each of these smaller squares, one value is randomly selected.

To further increase the sample size, the previous procedure is repeated. Ten squares are randomly picked with the Cholesky matrix, given by the green squares in figure 6.21a. These are divided in four, and from the section which contains no sample in the column or row one sample is selected.

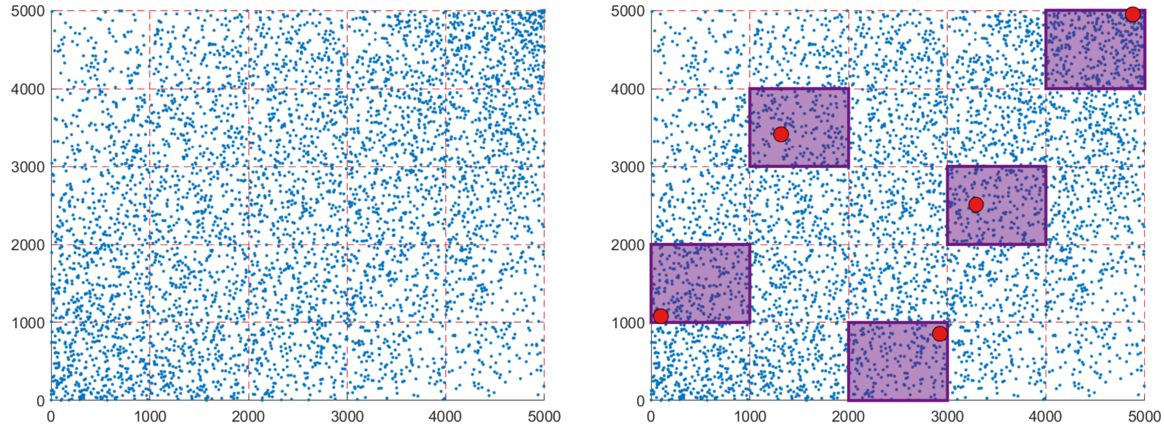

(a) (b)

Figure 6.19: Data points containing the rank of the total wave energy in x- and y-direction. In (a) the ranked data points are divided in five equal density rows and columns. In (b) one rectangle is selected in each row and column, and a random samples is selected in each rectangle.

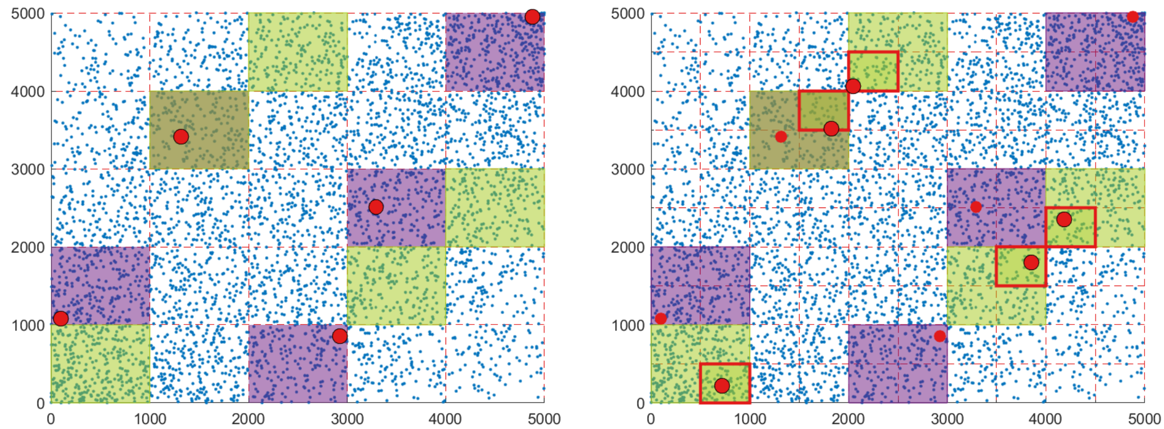

(a) (b)

Figure 6.20: Increasing the sample size from five to ten. In (a) five additional rectangles are selected in green. In (b) all rectangles are split into four. Of each large green rectangle, the smaller square which contains no previous selected data point in its row or column is selected, highlighted by a red border. Out of these smaller squares a random data point is sampled.

6.5. Wave transformation to near-shore

The sampled wave time series are offshore wave data from IJmuiden Munitiestortplaats (IJM), Eierlandsegat (EIE), and Europlatform (EUR). The last step in generating synthetic data as input for XBeach is to transform this offshore wave data to the nearshore location of the case study.

The results of the transformed time series are given in figure 6.22 where the first 5 samples of the time series are given. Each sample is given by a different colour. The gaps in the time series are due to the offshore directed waves, where the beach profile is assumed to be stable (section 3.4.5)

While until now in this chapter the wave period was given as the mean zero down-crossing period (T_{m02}), now it is transformed to the peak period. In the transformation table, the (T_{m02}) is transformed to the T_p by multiplication with a factor 1.28, which is a standard factor for a JONSWAP spectrum.

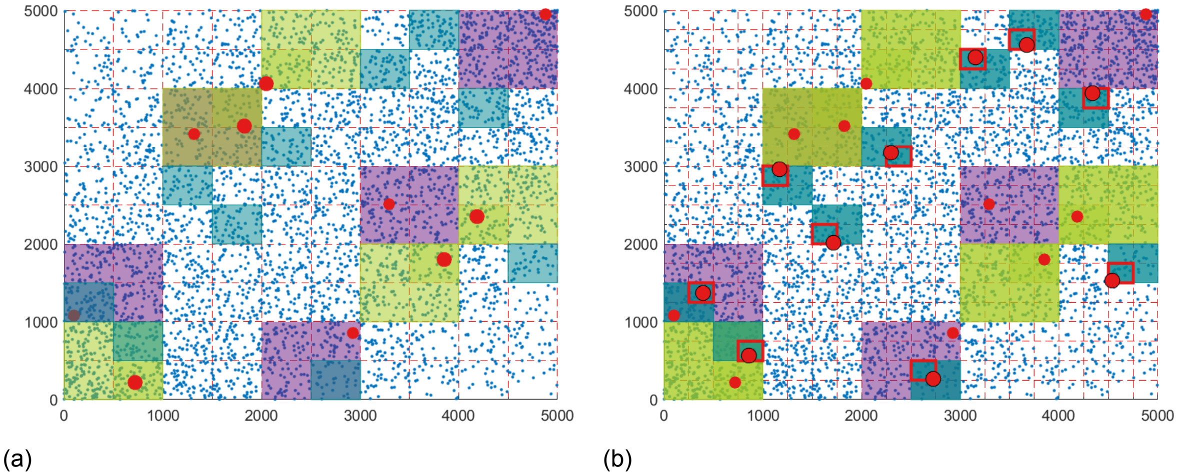

Figure 6.21: The process of increasing the sample size from 10 to 20. Similar to the method in figure 6.20

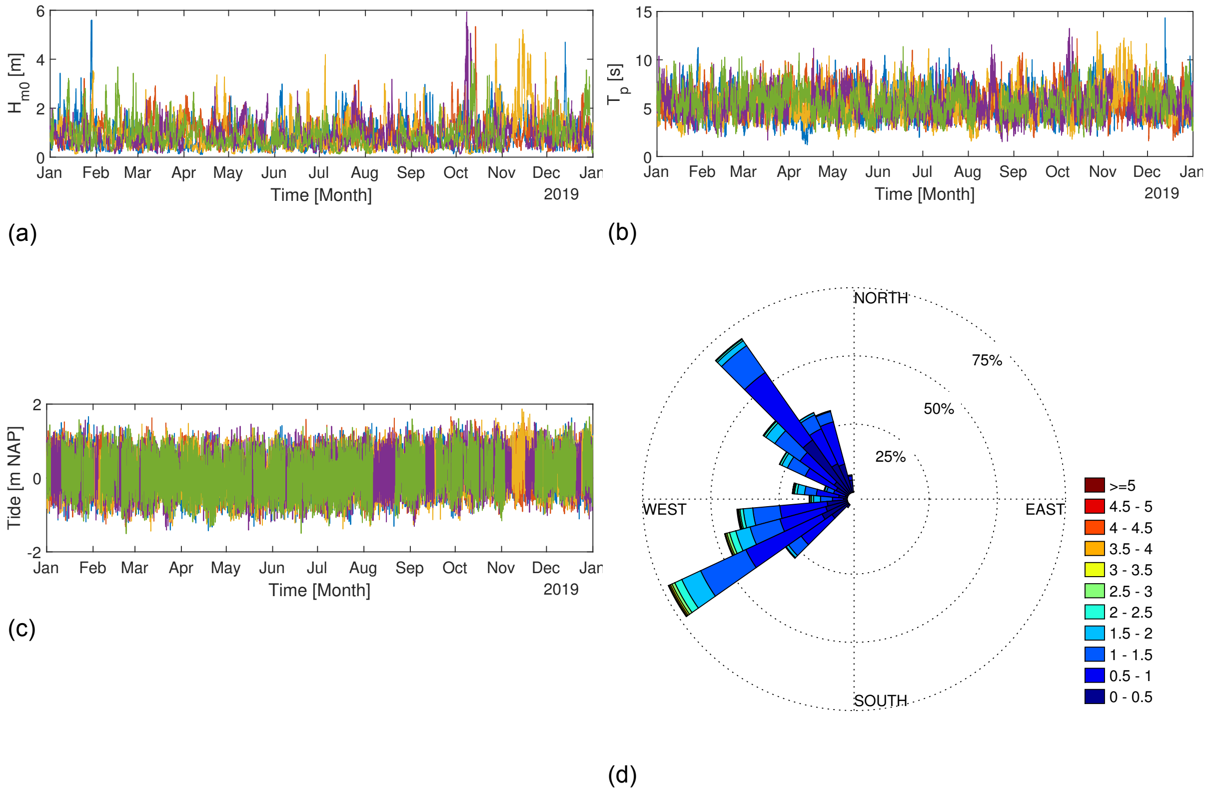

Figure 6.22: Results of the transformed synthetic hydrodynamic data. In (a) the time series of the significant wave height (H_{m0}) is given, (b) shows the peak period (T_p), (c) shows the water level, and (d) is a wind rose of the wave directions of the first five samples. The first five time series of the transformed data are given, each time series in (a), (c), and (d) is indicated by a different colour.

6.6. Validation

To validate the synthetic time series, the 20 samples of the synthetic wave time series, transformed to the nearshore study location, are compared with the transformed observed wave time series. The time series of the observed significant wave heights (figure 6.23a) give a similar pattern as the synthetic significant wave heights (figure 6.23b). However, the seasonality is more obvious in the observed wave time series. This is was already observed with the wave time series at IJmuiden Munitiestortplaats, and this behaviour remains in the transformed time series. The mean of the wave heights during the storm season, from October to April, is higher for the observed wave heights than for the synthetic wave heights. During the calm season, from April to October, the mean of the significant wave height is lower for the observed data than for the synthetic data (table 6.6).

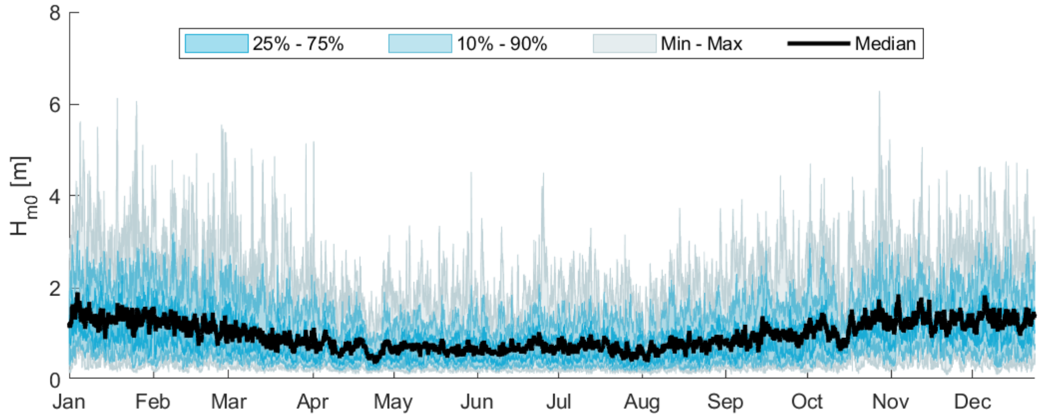

(a)

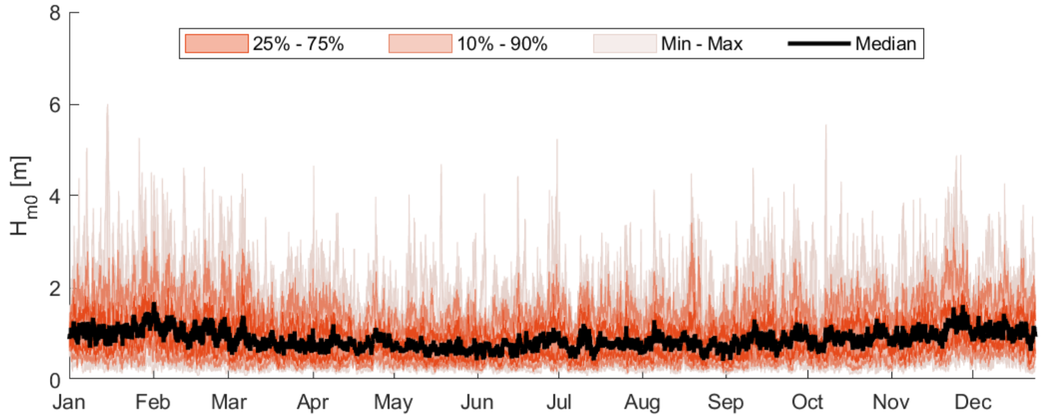

(b)

Figure 6.23: Variability of the significant wave height. In (a) a fan chart with the significant wave height with 27 years of transformed wave data from IJmuiden Munitiestortplaats, Europlatform, and Eierlandsegat, to the location of the Honsbossche Dunes. In (b) the values of 20 years of synthetic generated wave data.

Table 6.6: Mean values of synthetic and observed significant wave heights

	Total mean [m]	Mean storm season [m]	Mean calm season [m]
Observed H_{m0}	0.99	1.21	0.77
Synthetic H_{m0}	0.93	1.0	0.86

To further analyse the source of the difference between the synthetic wave time series and the observed wave time series, the stationary components and non-stationary components are separated. The moving average component (μ^{Hm0}) of the synthetic time series shows a similar pattern as the moving average component of the observed time series (figure 6.24a and 6.24b). The observed component shows more short term fluctuations with a larger variance, which are not represented in the synthetic time series. The magnitudes and patterns of the seasonal mean are similar for the synthetic data and the observed data.
For the standard deviation (σ^{Hm0}) of the seasonal component, the synthetic data represents the observed data quite well (figure 6.24c and 6.24d). Similar to the moving average, the standard deviation of the observed time series contains more short term fluctuations. The difference in the short term fluctuations between the observed and the synthetic time series are not the reason behind the differences in the final time series, as the final time series of the significant wave heights appear to show more short term fluctuations with the synthetic data.
So both the mean and the standard deviation of the seasonal components appear to be properly sim-

ulated. The more pronounced seasonality in the results of the wave time series of the significant wave heights, seem not to emerge from the model of the seasonal components.
The origin of the seasonality difference appears to be the model for the stationary component. The stationary component of the observed significant wave height (z^{Hm0}) still appears to contain some seasonality, as the median is higher in the storm season than in the summer season (figure 6.24e). The stationary component of the synthetic significant wave heights do not show this seasonality (figure 6.24e).

The cause of this remaining seasonal trend may lie in the process of decoupling the observed wave time series.

Despite this difference in seasonality, the synthetic wave time series represent the observed wave time series reasonable well. These synthetic wave time series are considered to be adequate to use for the stochastic forecasting. Further improvement of the synthetic data is therefore beyond the scope of this study.

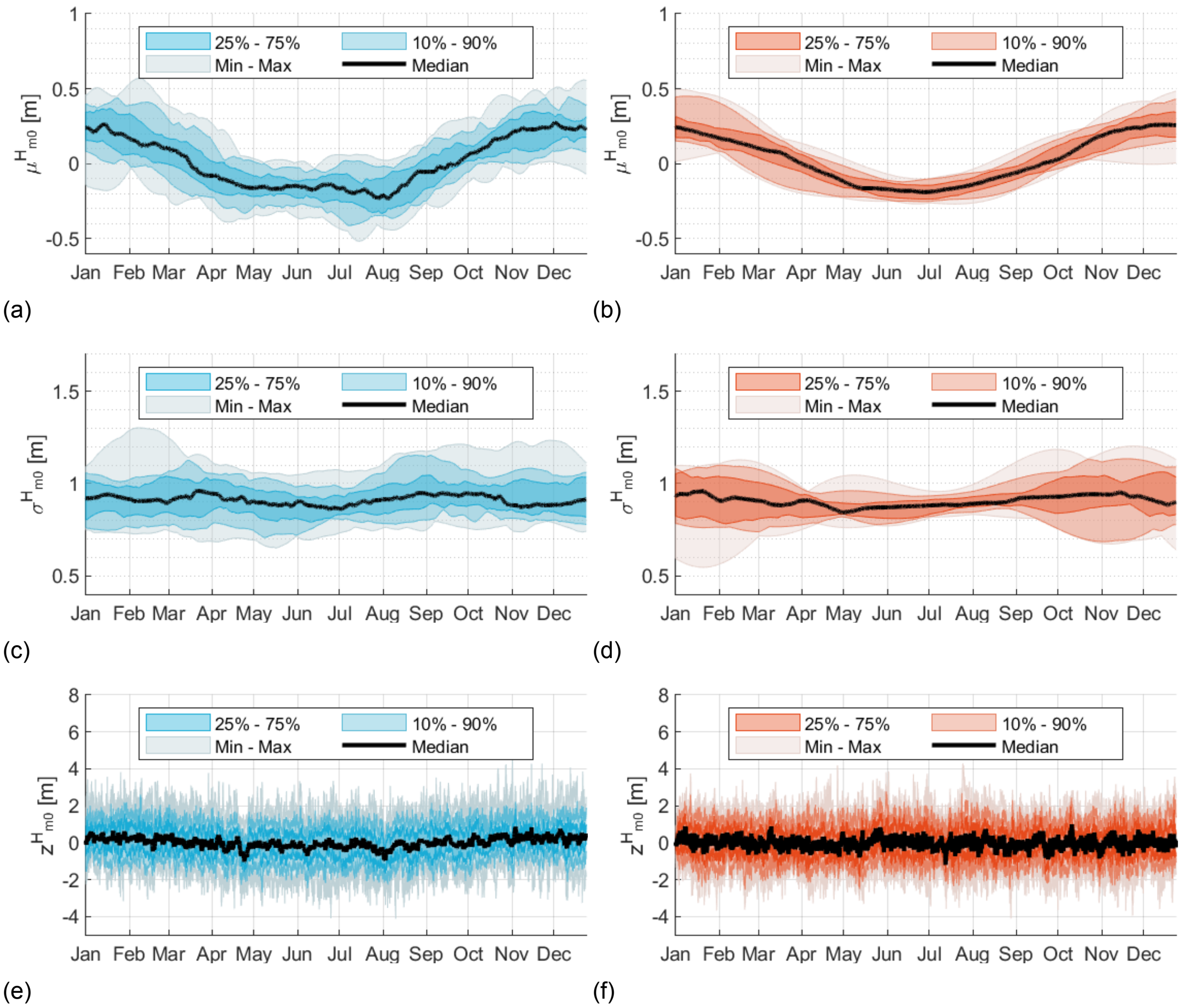

Figure 6.24: Time series of the significant wave height split in a stationary and a non-stationary component. The observed data is given in blue and the synthetic data in red. Figures (a) and (b) show the slowly varying mean of the significant wave heights. (c) and (d) show the slowly varying standard deviation. The stationary components for the observed and synthetic time series are given in (e) and (f).

6.7. Conclusion

The sub-question which is answered in this chapter is "How can stochastic forcing conditions be generated for a near-shore location?". These stochastic forcing conditions consist of time series of hydrodynamic conditions of the significant wave heights, mean zero-crossing periods, wave directions, and water levels. To answer this question, an advanced method for generating wave time series, based on ARMA processes, is applied for the location of the Hondsbossche Dunes. This results in a set of 20 time series of one year, with a one-hour interval rate.

The result shows how stochastic forcing conditions can be generated for a near-shore location and thereby answers the sub-question. Whether this method is effective is debatable and depends on the purpose. The advantages and disadvantages of this method can be summarised as follows:

+ The generated time series contain seasonal differences
+ The generated time series contain storm behaviour
+ The method is easily extended to other locations

– The method contains many modelling steps, this can introduce additional uncertainties
– Generating the wave time series is relatively time-consuming compared to other methods.

For the synthetic wave time series generated in this chapter, the main differences with the observed wave time series are the magnitudes of the seasonal differences. This inaccuracy seems to result from an error in the decomposition of the wave time series into a stationary and non-stationary component. This inaccuracy is not necessarily a deficiency in the method, as this did not occur in the results of this method in Jäger (2018). This inaccuracy can likely be resolved in further research, which is beyond the scope of this study. The generated synthetic wave time series are considered accurate enough to use as forcing conditions for the stochastic forecasting with XBeach.

7

Stochastic forecasting with XBeach

The calibrated XBeach model (chapter 5) and the synthetic forcing time series (chapter 6) are used for a stochastic beach width prediction. In this chapter, the stochastic XBeach model is examined. First, the sample size is reviewed in section 7.1, in section 7.1.1 the beach width development results of the XBeach model are presented and explained, which is the principal result of this study. In subsection 7.1.2 this result is validated.

7.1. Sample size evaluation

The sample size is evaluated by varying the sample size and analysing the resulting distribution of the beach widths until the sample size is considered sufficient. The sample size is considered to be sufficient when increasing the number of samples does not affect the probability density function of the resulting beach width. A number of 5, 10, and 20 time series are successively sampled and used as XBeach input. The probability density of the beach width difference changes significantly when increasing the sample size from 5 to 10 (figure 7.1a). When increasing the sample size from 10 to 20, only little difference is observed in the probability density functions. The median values seem to converge towards around -50 m (figure 7.1b). The domain is 111 m for all sample sizes because the smallest and largest values for the 20 samples, already occur in the first five samples. Note that the sample size is analysed by a kernel smoothing density estimate, therefore the curves are smooth, even for a sample size of 5. A sample size of 40 is expected to show a similar probability density distribution as 20 samples. Verifying this would require an extra week of computation time. For this study, the convergence towards the sample size of 20 is considered enough and the result for 40 samples is not examined.

7.1.1. Beach width development

The primary result of the XBeach model with synthetic data is the beach width development for each sample. For all 20 samples, a beach profile is generated with time steps of one day. These 20 XBeach computations for one year of data result in 20 beach profile developments. After the simulation with a run duration of one year, the resulting beach profiles show a range of outcomes (figure 7.2). The initial profile shows a high beach area at a bed level of 3 m, at the x-coordinates between 2200 m and 2350 m. In all resulting profiles, this nourished beach area decreases. In the least severe case, the high beach area is approximately halved. In the most severe case, the nourished area of + 3 m is totally dispersed.

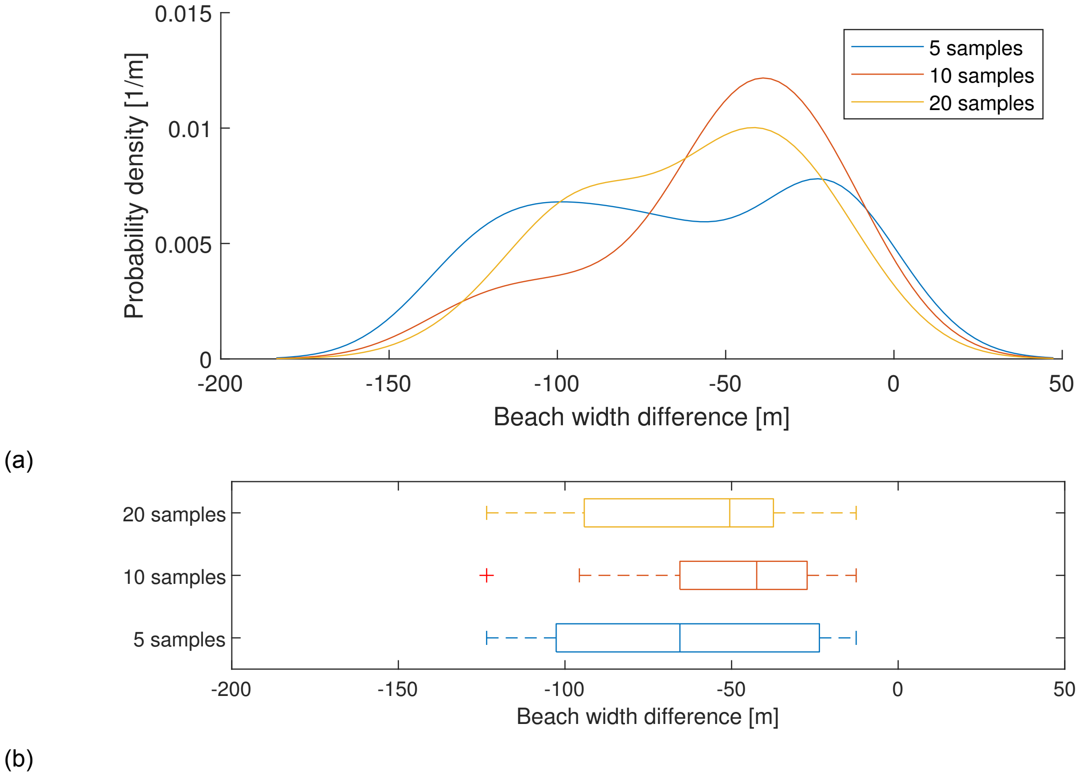

Figure 7.1: Distribution of the beach width difference after one year with respect to the initial beach width, with a sample size of 5, 10, and 20. In (a) the Probability density functions of the beach width difference is given per sample size. In (b) box plots are given for each sample size.

The beach widths of these profiles are determined by a volume integration between the mean high water level and the mean low water level (figure 2.1 section 2.1). To analyse the beach width difference, the initial beach width is subtracted from the simulated beach width for each profile. The 20 beach width difference profiles are summarised in a fan chart showing the range of possible values and their likelihood (figure 7.3). When looking at the median of the fan chart, a gradual reduction in beach width is

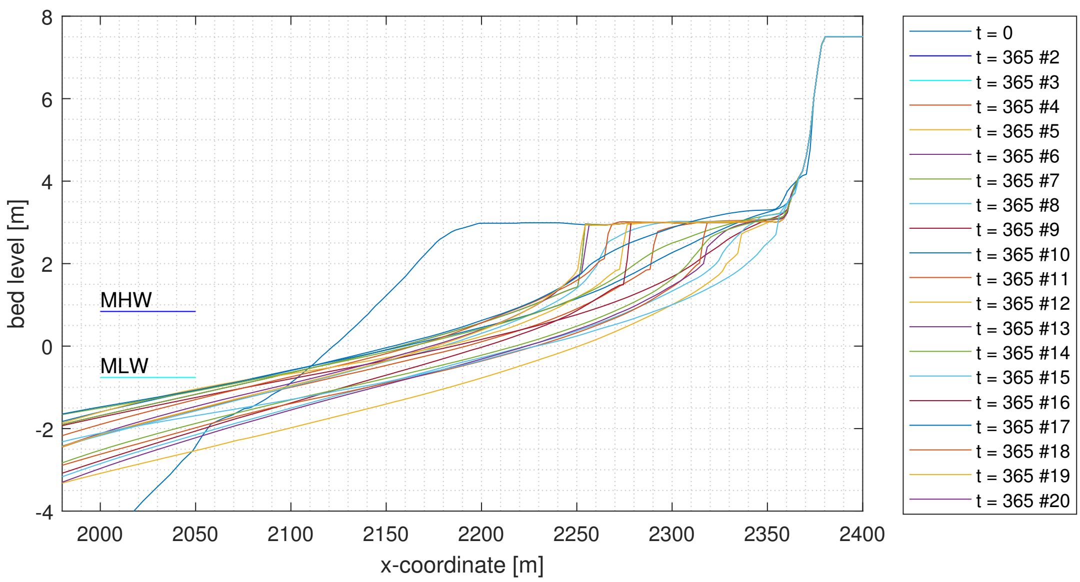

Figure 7.2: Final beach profiles generated with XBeach. The blue line with 't = 0' gives the initial profile, the other profiles are the results after 265 days of synthetic wave forcing.

observed. During the storm season, from October to April, this reduction is stronger than in the summer season from April to October. So the seasonal differences in the wave time series are reflected in the beach width results. The model results show a probability of 80% that the beach width after one year of wave exposure has changed by between -18 m and -98 m.

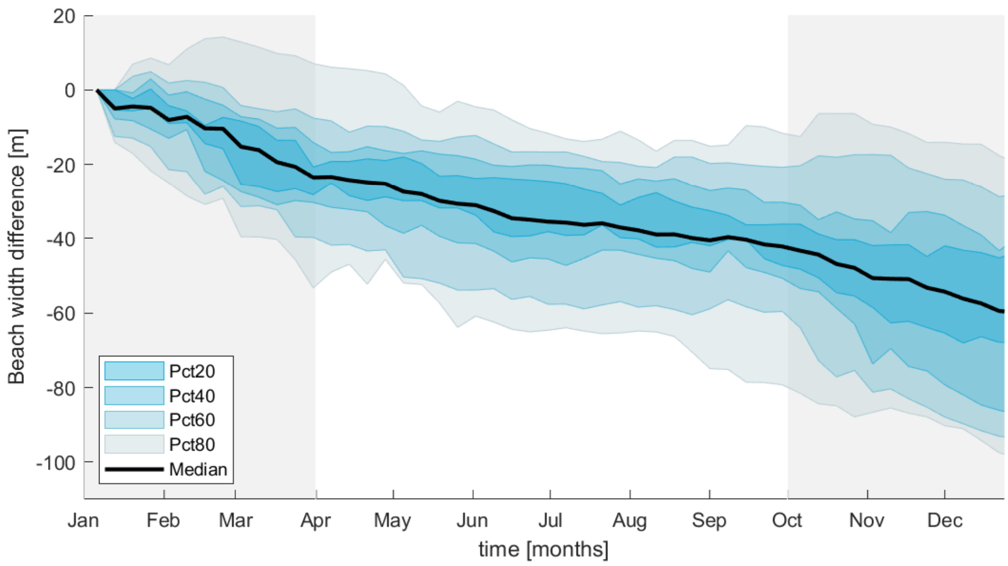

Figure 7.3: Fan chart containing the development of the beach widths with respect to the initial beach width. The fan chart data are based on the 20 beach profiles resulting from the XBeach models with synthetic data. The median and the 20%,40%,60%, and 80% probability ranges are shown. The winter period, between October and April, is shaded in grey.

Remarkably, the results show that the beach width can also increase by over 20 m within two months, suggesting accretion on the study location. However, when taking a closer look at the intermediate cross-shore profiles, the increasing beach width appears not to be a result of solely accretion, but also of erosion. When the waves hit the dune foot in an event where high tide and high waves coincide, a significant amount of sediment is transported from the higher beach and spread over the foreshore, causing an increased beach width (figure 7.4).

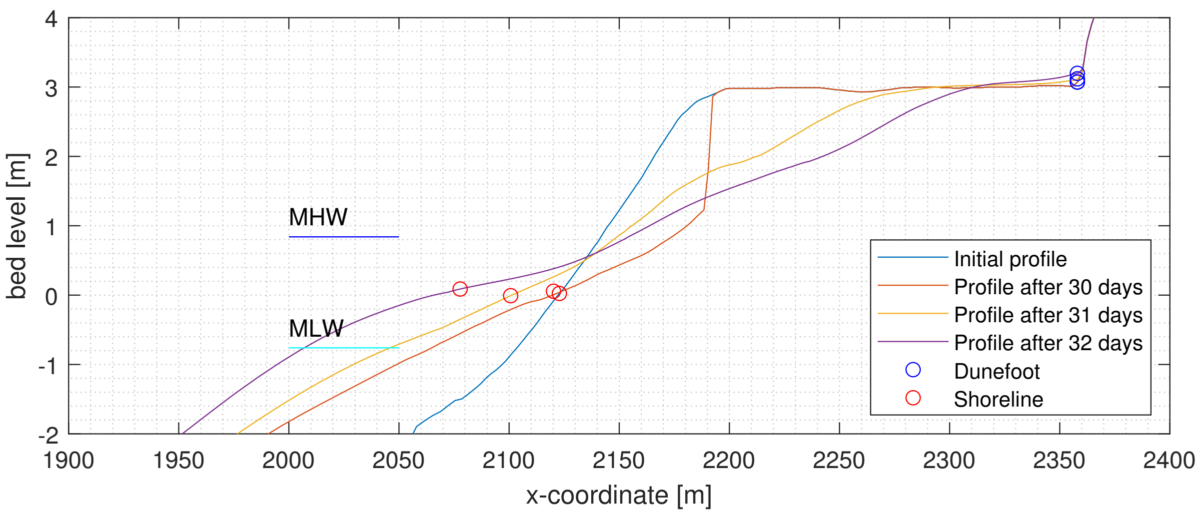

Figure 7.4: Illustration of a beach width increase during an energetic event. The initial profile is given in blue, the orange line gives the pre-storm profile after a model time of 30 days. The yellow profile gives a profile during the storm at 31 days and the post-storm profile is given in purple. The shoreline and dune foot are indicated by a red and blue 'o' respectively.

7.1.2. Validation

It is difficult to validate the synthetic wave data with these observed data points. The synthetic wave data are based on a range of hydrodynamic time series, while the observed data points are only based on one time series, i.e. the observed hydrodynamic conditions. This must be kept in mind for the validation.

To validate the model, the weekly averaged beach width change of the forecast data is compared with the beach width change per day of the observed data (figure 7.5).

The beach width change is weekly averaged because the period between the observed data points is in the order of weeks. Shortening the period where over the data are averaged, increases the fluctuations and bandwidth of the fan chart. Conversely, increasing the interval over which the data are averaged flattens would flatten and decrease the width of the fan chart. This behaviour should be kept in mind when comparing the synthetic with the observed beach width change per day.

During the winter season, the magnitude of the beach width change per day is larger than during the summer season. Furthermore, the probability range of the beach width change per day is larger in the winter season. The synthetic data show some fluctuations, especially in the winter season. These fluctuations are due to coinciding events of either a high, or a low beach width change from the different samples. These coinciding events are by chance. There is no physical reason that would clarify that the probability range of the beach width change per day is larger at the beginning of November than at the end of November, while the results do suggest this. Taking a larger sample size would flatten these fluctuations.

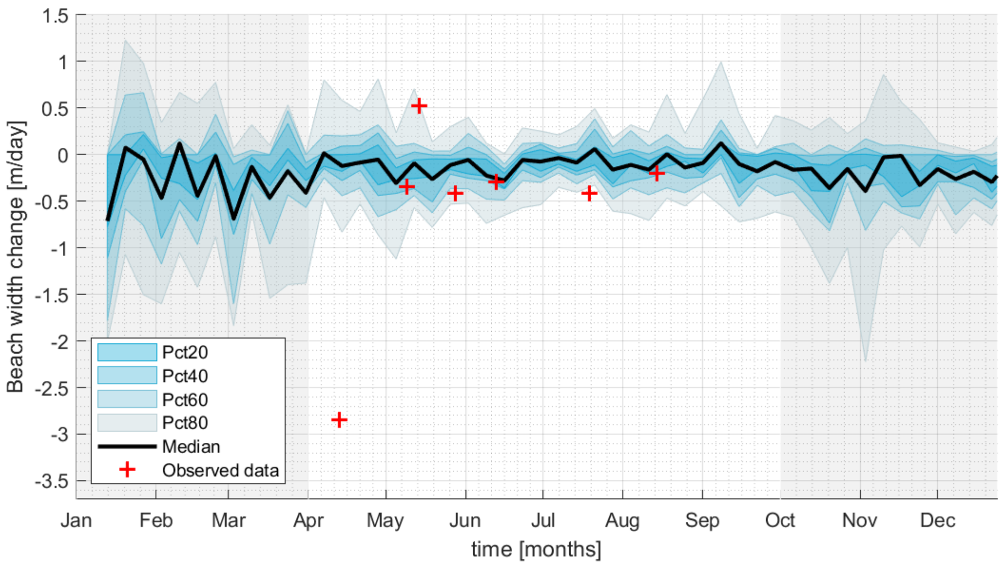

Figure 7.5: Illustration of the beach width change per day. The black line gives the median of the beach width change per day from the XBeach forecast. These data are weekly averaged. The blue colours indicate the 20%, 40%, 60%, and 80% probability ranges. The red '+' markers indicate the observed data.

The observed data points show the average beach width change per day between the surveys from April to September. The first point shows a beach width decrease per day between the first and the second survey. With a beach width change of -2.8 m per day, this data point falls outside the 80% probability range of the synthetic data. This first survey was shortly after the nourishment. Possibly, the beach width change is more extreme during the first weeks after a nourishment. A likely reason for a more extreme beach width change shortly after the nourishment is because the beach is not yet in a natural profile. The other observed beach width change data points are in better correspondence with the synthetic data. The third point shows an increase of 0.5 m, which is relatively high compared to the synthetic data, but not an exceptional value. The data point in July, 19th, lies just outside the 80% probability range; however, this is due to the coincidental fluctuations. The other data points are all just below the median of the synthetic results, but well within the probability ranges. This indicates a high, but not extraordinary beach width decrease per day in the observed data.

To further compare the synthetic to the observed results, the mean and standard deviation of the beach width decrease per day is analysed (table 7.1). The mean and standard deviation of the synthetic data is divided in the winter and summer period. The observed data is only gathered during the summer period. Therefore the observed data should be compared to the synthetic data in summer. The mean and standard deviation of the observed data is divided into the data sets both in- and excluding the first data point. The mean of the beach width change per day for the synthetic data is -0.10 m. This is 140% difference with the observed value of -0.57. When excluding the first data point, the synthetic data and the observed data are 62% apart, with an observed mean of -0.19 m. So the magnitude of the mean of the synthetic data is slightly low compared to the observed data. Also for the standard deviation, the synthetic data seems to be inaccurate when including the first data point, with a 79% difference between the synthetic data and the observed data. While excluding the first data point results in a 31.2% difference. The standard deviation of the synthetic data is high compared to the observed data.

The synthetic data consists of a set of 20 time series. The mean of the beach width change per day for the synthetic data is actually the mean of the 20 means. The standard deviation of these 20 mean beach width change per day values is 0.08 m. So the observed mean beach width change per day of the data points excluding the first anomaly deviates slightly more than one standard deviation of the synthetic mean during summer. This can be a reasonable difference. The standard deviation of the 20 standard deviations of the beach width change per day during the summer is 0.11 m. So the observed standard deviation is less the one standard deviation apart from the synthetic standard deviation.

Overall the observed beach width change per day falls well in the range of possible synthetic data values, except for the first data point.

Table 7.1: Mean and standard deviation of the weekly averaged beach width change per day for the synthetic and the observed data. For the synthetic data, the values are separated in the winter and summer period. For the observed data, data is only gathered during the summer period. The mean and standard deviation of the observed data are separated in data points 1:7, including the first outlying observation, and 2:7, excluding the first outlying observation.

	Synthetic data			Observed data	
	Winter	Summer	All	Data points 1:7	Data points 2:7
Mean [m]	-0.22	-0.10	-0.17	-0.57	-0.19
Standard deviation [m]	0.81	0.46	0.67	1.06	0.36

7.2. Conclusion

This chapter examined the stochastic beach width forecast by use XBeach. The sample size used for the stochastic forecasting is 20, defined on the basis of the convergence of the probability density distribution of beach width results. 20 sets of synthetic hydrodynamic forcing time series of one year are used as XBeach input. This results in a range of 20 possible beach profile developments. The beach width development of this stochastic forecast shows a gradual reduction of the beach width. The seasonal differences which are present in the wave data are reflected in the resulting beach widths. After one year, the beach width change has a median of -60 m and a probability of 80% that the beach width has changed between -18 m and -98 m. There is a 10% chance that the beach width decrease is larger than 99 m after one year. Finally, for the validation, the beach width change per day of the synthetic wave data is compared to the observed data. Apart from the first data point, the observed results are in the same range as the synthetic results. The first observed data point might be an anomaly because it was shortly after the additional nourishment and can, therefore, be left out of the validation. The mean values of the beach width change per day are -0.10 and -0.19 for the synthetic and observed values respectively. So the magnitude of the observed beach width change per day is large compared to the synthetic data. The standard deviation values of the beach width change per day are 0.46 and

0.36 for the synthetic data and the observed data respectively. The standard deviation of the observed data is high low compared to the synthetic data. Overall the observed beach width change per day falls well in the range of possible synthetic data values.

8 Discussion

In this study, a beach width prediction is carried out within a stochastic framework. This chapter summarises the key findings and clarifies the limitations of this study.

8.1. Key findings

This study demonstrates a method for an uncertainty assessment for beach width predictions within a stochastic framework for a recently nourished beach. This directly fulfils the main research objective, i.e. "Examine an uncertainty assessment method for beach width predictions by carrying out a beach width prediction within a stochastic framework at a recently nourished beach". The main result is a stochastic beach width prediction for the location of the Hondsbossche Dunes, directly after a nourishment. This stochastic beach width prediction shows the possible beach width development over one year, with its probability of occurrence. After one year, the results show that with an 80% probability the beach width decrease is between 18 m and 99 m.

The stochastic XBeach predictions give a good insight in the possible development of the widths of a beach with different annual wave forcing. A traditional deterministic model gives a 'most likely' scenario. The added value of this research are the probability ranges of the forecasting. A beach width prediction model has a large uncertainty, which should not be omitted. A relevant question which can be answered with a stochastic beach profile forecasting method can be "What is the probability that a new nourishment has to take place within a certain period?". The added value of this study lies not solely in the values found in the stochastic beach width prediction, but more in the method developed for this prediction.

This study combines an extensive method for generating stochastic wave conditions, with beach width modelling. The method used to create stochastic forcing conditions is based on Autoregressive-Moving Average Models. The beach width is modelled with an 1D XBeach model. In previous research, these two parts are separately studied before. An examination of the combination of these two parts is a useful contribution to the existing scientific knowledge.

The in this study developed stochastic beach width forecasting method, could be extended to other locations. Potential locations where this method can be applied are coastal regions where sufficient hydrodynamic data are available and an XBeach model can be applied. Besides applying the model at other locations, the model can potentially be used with a different simulation period of multiple years.

8.2. Limitations

There are some limitations to the created model, these limitations are discussed in this section.

Uncertainties

The uncertainty range from the result of this study is only based on the intrinsic forcing uncertainty for a beach width prediction, i.e. the uncertainty of future hydrodynamic conditions. Besides this uncertainty, there is a whole range of additional uncertainties which are not explored and included in this study. In Kroon et al. (2019) the effect of the model uncertainty is compared to the effect of the wave variability by varying both the wave climate and a model calibration factor. For multi-year time scales, the influence of model uncertainties can become dominant. Kroon et al. (2019) found that after a simulation period of 2.5 years the model uncertainty accounts for 50% of the total variance. Ignoring these model uncertainties leads to a too narrow bandwidth of the future beach width forecast. Therefore it is recommended that, in future research, epistemic uncertainties are taken into account for stochastic beach width forecasting.

Sampling parameter

With Latin Hypercube sampling, 20 hydrodynamic time series resulting in beach profiles are sampled, which should represent the whole range of possible results. This sampling is based on the total wave energy in x-, and y-direction. These parameters are used as sampling parameters based on the assumption that there is a strong correlation between the total beach erosion and the total wave energy. This assumption of the correlation between the total wave energy in x- and y-direction and the total beach width reduction is checked using the scatter plots (figure 8.1). No significant correlation is found between the total beach width decrease and the total wave energy. The correlation coefficient between the total wave energy and the beach width decreases is $r = 0.09$. The correlation between the beach width decrease in x- and y-direction give $r = 0.09$ and $r = 0.01$ respectively.

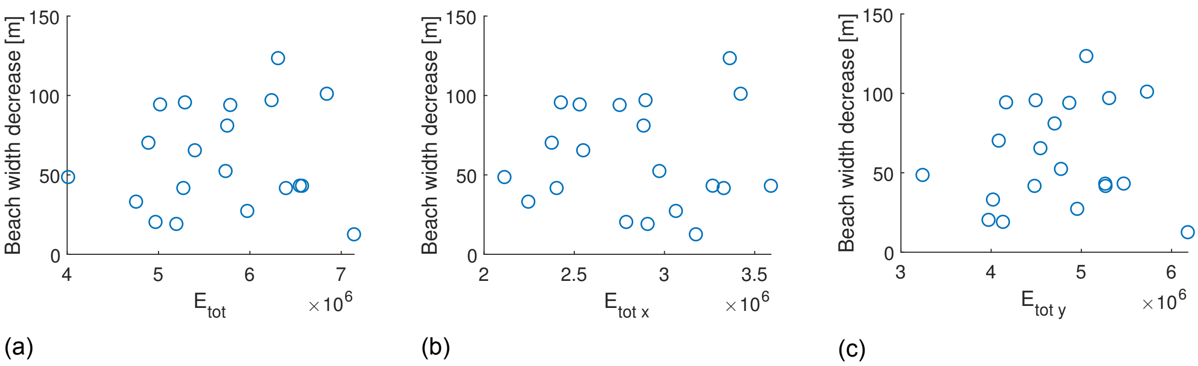

Figure 8.1: Scatter plots with the total wave energy and the total beach width decrease for all 20 simulations. In (a) the total wave energy in x- and y-direction is plotted against the total beach width decrease. In (b) and (c) the relation between the total beach width decrease and the total wave energy in x- and y-direction are given. The graphs reveal no significant correlation.

Apparently, the assumption of a strong correlation between the total wave energy and the beach width decrease is false. The reasoning behind this assumption is, that sampling 20 time series with a stratified wave energy in x- and y-direction leads to beach widths with a similar stratification, depicting the total range of possible beach widths. Since this assumption turns out to be false, the sampling method is random and the Latin Hypercube method loses its effect. However, convergence in the probability density of the beach widths indicates that the sample size is large enough (figure 7.1).

When analysing the individual beach width development in the results, the intensity of the strongest storms are more likely to be significant for the total beach width decrease. Especially when the highest water levels coincide with high significant wave heights, serious erosion takes place. Further research is recommended to indicate a more suitable sampling parameter.

Beach width as result

The beach width is the main parameter of interest in this study. However, an increase in beach width can also be the result of a high energy event, as explained in section 7.1.1. In the case used in this study, the beach is recently nourished and does not have a natural profile. When sediment from the higher part of the beach erodes, it can be deposited close to the shoreline, leading to an increase in beach width. An increase of the beach width does not always indicate less flood risk, as it can be the result of dune erosion after a severe storm.

Limitations in the synthetic time series model

In the simulation of the synthetic time series room for improvement can be found in several parts.

The surge should be simulated in more detail. The surge is of great influence in the development of the beach width because when an event with large significant wave heights coincides with a high water level, severe erosion can take place which is significant for the development of the beach profile.

The magnitude of the seasonality in the time series of the significant wave heights and the peak wave periods are underestimated in the synthetic time series in this study. The origin of the difference in the magnitude of the seasonality appears to be in the decoupling of the time series in seasonal and stationary components. This is not a flaw in the method, but in this study, choice was made not to further investigate and correct this, but to carry on with the results. Further research could investigate the impact of this deficiency and potentially correct this.

The limitations in the synthetic time series, are expected to be reflected in the beach width forecast. Although some seasonality is present in the beach width forecast, this seasonality is likely to be underestimated, just as in the hydrodynamic forcing conditions. The limited seasonality in the hydrodynamic conditions lead to an overestimation of the wave heights in summer and an underestimation of the wave heights during winter. During the summer season, the modelled beach width are therefore also likely to be overestimated, whereas the beach width decrease in winter is likely to be underestimated. The underestimation of the waves in winter is likely to be of greater effect than the overestimation in summer because in winter more, and higher storms are present. Therefore the overall effect of the limited seasonality is expected to result in an underestimated total beach width decrease.

The method whereby the synthetic time series are created is quite time consuming, as it contains many modelling steps. For academic purpose, an extensive description of the hydrodynamic behaviour is desired on a high temporal resolution. For practical purposes, a simplified method for the generation of synthetic wave data might be more sensible. The large number of modelling steps in the creation of the synthetic wave data can lead to more model uncertainties. In further research, it is interesting to compare the wave simulation method based on ARMA models as described in this study, to a wave simulation model based on a random monthly selection.

During the process of transforming the offshore wave time series to the nearshore, the wave periods appear to lose accuracy. During the validation of the transformed data, the correlation between the transformed peak period, and the observed peak period appears to be weak. However, the inaccuracy is not clearly bias to either side. So the wave period is both under- as overestimated. Therefore the influence of this limitation is expected to be low, although, this is not affirmed in this study.

One fixed value for the longshore transport gradient

This study shows that the longshore transport gradient is an important parameter for the calibration of the XBeach model at the study location. The study location is on the convex-seaward crest of a perturbation in the shoreline so structural erosion is likely as described in section 5.2. This is successfully simulated by the longshore transport gradient. However, when the perturbation flattens over time due to erosion, the longshore transport gradient decreases until the shoreline becomes stable. In XBeach only one fixed value of the longshore transport gradient can be taken. When in the forecast the magnitude of the perturbation decreases, the longshore transport gradient is expected to decrease and the XBeach model will overestimate the amount of longshore volume loss. Especially for longer forecasting periods, this is likely to become a problem.

9 Conclusion

When executing beach profile development forecasts, engineers should be aware of the uncertainty range of the resulting forecast. In this study, a method for probabilistic beach profile forecasting with XBeach is developed for beach width predictions at a recently nourished beach. To illustrate this, the method is applied on the Hondsbossche Dunes as a case study. In contrast with traditional deterministic beach width modelling with one outcome, the modelling in this study results in a beach width forecast with a range of the possible outcomes and their probabilities of occurrence. This range of possible outcomes is depending on the variability in the forcing conditions.

The in this study examined method for beach width predictions within a stochastic framework starts with an analysis of the behaviour of the recently nourished beach at the Hondsbossche Dunes. By a survey on the dry part of the beach, observed beach profile data are gathered. By analysing the differences between the subsequent surveys, the morphological evolution of the beach, in the first four months after the nourishment, is evaluated. The most severe erosion takes place at the largest cross-shore extent of the additional nourishment, where the beach width decreases with 52 m in the first four months after the nourishment. A both ends of the nourishment in longshore direction, accretion takes place. This is due to the longshore diffusion of the nourishment volume. After one year, the initial planform of the nourishment is dissipated over the coastline.

The next step is an analysis of the local hydrodynamic conditions, to generate synthetic wave time series. Offshore wave time series of the significant wave height, mean zero-crossing period, wave direction, and water level are decomposed into segments with different physical properties. These segments are separately simulated and thereafter combined to create a set of synthetic time series. The seasonal components of the hydrodynamic conditions are simulated using Fourier series, and the stationary components are simulated with ARMA models. A number of 5000 synthetic time series with a period of one year and one hourly interval are generated to represent a full range of possible conditions. The size of these synthetic time series is decreased to a set of 20 characteristic time series by Latin Hypercube sampling. The resulting synthetic wave time series consist of realistic time series containing natural variations such as seasonal differences, storm, and calm conditions. The seasonal difference in the synthetic wave time series is less explicit than in the observed wave time series, this leaves room for improvement.

To evaluate the possible future coastal development due to the synthetic forcing conditions, a 1D XBeach model is calibrated and validated to match the observed changes in beach width.

The 20 selected hydrodynamic time series are used as forcing conditions for the XBeach model. This results in a range of possible beach profile developments. These results indicate the possible beach width development with its probability of occurrence. After one year, the beach width change has a median of -60 m and a probability of 80% that the beach width has changed between -18 m and -98 m. Furthermore, there is a 10% chance that the beach width decrease is larger than 98 m after one year. The probability ranges of the beach width development are the main result of this study. This gives a more realistic idea of the possible development of the beach width at the Hondsbossche Dunes after the installation of an additional nourishment than a deterministic forecast.

To reflect these findings to literature is difficult because not many comparative publications with stochastic beach width models with similar time scales and conditions exist. A comparable publication is the annual prediction of shoreline erosion and subsequent recovery (Davidson et al., 2017). Davidson et al. (2017) used random monthly sampling to create stochastic forcing conditions and the model ShoreFor for annual beach width predictions for the location of Perranporth (UK). In this study, a shoreline displacement after a year of approximately between -40 m and 20 m is found. The uncertainty range of 60 meters at Perranporth is comparable to the 80 m uncertainty range at the Hondsbossche Dunes (both with a probability of 80%) found in this study, considering the differences in location, used models, and methodologies.

Since the method used in this study is described extensively, this can be applied anywhere where XBeach models are applicable and sufficient wave data are available. This study is relevant because previous methods of beach width forecasting do indicate the most probable beach profile development, but no probability of occurrence. As beach profile forecasting depends on highly uncertain wave conditions more insight in the uncertainty range of a forecast is desired. This gives a more realistic idea of the possible beach width development. Hereby the probability that nourishments have to take place within a certain period, can be indicated. This can be useful for better budgeting decisions in beach nourishment contracts with maintenance obligation, as the Hondsbossche Dunes. Also, beach nourishment volumes can be optimised with this improvement in beach width modelling.

Recommendations

In further research, stochastic beach width forecasting can be further optimised in the combination with long term process-based modelling. An important improvement can be made in the generation of synthetic forcing conditions resulting in better seasonal behaviour. In this study, the focus lies on the intrinsic uncertainties of the forcing conditions for an XBeach model. It is recommended to incorporate the significant epistemic uncertainties. This can further improve the validity of the stochastic forecasting.

Several parts of the method to create stochastic hydrodynamic forcing conditions can be further improved. Some of these are; a more appropriate sampling parameter for Latin Hypercube sampling; a more detailed model for the surge; accurate decoupling in stationary and non-stationary components; improvements in the accuracy of the transformation of the wave period from offshore to the nearshore. Further research could examine whether improving these modelling steps is important and if so, make these improvements.

In this study, a 1D XBeach model is used to model the beach width development. To account for longshore gradients, a constant longshore transport gradient is implemented. With increasing computational power, stochastic forecasting with a 2D XBeach model could be feasible, albeit with a shorter period. For a location with a longshore transport gradient, such as the Hondsbossche Dunes, the possibility of a stochastic 2D XBeach model can be investigated.

It is evident that for beach width forecasting, uncertainty ranges have to be taken into account. It is, however, unclear what the most adequate and efficient way is to take these uncertainty ranges into account. This study contributes to the understanding of the possibility to use ARMA models for generating hydrodynamic forcing conditions. An interesting followup from this study would be to put this method in perspective to other methods, such as random monthly sampling. Questions to be asked are ”to what extent do the complex modelling steps of the ARMA method contribute to the accuracy?” And ”do these extra modelling steps create additional epistemic uncertainties?”

References

Acharya, A. S., Prakash, A., Saxena, P., & Nigam, A. (2013). Sampling: Why and how of it. *Indian Journal of Medical Specialties*, *4*(2), 330–333.

Ashton, A. D., & Murray, A. B. (2006). High-angle wave instability and emergent shoreline shapes: 1. modeling of sand waves, flying spits, and capes. *Journal of Geophysical Research: Earth Surface*, *111*(F4).

Bart, L. (2017). Long-term modelling with xbeach: combining stationary and surfbeat mode in an integrated approach.

Bosboom, J., Reniers, A., & Luijendijk, A. (2014). On the perception of morphodynamic model skill. *Coastal Engineering*, *94*, 112–125.

Boukhanovsky, A. V., Lopatoukhin, L. J., & Soares, C. G. (2007). Spectral wave climate of the north sea. *Applied Ocean Research*, *29*(3), 146–154.

Box, G. E. (1979). Robustness in the strategy of scientific model building. In *Robustness in statistics* (pp. 201–236). Elsevier.

Box, G. E., Jenkins, G. M., Reinsel, G. C., & Ljung, G. M. (2015). *Time series analysis: forecasting and control*. John Wiley & Sons.

Brockwell, P. J., Davis, R. A., & Calder, M. V. (2002). *Introduction to time series and forecasting* (Vol. 2). Springer.

Callaghan, D., Nielsen, P., Short, A., & Ranasinghe, R. (2008). Statistical simulation of wave climate and extreme beach erosion. *Coastal Engineering*, *55*(5), 375–390.

Dagalaki, V. (2018). *Towards multi-model coastline change uncertainty quantification & aggregation* (Unpublished master's thesis). TU Delft.

Davidson, M. A., Turner, I. L., Splinter, K. D., & Harley, M. D. (2017). Annual prediction of shoreline erosion and subsequent recovery. *Coastal Engineering*, *130*, 14–25.

Dean, R. G. (2003). *Beach nourishment: theory and practice* (Vol. 18). World Scientific Publishing Company.

de Jongh, L. (2017). *Initial morphological evolution of a mega nourishment: The hondsbossche dunes one year after construction* (Unpublished master's thesis). TU Delft.

den Bieman, J. P., Stuparu, D. E., Hoonhout, B. M., Diermanse, F. L., Boers, M., & van Geer, P. F. (2014). Fully probabilistic dune safety assessment using an advanced probabilistic method. *Coastal Engineering Proceedings*, *1*(34), 9.

de Schipper, M. A., Darnall, J., de Vries, S., & Reniers, A. (2017). Beach scarp evolution and prediction. *Coastal Dynamics 2017*.

de Schipper, M. A., de Vries, S., Ruessink, G., de Zeeuw, R. C., Rutten, J., van Gelder-Maas, C., & Stive, M. J. (2016). Initial spreading of a mega feeder nourishment: Observations of the sand engine pilot project. *Coastal Engineering*, *111*, 23–38.

Dillingh, D. (2013). *Kenmerkende waarden kustwateren en grote rivieren* (Tech. Rep.). Report 1207509-000-ZKS-0010. Delft, The Netherlands: Deltares.

Fockert, A., & Luijendijk, A. (2010). *wave look-up table* (Technical Memo). Boussinesqweg 1, 2629 HV Delft: Deltares. (report 1002337-002-ZKS-0001)

Guillén, J., Stive, M., & Capobianco, M. (1999). Shoreline evolution of the holland coast on a decadal scale. *Earth Surface Processes and Landforms: The Journal of the British Geomorphological Research Group*, *24*(6), 517–536.

Hall, C. M. (2001). Trends in ocean and coastal tourism: the end of the last frontier? *Ocean & coastal management*, *44*(9-10), 601–618.

Holthuijsen, L. H. (2010). *Waves in oceanic and coastal waters*. Cambridge university press.

Iman, R. L., & Conover, W.-J. (1982). A distribution-free approach to inducing rank correlation among input variables. *Communications in Statistics-Simulation and Computation*, *11*(3), 311–334.

Jäger, W. (2018). *Multivariate methods for coastal and offshore risks* (Unpublished doctoral dissertation). Delft University of Technology.

Jones, R. H. (1980). Maximum likelihood fitting of arma models to time series with missing observations. *Technometrics*, *22*(3), 389–395.

Keijsers, J. G., Poortinga, A., Riksen, M. J., & Maroulis, J. (2014). Spatio-temporal variability in accretion and erosion of coastal foredunes in the netherlands: regional climate and local topography. *PloS one*, *9*(3), e91115.

Kriebel, D. L., & Dean, R. G. (1993). Convolution method for time-dependent beach-profile response. *Journal of Waterway, Port, Coastal, and Ocean Engineering*, *119*(2), 204–226.

Kroon, A., de Schipper, M. A., van Gelder, P. H., & Aarninkhof, S. G. (2019). *Incorporating model uncertainty in building with nature designs.* (Preprint submitted to Coastal Engineering)

Li, L. (2010). A fundamental study of the morphological acceleration factor.

McKay, M. D., Beckman, R. J., & Conover, W. J. (1979). Comparison of three methods for selecting values of input variables in the analysis of output from a computer code. *Technometrics*, *21*(2), 239–245.

Murphy, A. H. (1988). Skill scores based on the mean square error and their relationships to the correlation coefficient. *Monthly weather review*, *116*(12), 2417–2424.

Pebesma, E. J., & Heuvelink, G. B. (1999). Latin hypercube sampling of gaussian random fields. *Technometrics*, *41*(4), 303–312.

Ranasinghe, R., Swinkels, C., Luijendijk, A., Roelvink, D., Bosboom, J., Stive, M., & Walstra, D. (2011). Morphodynamic upscaling with the morfac approach: Dependencies and sensitivities. *Coastal engineering*, *58*(8), 806–811.

Rijkswaterstaat. (n.d.). *Waterinfo actuele waterdata.* Retrieved 2018-10-30, from `https://waterinfo.rws.nl/`

Roelvink, v. D., Van Dongeren, A., McCall, R., Hoonhout, B., Van Rooijen, A., Van Geer, P., … Quataert, E. (2015). Xbeach technical reference: Kingsday release. *Model description and reference guide to functionalities*.

Ruessink, B., & Jeuken, M. (2002). Dunefoot dynamics along the dutch coast. *Earth surface processes and landforms*, *27*(10), 1043–1056.

Ruggiero, P., List, J., Hanes, D., & Eshleman, J. (2007). Probabilistic shoreline change modeling. In *Coastal engineering 2006: (in 5 volumes)* (pp. 3417–3429). World Scientific.

Sadegh, M., Ragno, E., & AghaKouchak, A. (2017). Multivariate copula analysis toolbox (mvcat): Describing dependence and underlying uncertainty using a bayesian framework. *Water Resources Research*, *53*(6), 5166–5183.

Sallaberry, C. J., Helton, J. C., & Hora, S. C. (2008). Extension of latin hypercube samples with correlated variables. *Reliability Engineering & System Safety*, *93*(7), 1047–1059.

Scheel, F., de Boer, W. P., Brinkman, R., Luijendijk, A. P., & Ranasinghe, R. (2014). On the generic utilization of probabilistic methods for quantification of uncertainty in process-based morphodynamic model applications. *Coastal Engineering Proceedings*, *1*(34), 88.

Sterl, A., Brink, H. v. d., Vries, H. d., Haarsma, R., & Meijgaard, E. v. (2009). An ensemble study of extreme north sea storm surges in a changing climate. *Ocean Science Discussions*, *6*(2), 1031.

Țene, M., Stuparu, D. E., Kurowicka, D., & El Serafy, G. Y. (2018). A copula-based sensitivity analysis method and its application to a north sea sediment transport model. *Environmental Modelling & Software*, *104*, 1–12.

The Netherlands Space Office Satellietdataportaal. (2018). *2018-04-07 0.8m triplesat.* Retrieved from `https://satellietdataportaal.nl/wmslayer/20180407_094625_Tri` (Online; accessed April 15, 2018)

Van Gelder, P. (2000). Statistical methods for the risk-based design of civil structures.

Van Rijn, L., Walstra, D., Grasmeijer, B., Sutherland, J., Pan, S., & Sierra, J. (2003). The predictability of cross-shore bed evolution of sandy beaches at the time scale of storms and seasons using process-based profile models. *Coastal Engineering*, *47*(3), 295–327.

Verhagen, H. J. (1989). Sand waves along the dutch coast. *Coastal Engineering*, *13*(2), 129–147.

A

Comparison between Wave Buoy and Transformation table

In this appendix the wave data from the wave buoy are compared to the data from the transformation table. This comparison is made for the significant wave height, the peak period, and the wave direction.

A.1. Significant wave height

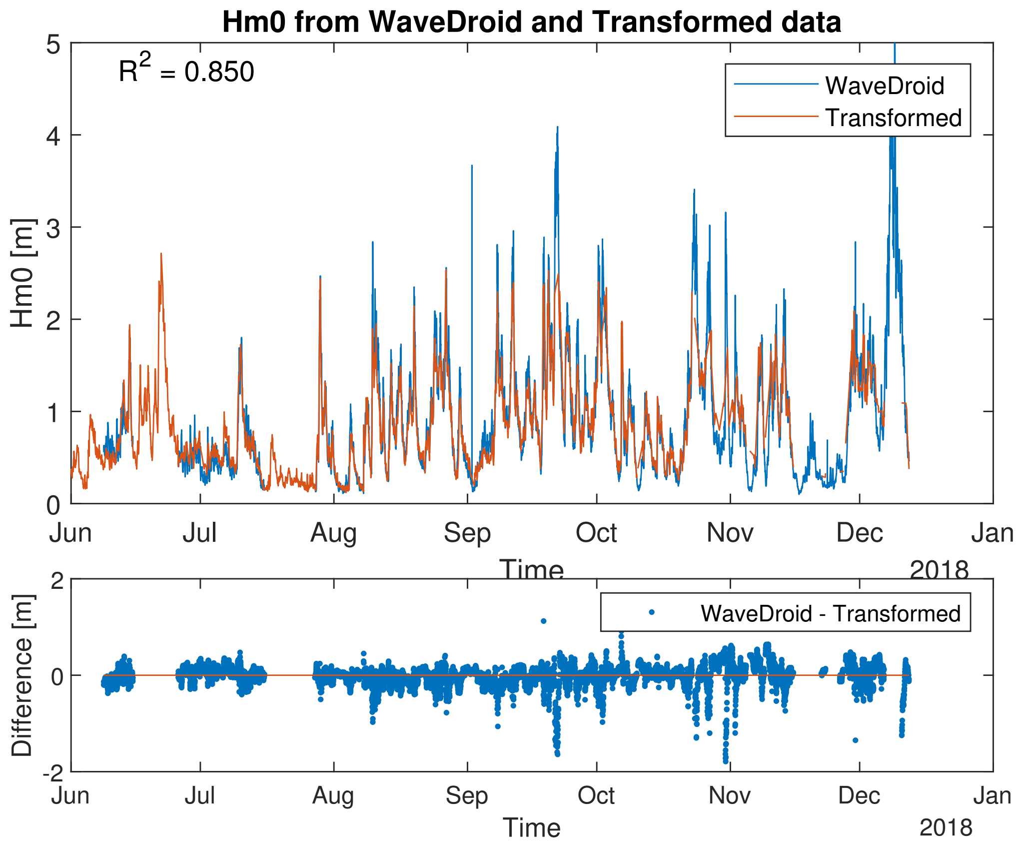

Figure A.1: Comparison of the significant wave heights measured by the local wave buoy, and the significant wave heights transformed with the wave transformation table

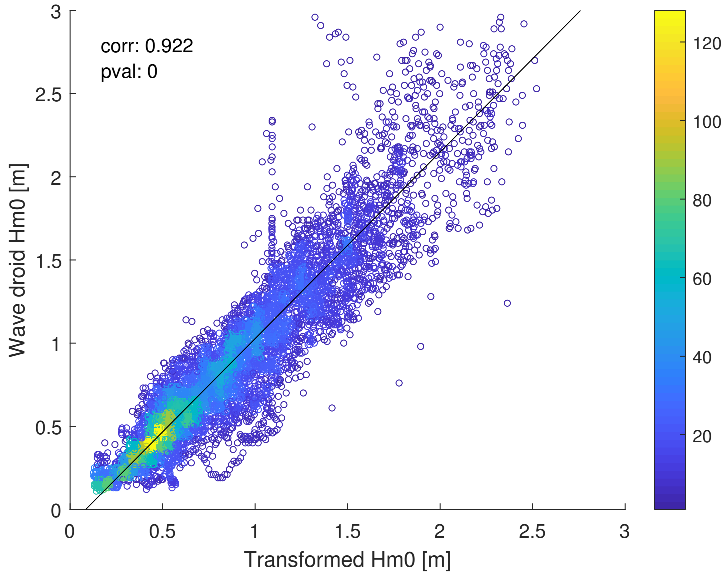

Figure A.2: Density scatter for the significant wave height with the significant wave height derived from the transformation table on the x-axis, and the significant wave height derived from the local wave buoy on the y-axis.

A.2. Wave peak period

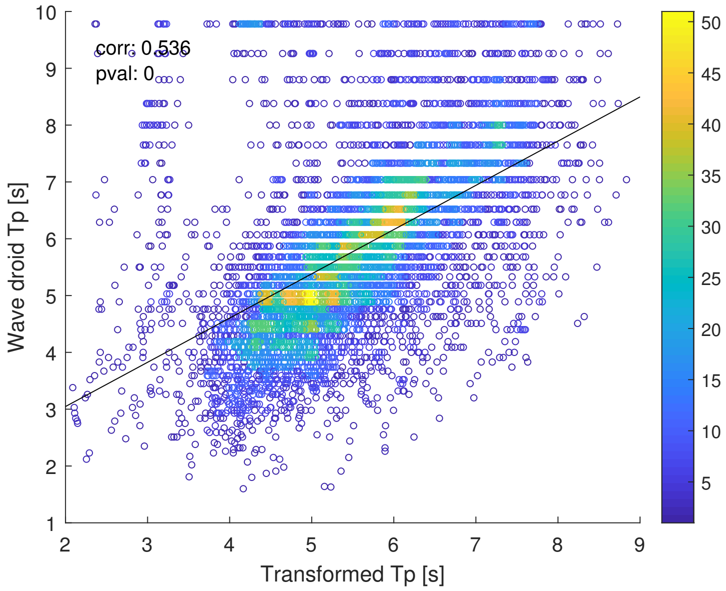

Figure A.3: Density scatter for the peak period with the peak period derived from the transformation table on the x-axis, and the peak period derived from the local wave buoy on the y-axis.

A.3. Wave direction

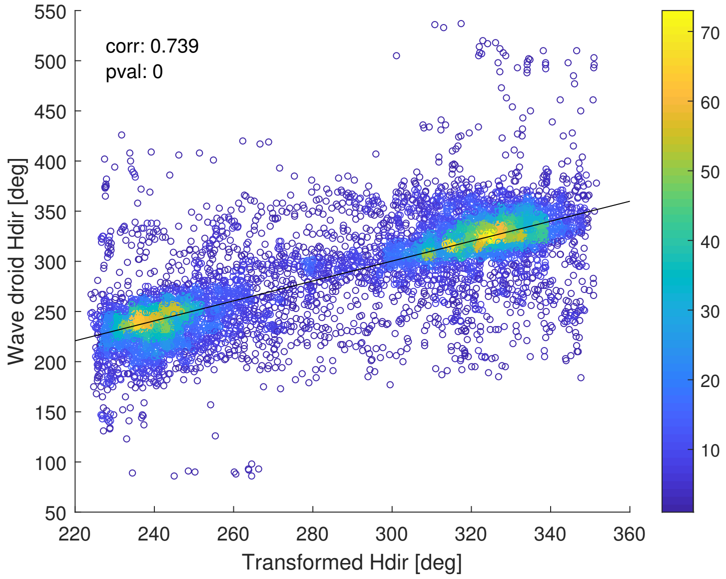

Figure A.4: Density scatter for the wave direction with the wave direction derived from the transformation table on the x-axis, and the wave direction derived from the local wave buoy on the y-axis.

B

Survey Data

B.1. Elevation maps

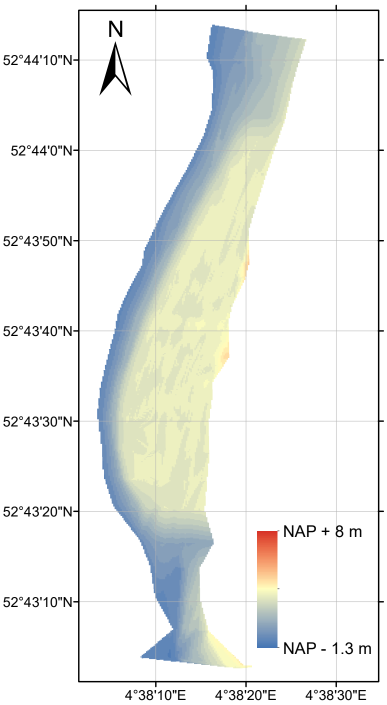

(a)

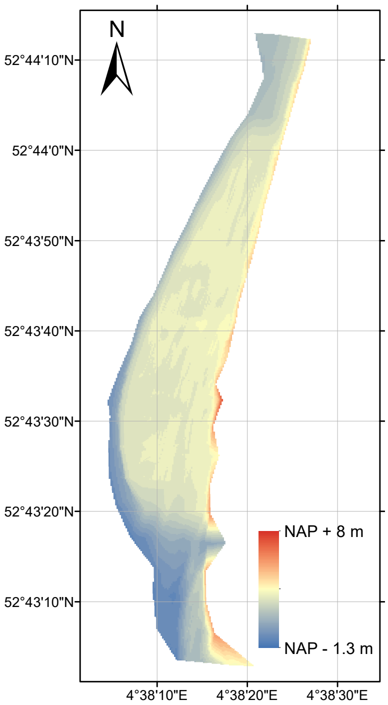

(b)

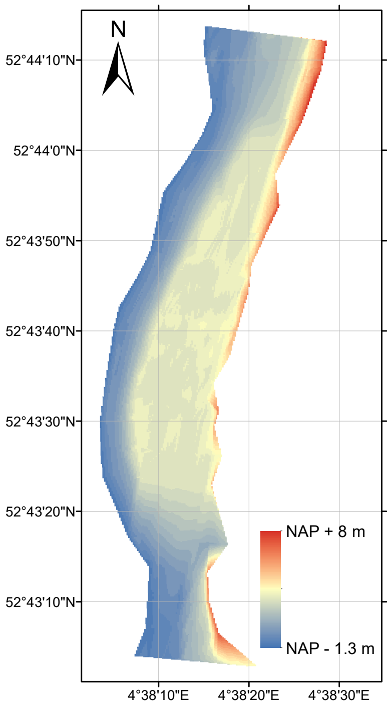

(c)

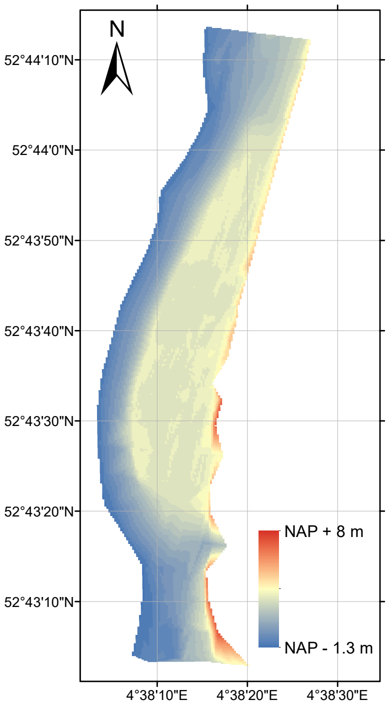

(d)

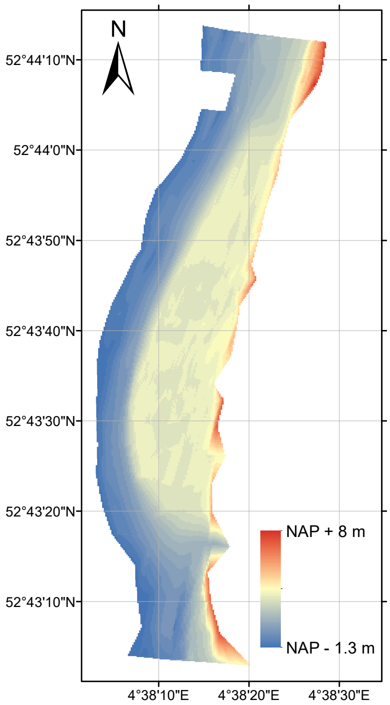

(e)

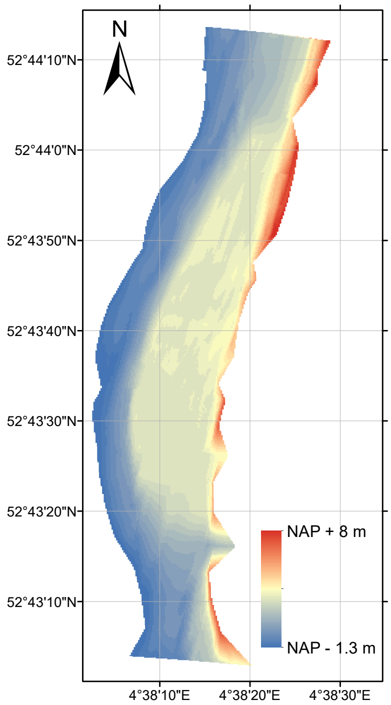

(f)

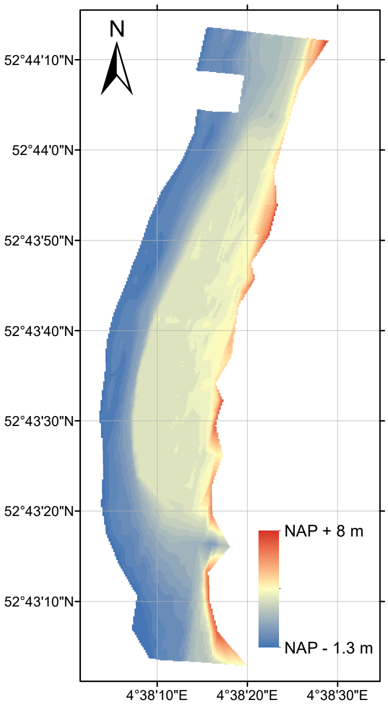

(g)

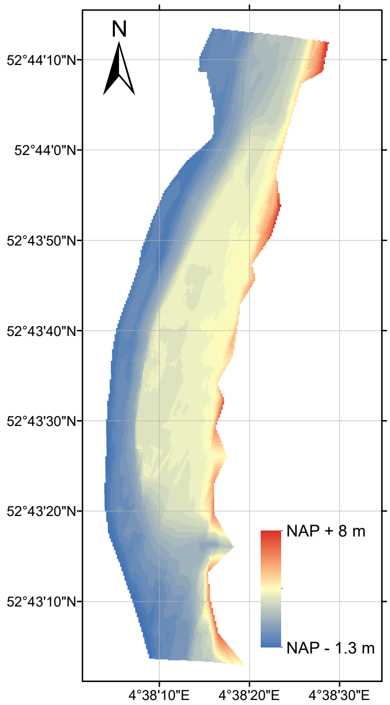

(h)

Figure B.1: Elevation maps created from survey data.

B.2. Erosion and accretion

(a)

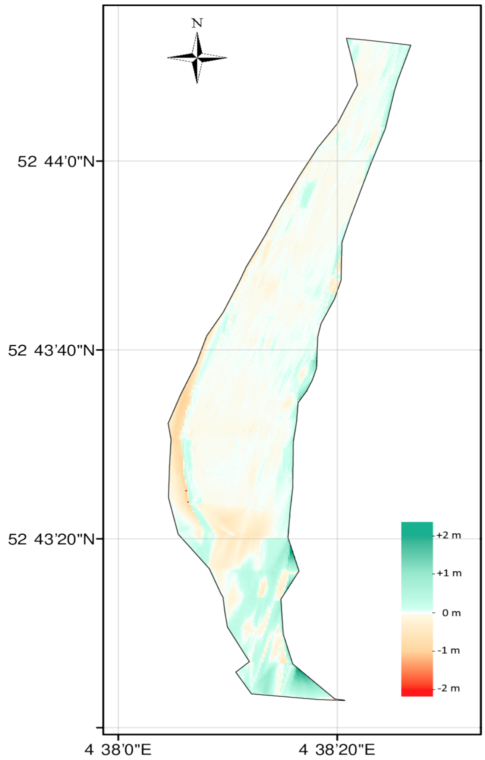

(b)

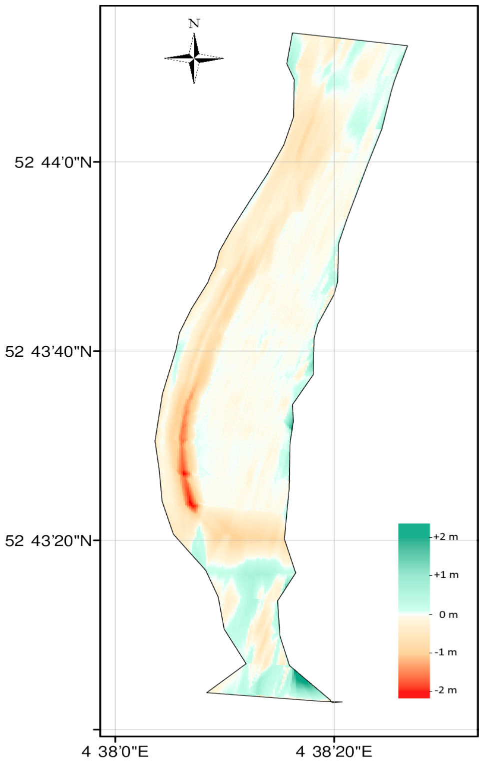

(c)

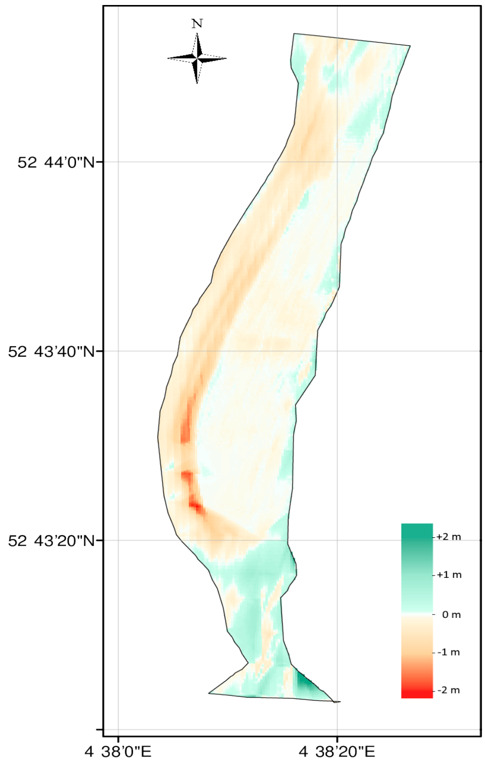

(d)

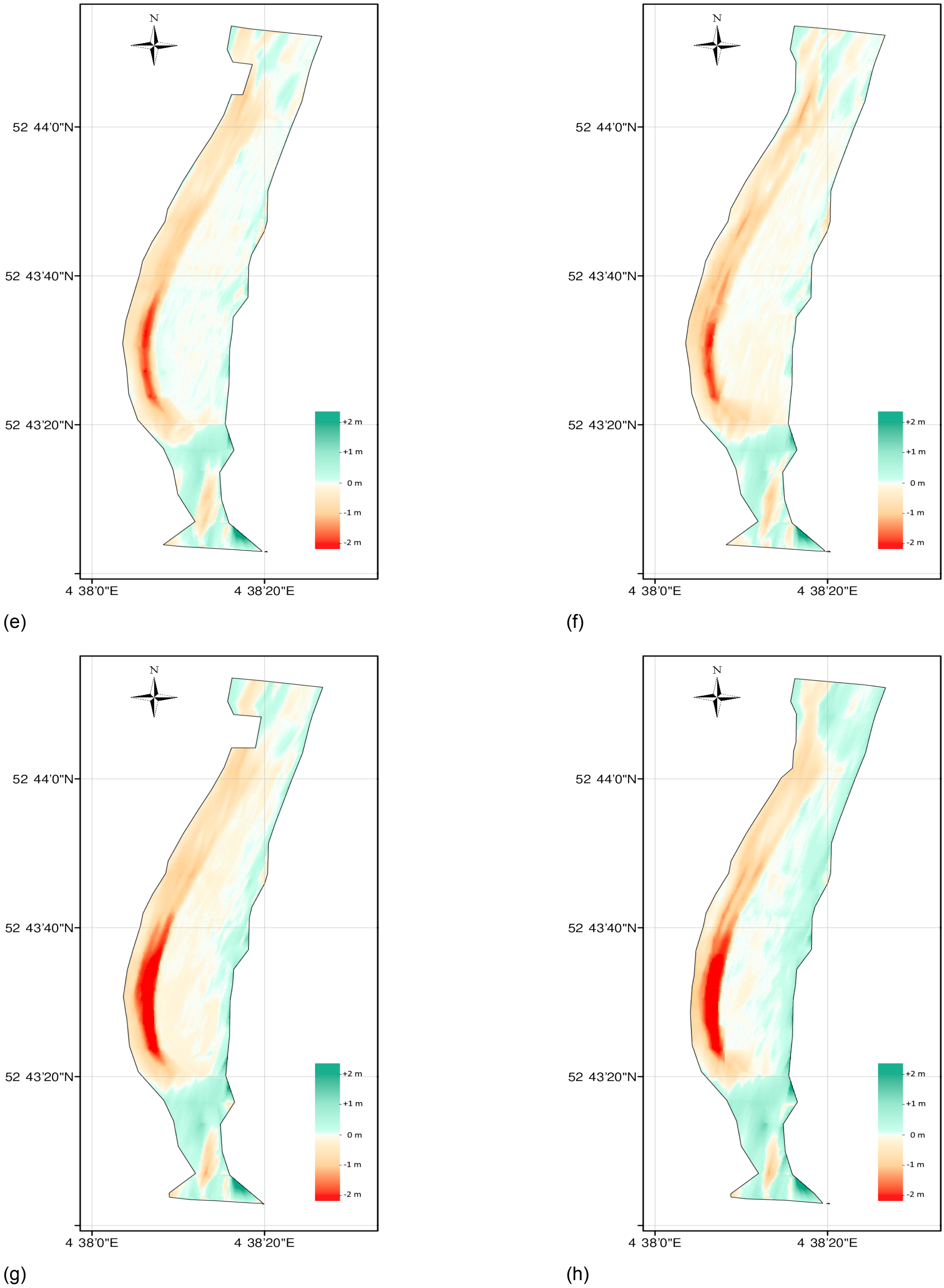

Figure B.2: Erosion and accretion maps. These erosion and accretion maps are created by subtracting the initial elevation map (figure B.1a) from the subsequent elevation maps (figure B.1b to B.1h). Erosion is indicated by red colours and accretion is indicated by green colours. For orientation, B.2a contains a satellite image of the study area.

B.3. Beach profiles at section KK

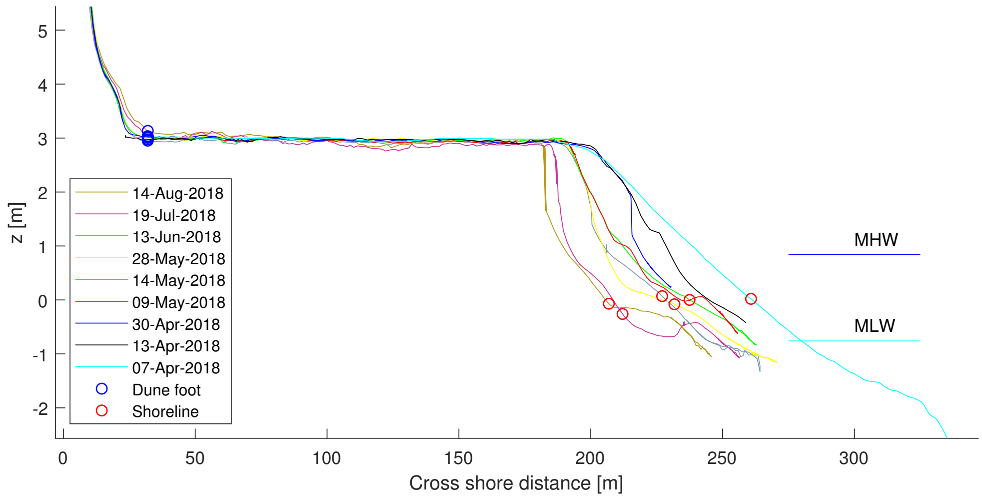

Figure B.3: Beach profiles at section KK. Each survey date is given by a different colour. The location of the dune foot and the shoreline are given by a blue and red 'o' respectively.

B.4. Satellite images

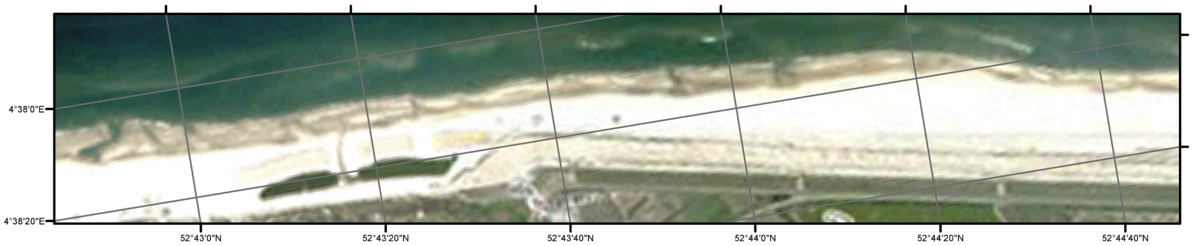

(a)

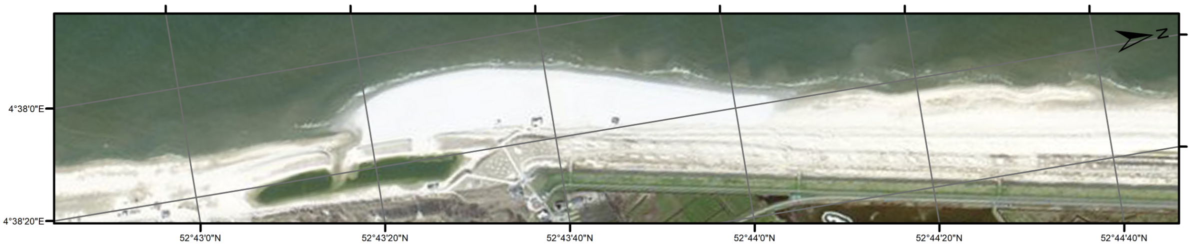

(b)

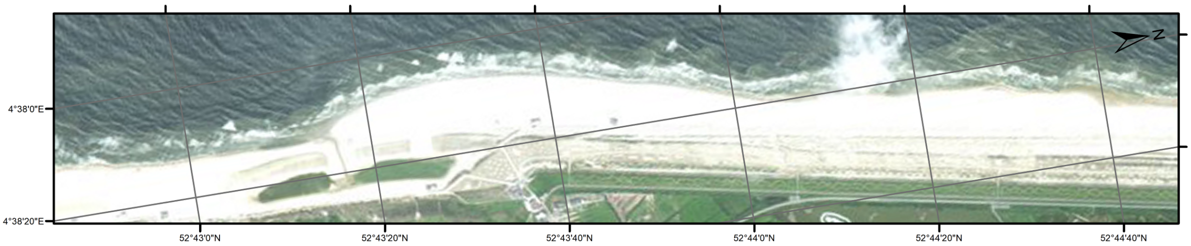

(c)

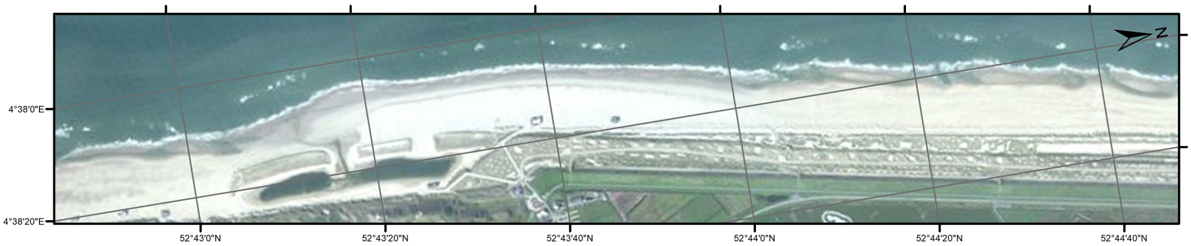

(d)

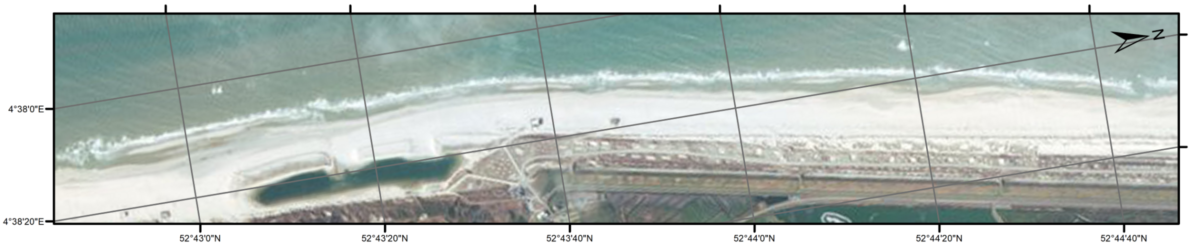

(e)

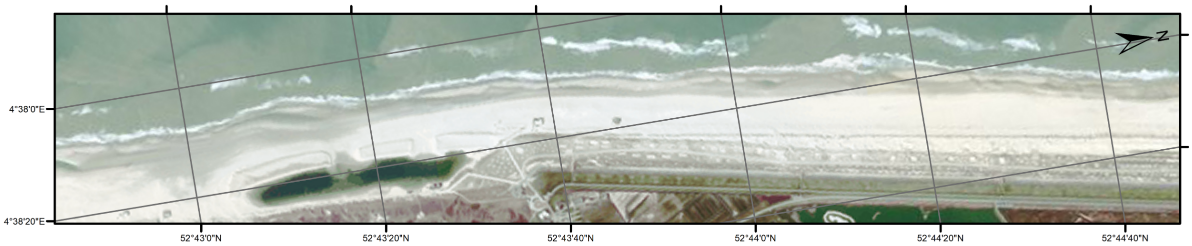

(f)

Figure B.4: Periodic captures of satellite images of the location of the additional nourishment (The Netherlands Space Office Satellietdataportaal, 2018). In (a) the situation eight months before the additional nourishment is given, at July 6, 2017. In (b) the situation just after the nourishment at April 7, 2018. In (c) the satellite image at June 6, 2018. In (d) the situation at October 5, 2018. In (e) the situation of March 2, 2019. In (f) the situation at April 1, 2019, One year after the nourishment.

C

XBeach settings

Params.txt file

```
%%%%%%%%%%%%%%%%%%%%%%%%%%%%%%%%%%%%%%%%%%%%%%%%%%%%%%%%%%%%%%%%%%%%%%%%%%%%%%%%
%%% XBeach parameter settings input file                                     %%%
%%%                                                                          %%%
%%% date:     11-Feb-2019 10:57:00                                           %%%
%%% function: xb_write_params                                                %%%
%%%%%%%%%%%%%%%%%%%%%%%%%%%%%%%%%%%%%%%%%%%%%%%%%%%%%%%%%%%%%%%%%%%%%%%%%%%%%%%%

%%% Bed composition parameters %%%%%%%%%%%%%%%%%%%%%%%%%%%%%%%%%%%%%%%%%%%%%%%%%

D50          = 0.000250
D90          = 0.000375

%%% General %%%%%%%%%%%%%%%%%%%%%%%%%%%%%%%%%%%%%%%%%%%%%%%%%%%%%%%%%%%%%%%%%%%%

%%% Grid parameters %%%%%%%%%%%%%%%%%%%%%%%%%%%%%%%%%%%%%%%%%%%%%%%%%%%%%%%%%%%%

depfile      = bed.dep
posdwn       = 0
nx           = 570
ny           = 0
vardx        = 1
xfile        = x.grd
xori         = -500
yori         = 0
thetamin     = -90
thetamax     = 90
dtheta       = 20

%%% Model time %%%%%%%%%%%%%%%%%%%%%%%%%%%%%%%%%%%%%%%%%%%%%%%%%%%%%%%%%%%%%%%%%

tstop        = 29361600
tintg        = 86400
tstart       = 1
```

```
%%% Morphology parameters %%%%%%%%%%%%%%%%%%%%%%%%%%%%%%%%%%%%%%%%%%%%%%%%%%%%%%

morfac       = 10
morstart     = 1
dryslp       = 1
lsgrad  = -0.003

%%% Sediment transport parameters %%%%%%%%%%%%%%%%%%%%%%%%%%%%%%%%%%%%%%%%%%%%%%

facua        = 0.1

%%% Roller parameters %%%%%%%%%%%%%%%%%%%%%%%%%%%%%%%%%%%%%%%%%%%%%%%%%%%%%%%%%%

beta         = 0.100000

%%% Tide boundary conditions %%%%%%%%%%%%%%%%%%%%%%%%%%%%%%%%%%%%%%%%%%%%%%%%%%%

zs0file      = tide.txt
tideloc      = 1

%%% Wave boundary condition parameters %%%%%%%%%%%%%%%%%%%%%%%%%%%%%%%%%%%%%%%%%

wbctype      = jonstable
wavemodel    = surfbeat

%%% Wave breaking parameters %%%%%%%%%%%%%%%%%%%%%%%%%%%%%%%%%%%%%%%%%%%%%%%%%%%

gamma        = 0.500000
alpha        = 1

%%% Wave-spectrum boundary condition parameters %%%%%%%%%%%%%%%%%%%%%%%%%%%%%%%%

bcfile       = JONSWAP.txt

%%% Output variables %%%%%%%%%%%%%%%%%%%%%%%%%%%%%%%%%%%%%%%%%%%%%%%%%%%%%%%%%%%

outputformat = netcdf

nglobalvar   = 6
H
zs
zb
hh
u
v


nmeanvar = 20
H
zs
zs0
zb
hh
u
v
ue
```

```
ve
urms
Fx
Fy
ccg
ceqsg
ceqbg
Susg
Svsg
R
D
DR
```

D

XBeach profiles comparison

D.1. Calibration

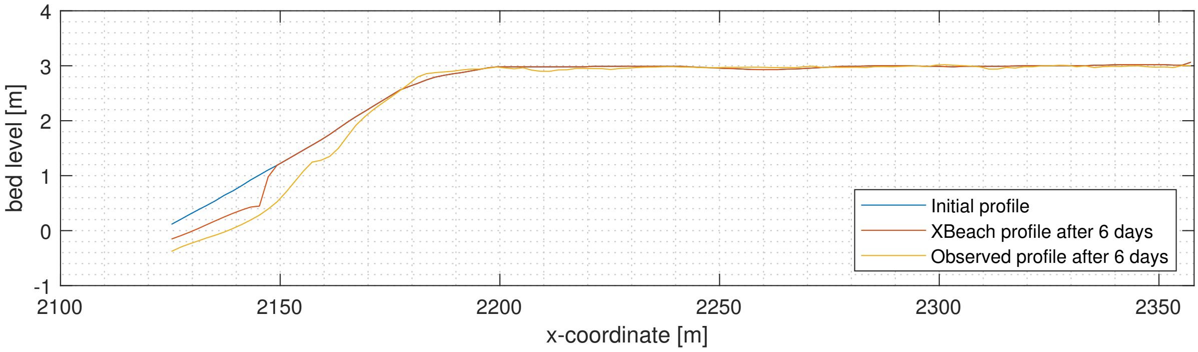

(a)

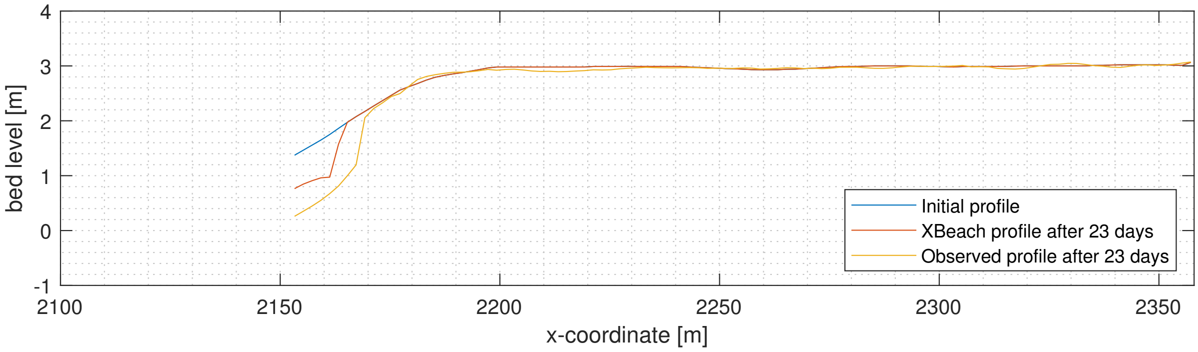

(b)

Figure D.1: First two profiles where the XBeach profile and the observed profile can be compared. In (a) the profiles at 13-04-2018, 6 days after the initial profile. In figure (b) the profiles at 30-04-2018, 23 days after the initial profile.

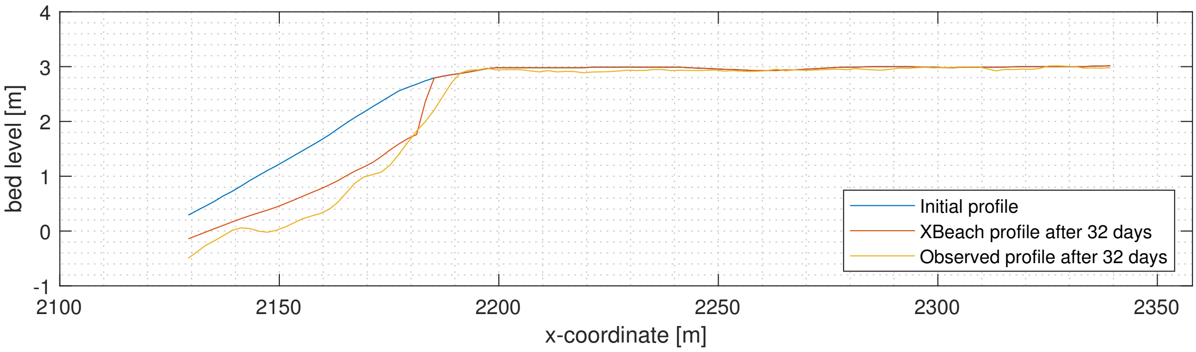

(c)

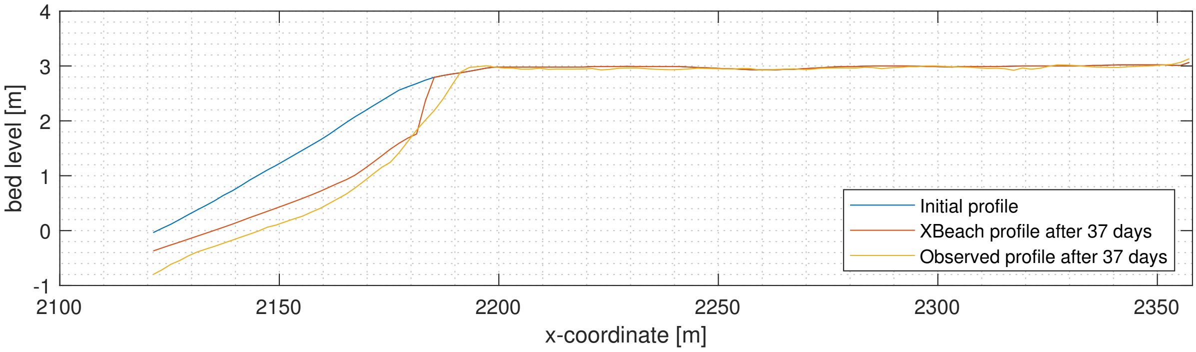

(d)

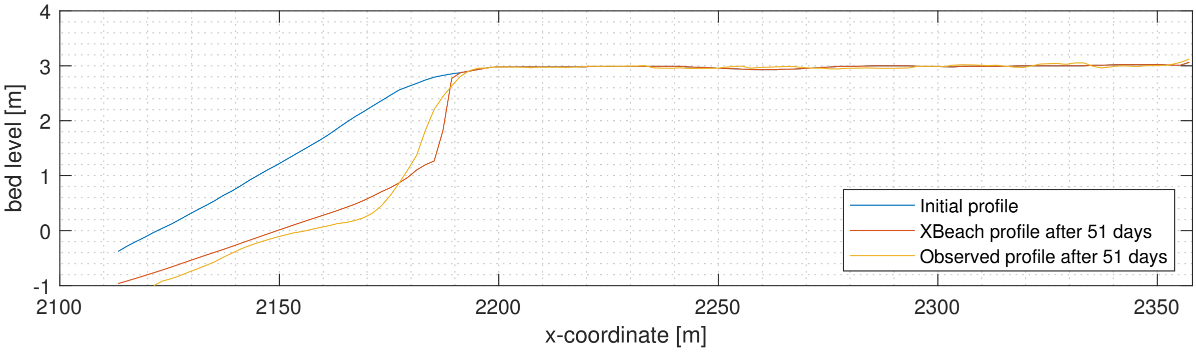

(e)

Figure D.1: Three figures where the XBeach profile and the observed profile can be compared. In (c) the profiles at 09-05-2018, 32 days after the initial profile. In figure (d) the profiles at 14-05-2018, 37 days after the initial profile. In figure (e) the profiles at 28-05-2018, 51 days after the initial profile.

D.2. Validation

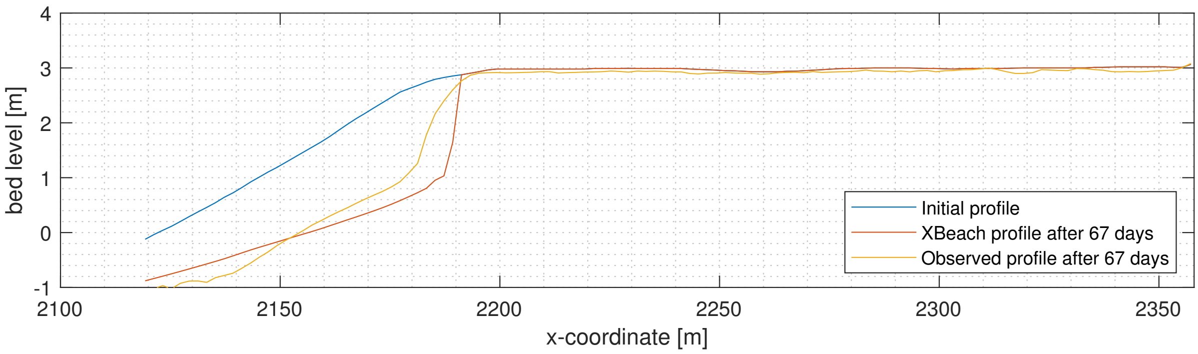

(a)

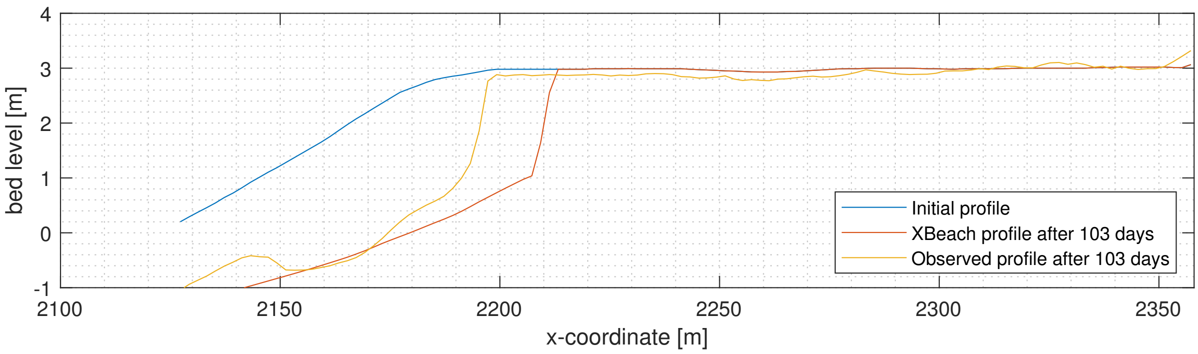

(b)

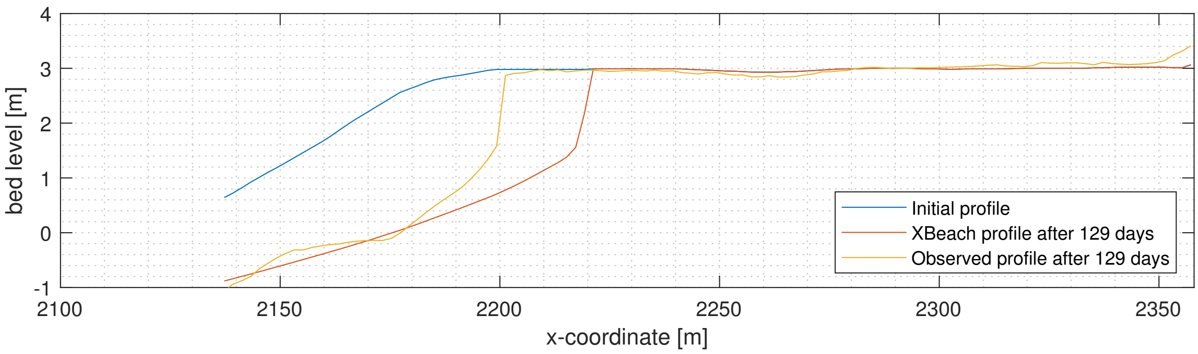

(c)

Figure D.2: Three figures where the XBeach profile and the observed profile can be compared. These tree profiles are from the validation period. In (a) the profiles at 13-06-2018, 57 days after the initial profile. In figure (b) the profiles at 19-07-2018, 103 days after the initial profile. In figure (e) the profiles at 14-08-2018, 129 days after the initial profile.